DROPLET MICROFLUIDICS COUPLED TO MICROCHIP ELECTROPHORESIS FOR HIGH-THROUGHPUT ENZYME MODULATOR SCREENING

by

Erik D. Guetschow

A dissertation submitted in partial fulfillment
of the requirements for the degree of
Doctor of Philosophy
(Chemistry)
in the University of Michigan
2016

Doctoral Committee:

Professor Robert T. Kennedy, Chair
Associate Professor Nikolaos Chronis
Professor Mark E. Meyerhoff
Associate Professor Brandon T. Ruotolo

To my family and friends

ACKNOWLEDGEMENTS

TABLE OF CONTENTS

LIST OF FIGURES

xi

LIST OF APPENDICES

LIST OF ABBREVIATIONS

APCE   Affinity Probe Capillary Electrophoresis

5-FAM   5-carboxyfluorescein

AMC   7-amino-4-methylcoumarin

Bag3   Bcl2-Associated Athanogene

BGE   Background Electrolyte

CE   Capillary Electrophoresis

CEC   Capillary Electrochromatography

CGE   Capillary Gel Electrophoresis

CPS1   Carbamoyl-phosphate Synthase 1

DMSO   Dimethyl Sulfoxide

EOF   Electroosmotic Flow

ESI   Electrospray Ionization

FRET   Fluorescence Resonance Energy Transfer

GAPDH   Glyceraldehyde-3-phosphate Dehydrogenase

HMDS   Hexamethyldisilazane

HMGCS2   3-hydroxy-3-methylglutaryl CoA Synthase 2

HPLC   High Pressure Liquid Chromatography

Hsp70   Heat Shock Protein 70

HTS	High-Throughput Screening
i.d.	Inner Diameter
IC$_{50}$	Half Maximal Inhibitory Concentration
K$_d$	Dissociation Constant
KO	Knockout (in regard to cell lines/mouse models)
LIF	Laser-Induced Fluorescence
MALDI	Matrix-Assisted Laser Desorption Ionization
MCE	Microchip Electrophoresis
MS	Mass Spectrometry
MWP	Multi-well Plate
NAD$^+$	Nicotinamide Adenine Dinucleotide
o.d.	Outer Diameter
PDC	Pyruvate Dehydrogenase Complex
PDMS	Polydimethylsiloxane
PFD	Perfluorodecalin
PFO	Perfluorooctanol
PKA	Protein Kinase A
PPI	Protein-Protein Interaction
SDH	Succinate Dehydrogenase
SIRT	Sirtuin
SOD1	Superoxide Dismutase 1

ABSTRACT

High-throughput screening (HTS) represents a powerful tool for drug discovery by allowing 10^4 to 10^5 assays to be completed within a single day. Typically, assays are performed in multiwell plates (MWPs) utilizing fluorogenic substrates for detection. These substrates increase development time and can introduce artifactual results. Therefore, alternate screening strategies based around natural substrates are necessary.

We developed a screening platform that couples nanoliter volume samples to microchip electrophoresis for analysis using a novel polydimethylsiloxane (PDMS)-and-glass microfluidic device. The system was demonstrated by screening a small library against protein kinase A (PKA), which regulates metabolism within the cell. It was chosen for its well-characterized kinetic parameters and commercially available peptide substrates. Sample throughput of 0.16 Hz was achieved allowing at least 6 replicate MCE injections from each sample in a high quality assay (Z'-factor = 0.8).

To demonstrate the ability to screen larger libraries, we developed a novel assay for sirtuin 5 (SIRT5) using a naturally derived peptide substrate. SIRT5 impacts metabolism and has reported oncogenic functions making inhibitor identification of clinical importance. Compared to the PKA assay previously developed, assay throughput was increased 3-fold and 1406 samples were analyzed within 46 minutes (0.5 Hz). Using a 250 ms separation, each assay sample could be analyzed 8 times by MCE generating

over 11,000 electropherograms. Several previously unreported inhibitors of SIRT5 were identified and verified by dose-response analysis.

Finally, work toward miniaturization of high-throughput assays was demonstrated by performing sample preparation and analysis completely within nanoliter volume droplets. A simple to use and easy to fabricate PDMS microfluidic device was developed to allow addition of assay reagents to nanoliter volume samples. Reagent use, relative to assays performed in 384 well plates, could be reduced 1,000-fold and sample-to-sample carryover was less than 5 percent under typical experimental conditions. Analysis of samples prepared in droplet format was demonstrated with droplets containing a fluorescent dye and addition of a fluorescent peptide. These samples could be analyzed by MCE at 0.33 samples per second but increased throughput should be possible by using higher flow rates.

CHAPTER 1: INTRODUCTION

High-Throughput Screening

High-throughput screening (HTS) has emerged in recent years as a powerful tool in drug discovery and other areas of biology and chemistry, such as catalyst discovery and protein engineering.[1, 2] High-throughput workflows are able to assay 10^4 to 10^5 compounds against a selected target within a single day. To achieve this level of throughput, most HTS utilizes multi-well plate (MWP)-based assays with robotic plate manipulation and liquid handling to massively parallelize sample preparation.[1-5] With the increasing size of compound libraries available, MWP density has increased from 96 to 1536 wells per plate in an effort to reduce assay time and sample consumption. Many technologies exist for high-throughput sample preparation ranging from bulk liquid dispensing (i.e. Thermo Fisher MultiDrop Combi) to compound library dispensing at nanoliter volumes (i.e. Caliper Life Science SciClone pin tool). These technologies allow even large compound libraries to be prepared in a timely manner.

Drug discovery has largely focused on five target families: G protein coupled receptors, kinases, proteases, nuclear receptors, and ion channels.[6] However, these families miss a large number of pharmacological targets within cells, such as other enzyme classes. Enzymes, which include kinases and proteases, efficiently catalyze chemical reactions to regulate cellular functions, such as metabolism, cell death, and

protein degradation. Indeed, many diseases and disorders have been linked to over- or under-expression of specific enzymes demonstrating their importance as pharmacological targets for disease intervention. Emphasizing this point, 50 percent of drugs on the market as of 2006 targeted enzymes (i.e. proteases and kinases).[7]

To achieve the throughput necessary for drug discovery, most assays utilize fluorescence detection methods. These tend to be robust, useful in homogenous assays found in HTS, and compatible with the small sample volumes associated with high-density well plates. To measure the effect of test compounds, a loss or gain of signal must be correlated to enzyme activity. For example, to detect β-galactosidase activity fluorescein-di-β-D-galactopyranoside (FDG), which consists of a fluorescein molecule conjugated to two galactopyranosyl moieties, is commonly used.[8] In the absence of β-galactosidase the substrates is non-fluorescent; however, removal of the galactopyranosyl moieties by the enzyme results in a fluorescent signal that correlates the β-galactosidase activity. Alternatively, coupled enzyme cascades, such as the commonly used Amplex Red system, can be used if fluorogenic substrates are unavailable. These assays stoichiometrically couple product formation in an assay of interest to a formation of a fluorescent product through a series of secondary enzymes. In many cases, this requires the development of novel fluorogenic substrates or optimization of coupled enzyme reactions for each assay[9] increasing assay development time and cost. Additionally, use of artificial substrates has the potential to generate false positive results due to possible non-physiological behaviors of the engineered substrates. To address these and other limitations, work has been done to develop HTS assays based on alternative detection

modes, such as liquid chromatography (LC), mass spectrometry (MS), surface plasmon resonance (SPR), and impedance, that avoid fluorogenic substrates.[9-16]

Several limitations exist for applying these alternative detection strategies to high-throughput screening. In the case of the optical assays, multi-analyte detection is difficult and most assays require multiple steps to generate a signal. For LC-MS assays, label-free analysis allows one to use natural peptides without needing to engineer a fluorophore; however, the throughput remains low due to slow LC separations.

Capillary and Microchip Electrophoresis for High-Throughput Screening

Although LC-MS methods tend to have low throughput unsuited to large-scale screening, other separations-based HTS methods, with potentially higher throughput, are possible. Capillary electrophoresis (CE), another separation technique, allows for rapid separation of analytes not possible by most LC-MS methods. This combined with the benefits of LC-MS methods, such as multi-analyte detection and spatial separation of interfering species, makes CE an attractive option for HTS. If fluorophores are required for detection, they can be placed remotely from the active peptide residue to reduce the likelihood of false positive results caused by non-specific interactions. Furthermore, peptide engineering to quench the fluorophore prior to enzymatic activity is not necessary because substrate and product can be separated prior to detection. To understand the potential of CE-based HTS, it will beneficial to discuss several fundamental aspects of CE and previous attempts at HTS by CE.

First established in 1981,[17] CE is typically performed fused-silica capillaries or on glass microfluidic devices, in which case it is called microchip electrophoresis (MCE),[18, 19] with the inlet and outlet connected to a voltage source (Figure 1-1). This development

addressed several limitations associated with existing electrophoretic methods (i.e. gel electrophoresis), such as slow separation speed and excessive joule heating. CE and MCE address these limitations by performing separations within narrow bore channels or tubes (i.e. 5-200 μm inner diameter) that afford better heat dissipation. Improved heat dissipation, in turn, allows application of higher voltages to achieve faster separations and improved performance.

In electrophoresis, analytes migrate through an electrically conductive buffer, called the background electrolyte (BGE), under the influence of an applied electric field. The speed and direction of migration, which ultimately affects analyte separation, is based on a combination of the electroosmotic mobility (μ_{EOF}) contributed by the buffer and the electrophoretic mobility (μ_{EP}) of the analyte.

Electroosmotic mobility is due to the formation of an electric double layer at the surface of the fused silica due to interactions between the negatively charged surface silanols and positive counter ions within the BGE (Figure 1-1, top). When an electric field (E) is applied, these ions move along the wall dragging the bulk solution and creating a net flow toward the cathode. This flow, called electroosmotic flow (EOF), moves with a velocity (v_{EOF}) determined by the following equation:

$$v_{EOF} = \mu_{EOF}E = \frac{\varepsilon\zeta}{\eta}E \quad \text{Eq. 1-1}$$

where ε is the permittivity of the BGE, ζ is the zeta-potential at the capillary wall, and η is the solution viscosity. This equation suggests that EOF is characteristic of the buffer composition and increases with applied electric field. The electrophoretic mobility is an intrinsic property of each analyte as is described as:

$$\mu = \frac{q}{6\pi\eta r} \quad \text{Eq. 1-2}$$

where q is the analyte charge and r is the Stoke's radius of the analyte. Finally, the net migration velocity of each analyte (v) will depend on contributions from both terms:

$$v = (\mu_{EOF} + \mu_{EP})E \quad \text{Eq. 1-3}$$

Therefore, analytes can be separated from one another based on their charge-to-size ratio. Under normal separation conditions (i.e. negatively charged surface and high pH buffers), EOF is directed toward the cathode (outlet), and cations migrate fastest, followed by all neutral compounds, and finally anions.

Compared to LC separations, which use pressure driven flow, EOF has a plug-shaped profile resulting in less band broadening during the separation. Additionally, assuming Joule heating, injection width, and analyte adsorption are mitigated, diffusion is the only source of band broadening. Under these conditions, theory suggests that increasing separation voltage (V) allows for shorter migration times (Eq. 1-4) and higher efficiency (Eq. 1-5),[20] where t_{mig} is migration time, L is capillary or channel length, N is number of theoretical plates, and D is the analyte diffusion constant.

$$t_{migration} = \frac{L}{(\mu_{EOF} + \mu_{EP})V} \quad \text{Eq. 1-4}$$

$$N = \frac{(\mu_{EOF} + \mu_{EP})V}{2D} \quad \text{Eq. 1-5}$$

As demonstrated by these equations, the separation length can be reduced to achieve faster separations without sacrificing efficiency by maintaining the same applied voltage (i.e. increasing the electric field). This is especially important for screening applications, in which high-throughput is essential, as it demonstrates fast and high quality separations are possible.
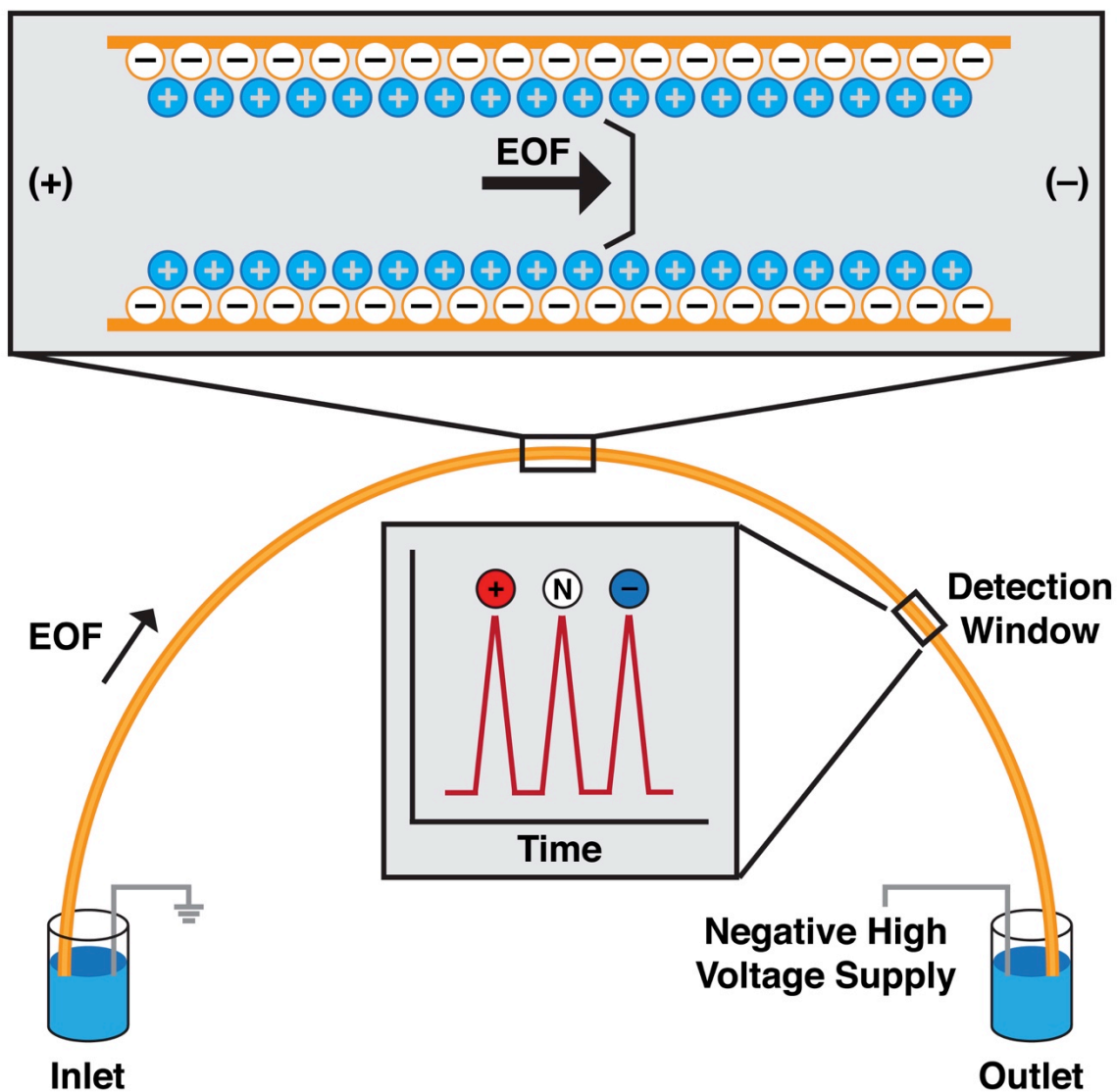
Figure 1-1. Schematic of capillary electrophoresis instrumentation and characteristics. The inlet and outlet of a fused silica capillary, filled with background electrolyte, are inserted into buffer vials connected to a high-voltage power supply. The external electric field generates an electric double layer due to interactions between the negatively charged surface and counter ions in the buffer (top grey box). This generates a plug-shaped electroosmotic flow. Analytes are separated based on differences in size-to-charge ratio with positive analytes migrating fastest and negatively charged analytes migrating slowest. All neutral analytes co-migrate with EOF.

Detection in CE or MCE is typically achieved through laser induced fluorescence

(LIF), UV absorbance spectroscopy, electrochemical detection, or mass spectrometry.

LIF is the most common detection method due to high sensitivity and simplicity.[21] Due to path length independence, the narrow bore of capillaries or microchannels does not limit detection efficiency and picomolar detection limits are possible. The primary disadvantage of LIF detection for high-throughput screening is the lack of natively fluorescent substrates and potential interactions caused by the fluorophore.

Because CE separates based on differences in size or charge, it is well suited to biochemical assay screening. The majority of enzymes induce changes on their substrate through removal of post-translation modifications, such as acetyl, succinyl, and phosphate groups, or cleavage of peptide bonds in the case of proteases. These changes in size and charge can be exploited to quickly separate substrate and product peptides. For example, SIRT1 targets the removal acetyl modifications from lysine residues. Under basic conditions typical of CE, the deactylated product peptide will have a higher net positive charge than the substrate due to exposure of the amine functional group on the lysine side change. This positive charge results in faster migration times for product peptides compared to substrate. This same idea can be exploited for monitoring protein-protein interactions through affinity probe capillary electrophoresis (APCE). In APCE, one protein is fluorescently labeled while the other remains unlabeled. The migration time of the labeled protein will shift depending on whether it is bound to the target protein or unbound; in turn, this can be used to quantify the degree of interaction. An example was the use of CE to identify small molecule inhibitors of the interaction between Heat Shock Protein 70 (Hsp70) and Bcl2-associated athanogene 3 (Bag3). Over 3000 compounds were tested, using a separation based on a combination of electrophoresis and pressure driven flow.[22]

One potential challenge of using CE or MCE with LIF detection for high-throughput screening is the effect of test compounds on migration time or analyte detection. In the case of migration time, test compounds could affect the electric double layer leading to enhanced or suppressed EOF and shifting migration times. However, most screening is done with compound concentrations below 20 µM and therefore should not have a significant impact on EOF. It is also possible that test compounds could fluoresce and lead to false positive results. However, deconvolution of signal from test compounds and substrates is possible due to the spatial separation achieved during CE or MCE. In conventional MWP assays, it would be impossible to screen natively fluorescent test compounds, as their signal would add to signal from the fluorogenic probe.

Although rapid separations are possible by electrophoresis, the bottleneck for high-throughput analysis remains sample introduction. Conventional CE or MCE systems use auto-samplers or manual sample dispensing to sequentially analyze samples leading to low sample throughput and large sample requirements. One group developed several small, labeled peptides based on the SIRT1 substrate, p53, for screening and demonstrated SIRT1 activity with several known modulators.[23, 24] In another example, a commercial CE system was used to identify protein-protein interaction inhibitors from a library of 3,000 compounds at a rate of 220 compounds per day.[22] In both examples, sample throughput was not significantly improved over typical LC-MS assays.

A commercial microfluidics system – the LabChip system – overcomes this limitation through the use of a 'sipper' sample loading method. In this design samples are arrayed in a MWP, and a short length of tubing connected the microchip is dipped into a sample well allowing sample to be pulled into the separation channel by applied vacuum

(Figure 1-2). Through interfacing to a MWP, samples can be prepared using existing high-throughput workflows and continuous operation is possible. The system was demonstrated in an assay for SIRT1 in which a fluorescently labeled peptide could be separated within 50 seconds.[25] However, this method does not achieve the potential of MCE-based screening because of band broadening induced by vacuum driven flow in the separation channel and throughput of only 0.02 samples per second.
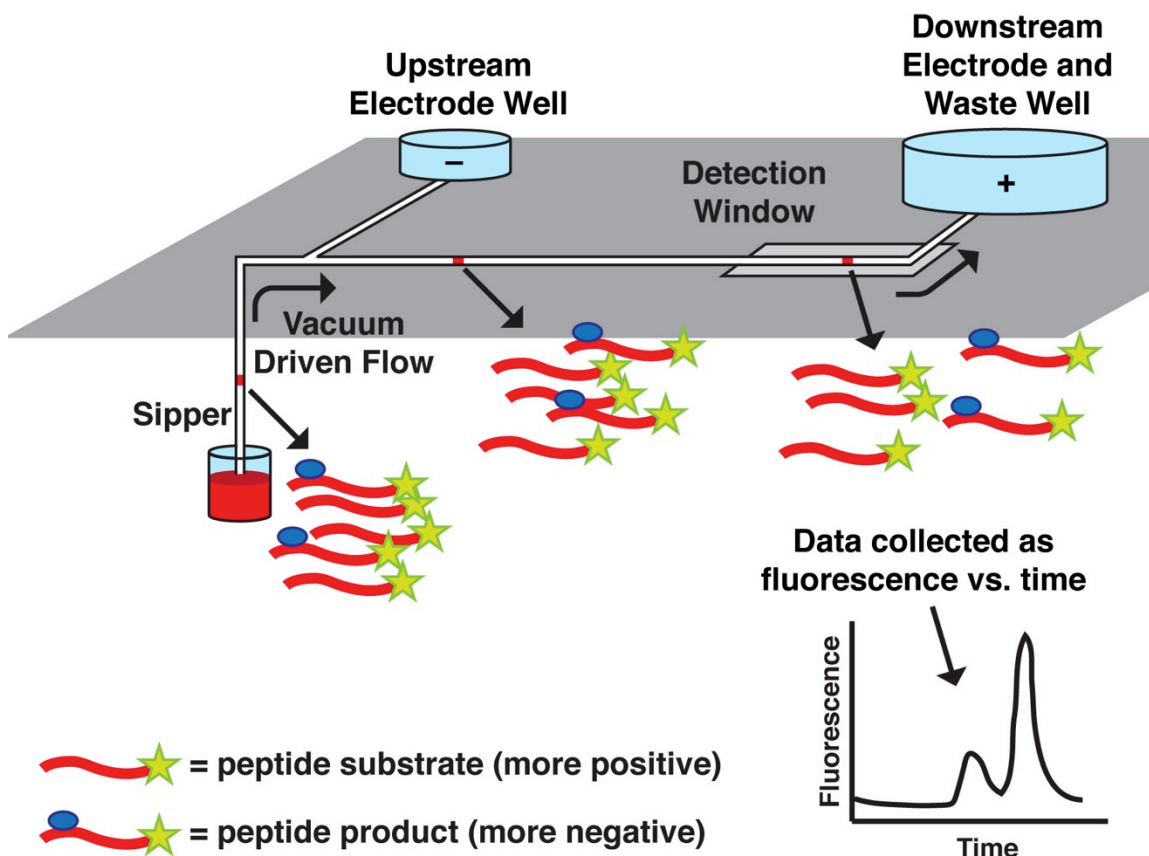
Figure 1-2. Schematic of the Caliper LabChip system for screening biochemical assays by microchip electrophoresis. At the top, shown coming in and out of the plane, is the microchip used for separation by a combination of electrophoresis and vacuum driven flow (applied at the outlet reservoir). Sample is introduced through a 'sipper' tube by interfacing to a multiwell plate. Labeled substrate and product peptides are separated based on differences in size-to-charge ratio and detected by fluorescence (shown bottom right).[26]

9

Segmented Flow for Low Volume Sample Handling

To improve throughput, samples could be introduced to microchips as segmented flow droplets. In such a method, aqueous samples (picoliter to microliter in volume) are encapsulated in an immiscible carrier phase, such as perfluorinated oil or air, allowing them to be easily manipulated without carryover.[27] In the clinical laboratory, this method has been used since the late 1950s to automate sample analysis for clinical tests, such as urea and blood glucose.[28, 29] Oil carrier phases have gained in popularity as they are much less compressible than air and analyte partitioning is minimized.[30] Droplet formation can be achieved in several ways. For generating a large number of droplets from a single sample, flow focusing and tee-junctions can be used.[31-34] To generate a few droplets of many samples, aspiration is used.[35-38] Once formatted, a number of manipulations, akin to conventional bench-top chemistry, can be performed within droplets such as splitting,[39-42] fusion,[43-47] mixing,[48-52] sorting,[53-56] reagent addition,[38, 50, 52, 57, 58] and dilution[59, 60] (Figure 1-3).

Droplet samples have the potential to drastically reduce sample consumption during HTS, which is doubly important because reagent cost and procurement are often a bottle neck during assay development and screening.[61] By combining the above droplet transformations, such as reagent addition and rapid mixing, screening reactions can be prepared at the picoliter or nanoliter scale instead of the microliter scale. Starting with droplets generated from existing compound libraries, enzyme and substrate could be dispensed directly into droplets, and results could be read directly by fluorescence. Using this method, one group reported a 1000-fold reduction in assay time and a 1-million-fold reduction in cost compared to a conventional assay.[53]
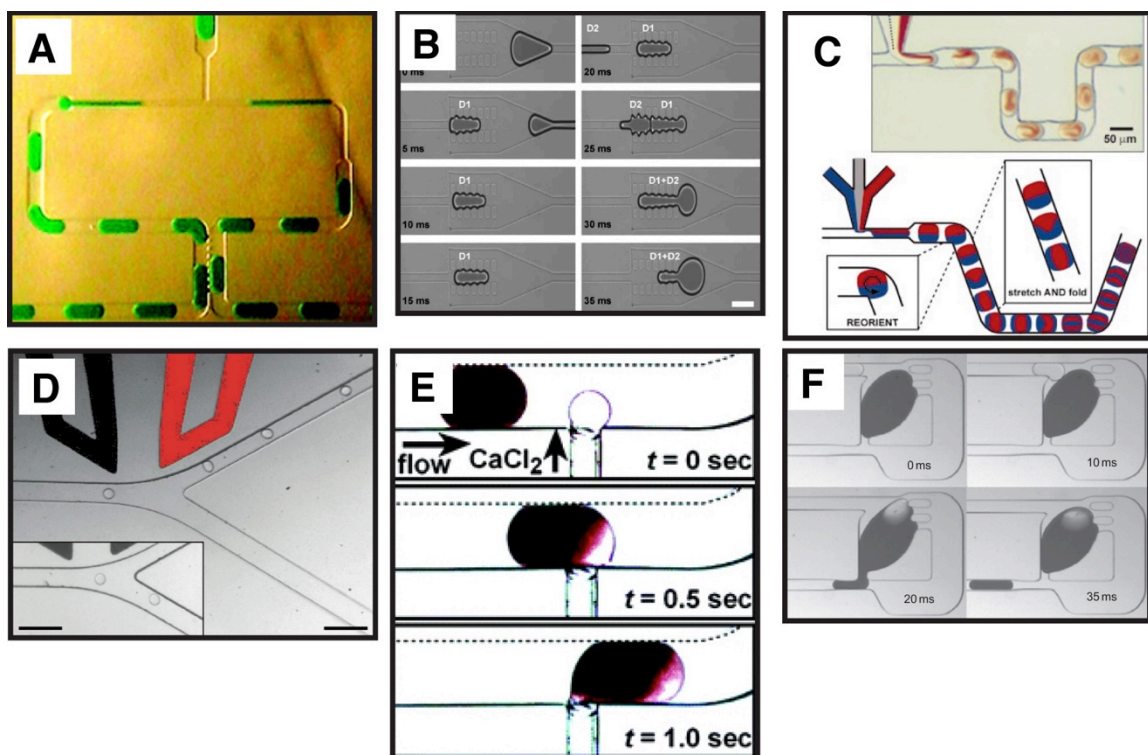
Figure 1-3. Examples of manipulations and transformations possible with droplet samples. A) Asymmetric splitting of primary droplets into smaller secondary droplets by control channel geometry.[42] B) Merging of two sequential droplets using a pillar array. The first droplet becomes stuck in the pillar array until merging with the second droplet. At this point, alternate flow paths for oil phase are blocked at the droplet is released.[46] C) Rapid mixing is achieved within droplets through integration of turns into the microfluidic network. At each turn the orientation of the droplet changes leading to advective mixing.[51] D) Fluorescence-activated droplet sorting (FADS) is achievable using external electrodes (shown in black and red at the top of the image). If a signal threshold is met, the electrode is energized causing droplets to deflect into the upper channel. Below the threshold, droplets automatically go into the lower channel (inset image).[54] E) Reagent addition scheme using a hydrophilic side channel to reduce carryover.[52] F) Serial dilution of droplets using a dilution chamber. Dilution droplets merge with the primary droplet (dark droplet centered in each frame) activating a fluidic valve and dispensing a tertiary droplet. Dilution of the primary droplet generates a serial dilution on chip.[59] Figures reproduced with permission from individual publishers.

Droplet strategies have been used in many novel applications related to high-throughput analysis. In one of the first applications of droplet microfluidics, enzyme kinetics for ribonuclease A were measured with better than 1 ms resolution through on-chip dilution and rapid mixing within droplets.[60] Building on this work, screening of

protein crystallization conditions using less than 4 nL of solution per sample was reported.[62] In a demonstration of HTS, high-resolution dose-response curves (10,000 points per compound) for a library containing 704 compounds against protein tyrosine phosphatase 1B were analyzed in 4.2 hours (~450 Hz).[63] Using more complex microfluidic platforms, drug cytotoxicity screening against encapsulated cells[64], directed evolution of enzyme mutants[53], generation of combinatorial reaction mixtures[65], and bacterial susceptibility to antibiotics[66] have been reported demonstrating that multiple steps and transformations of droplet samples are possible.

The low sample requirements for CE and MCE (typically less than a few hundred picoliters) and the ability to manipulate droplets in a high-throughput manner make them a natural solution to sample introduction bottlenecks. Several groups have developed methods for coupling droplet-based samples to electrophoretic analysis. Due the fact that most carrier phases are non-conductive, droplet streams must be desegmented (i.e. the aqueous samples and carrier phase separated) prior to analysis by electrophoresis. This is typically achieved through either passive, which functions without intervention, or active methods that require external forces to achieve phase segregation.

Passive droplet extraction is appealing because it requires no external input leading to simpler design and operation. These methods typically rely upon special channel geometries[67-70] or differences in surface chemistry.[71-76] Using a polydimethylsiloxane (PDMS) microfluidic device, one group developed a 'comb' structure that allowed selective removal of carrier phase from the droplet stream but prevent aqueous samples from passing due to high back pressure within the 'comb' (Figure 1-4A).[70] They used this method to couple an LC separation to CE to achieve 2D

separations. The same group used an oleophilic film to wick away carrier phase prior to analysis of droplet contents by capillary gel electrophoresis[71] or deposition for matrix assisted laser desorption ionization (MALDI)-MS (Figure 1-4B).[73] Another group reported the use of octadecyltrichlorosilane chemistry to pattern selected channels hydrophobic, within a glass microfluidic device, to achieve selective extraction of the aqueous samples. This method was used to analyze droplet samples from a microdialysis *in vivo* chemical monitoring and enzyme assay samples (Figure 1-4C).[75]

Active droplet extraction, while slightly more complex, affords opportunities to improve extraction robustness and selectivity.[77, 78] Using an applied electric field, aqueous droplets were merged with a parallel aqueous stream while the oil carrier phase continued toward a waste outlet. This was applied to couple droplet samples to electrospray ionization (ESI)-MS by extracting samples into an MS friendly buffer immediately prior to spray (Figure 1-4D).[77]

When coupled to electrophoretic analysis, the droplet sample is either wholly injected for analysis[70, 71, 76] or a portion is injected. In the former method, the oil phase is typically removed immediately prior to injection of the droplet onto the electrophoresis channel. While this method is the simplest to implement, poor separation efficiency is common because droplet volume is typically much larger than an ideal MCE injection volume. Separation time is directly proportional to droplet spacing and high efficiency separations will require the use of very small droplets. To improve separation efficiency, injection of a portion of each droplet sample could be done. In one design, the extracted sample passes the separation channel inlet resulting in the injection of a small sample plug.[72, 74] Therefore, injection volume is closely related to the sample flow rate and

droplet size. As with the previous method, separation time is directly proportional to droplet spacing. In another design, droplets were extracted before being sampled by EOF toward a voltage-gated injector. In effect, this is a dynamic sample reservoir allowing any combination of injection and separation parameters.[75, 79] Indeed, this approach yielded the highest efficiency separations (223,000 plates) from droplet samples. None of these methods, however, were demonstrated to be compatible with HTS, which requires analysis of many distinct samples with minimal carryover.
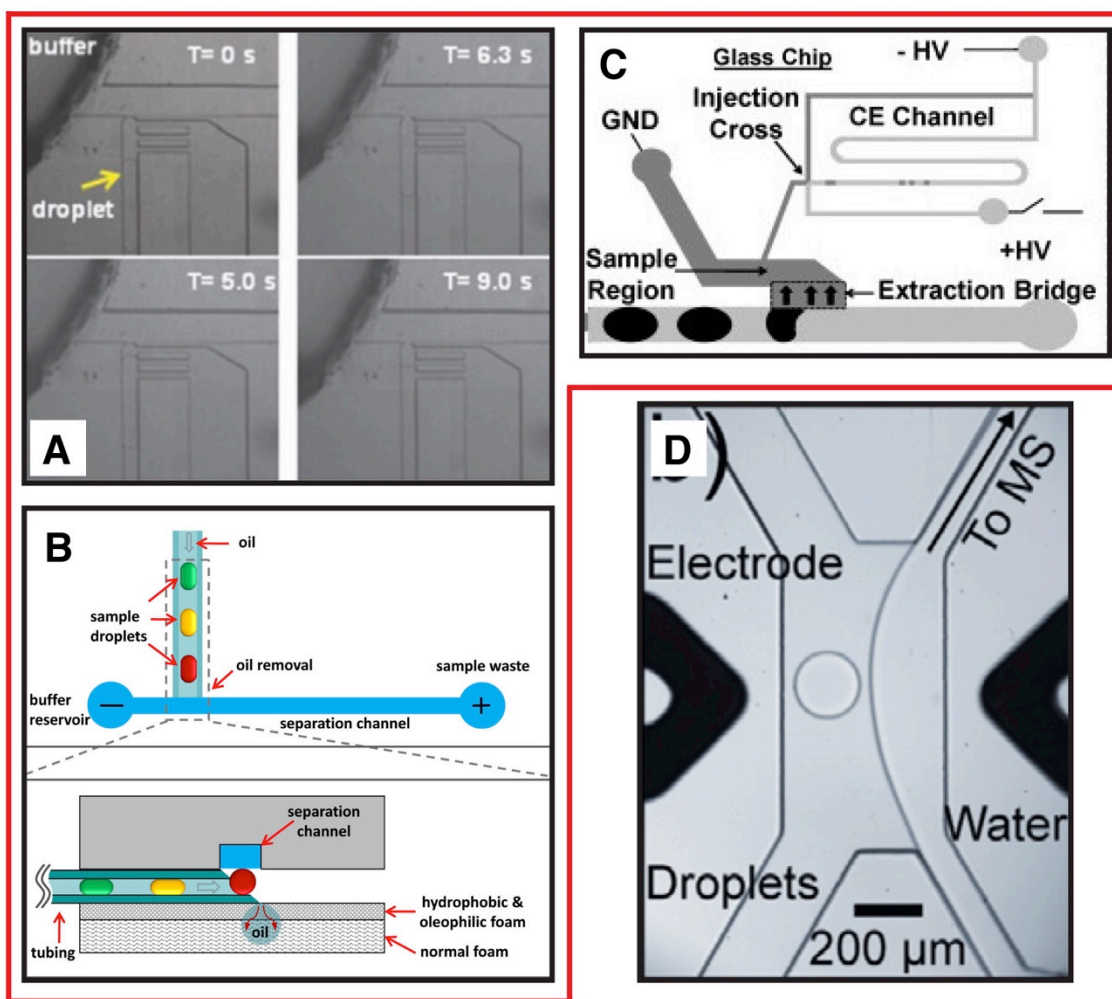
Figure 1-4. Examples of droplet desegmentation strategies for coupling to downstream analysis using either passive (examples in red box) or active strategies. A) Extraction of

droplets using special 'comb' channel geometry composed of thin PDMS pillars. Carrier oil is extracted through the pillars while the aqueous sample merges with the separation channel (top channel in each image).[70] B) Schematic diagram of a device using oleophilic foam/film to remove carrier oil prior to droplets merging with the separation channel. This method was used for analysis of droplets by gel electrophoresis.[71] C) Diagram of a glass device with modified surface chemistry for droplet extraction. The channel containing droplets is made hydrophobic through derivatization with octadecyltrichlorosilane while all other channels remain hydrophilic. Droplets are extracted across a thin 'extraction bridge' prior to analysis by MCE.[79] D) Active droplet extraction utilizing applied electric fields for analysis of droplets by mass spectrometry. Droplets flow parallel to and are merged with an aqueous stream upon entering the external electric field. Carrier phase, which is non-conductive, continues on unaffected.[77] Reproduced with permission from individual publishers.

One group has previously reported droplet-based sample introduction for high-throughput screening by MCE. In their study, droplet samples were introduced into a glass microfluidic device through a hydrophobic patterned channel where they were extracted and analyzed by MCE. They demonstrated analysis of GTPase activity using a 15 second separation (0.07 Hz) and throughput could be improved by simultaneous analysis of three samples within parallel electrophoresis channels.[72] While a significant improvement on other methods and the first true demonstration of HTS by MCE, the low throughput and carryover (7 percent) associated with this implementation limit the methods potential. Additionally, the authors characterized enzyme activity but did not demonstrate screening a chemical library.

Sirtuin Biology

Sirtuins (SIRTs) represent an evolutionarily conserved class of nicotinamide adenine dinucleotide (NAD^+)–dependent deacylases.[80-83] SIRT mediated deacylation reactions consume NAD^+ to generate a deacylated product, 2'-O-acetyl-ADP-ribose and nicotinamide. The sirtuin family is comprised of seven members located throughout the cell in areas such as the nucleus (SIRT1, SIRT2, SIRT6, and SIRT7), the cytoplasm

(SIRT1, and SIRT2), and the mitochondria (SIRT3, SIRT4, and SIRT5) (Figure 1-5).[84] Through modulation of lysine modifications on target proteins, sirtuins regulate many cellular functions, such as transcription, metabolism, and life span.[85-87] Initially identified as NAD^+-dependent deacetylases, only SIRT1 to SIRT3 have robust deacetylase activity while the deacetylase activity of SIRT4 to SIRT7 is reported as very weak or undetectable.[84, 88, 89] However, recent research has revealed a number of novel lysine post-translational modifications – such as acyl,[90, 91] succinyl,[88, 92] glutaryl,[93] malonyl,[94, 95] and crotonyl groups[96, 97] – providing alternate targets for sirtuin activity.
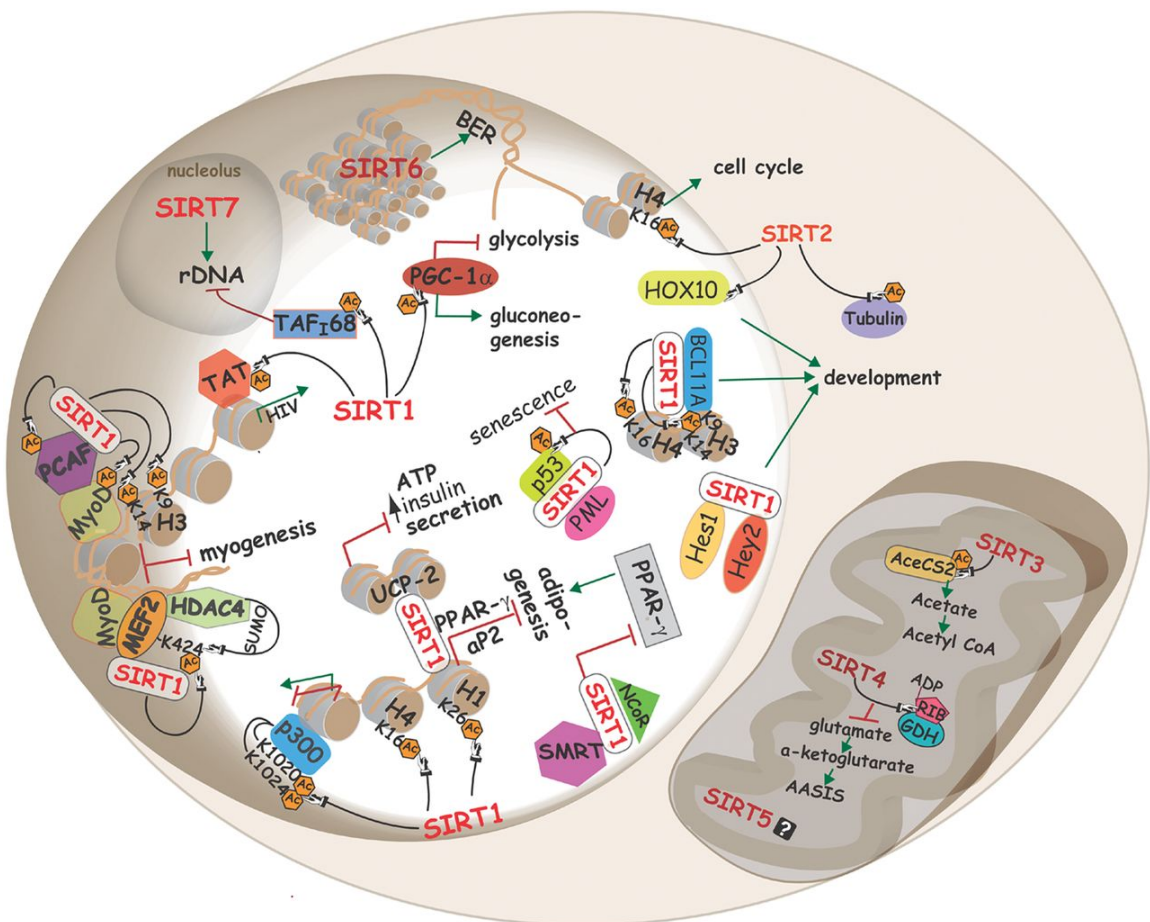
Figure 1-5. Primary cellular localization and function of sirtuins. SIRT1 and SIRT2 are present in the nuclear and cytosolic fractions.[82] SIRT3, SIRT4, and SIRT5 are located in

16

the mitochondria. SIRT6 and SIRT7 are located in the nuclear fraction. For well-studied sirtuins, their targets and affected cellular processes are labeled and suppression (red lines) or activation (green arrows) is noted. A black line connecting a sirtuin to an acetyl group denotes a specific acetyl-lysine target. Reproduced with permission from Portland Press.

One of the family members, SIRT5, readily catalyzes deacylation of negatively charged lysine modifications, such as malonyl, succinyl, and glutaryl moieties.[88, 92-94, 98, 99] Using x-ray crystallography, it was determined that the hydrophobic residues found in the substrate pocket of other sirtuins had been replaced by positively charged residues, such as arginine. This change may account for the unusual substrate preference of SIRT5.[88] Although no striking biological phenotype has been reported for SIRT5 KO mice,[100, 101] extensive hypersuccinylation and hypermalonylation is observed in SIRT5 KO cell lines suggesting that SIRT5 may be the primary regulator of negatively charged lysine modifications within the cell.[94, 98, 99]

Through removal of lysine modifications, SIRT5 regulates several metabolic enzymes (Figure 1-6).[102] Carbamoyl phosphate synthase 1 (CPS1), which catalyzes the first step of the urea cycle, has increased activity when desuccinylated or deacetylated.[100, 103] 3-hydroxy-3-methylglutaryl-CoA synthase 2 (HMGCS2), which is the rate-limiting enzyme in ketone body synthesis, is hypersuccinylated in the absence of SIRT5, and shows increased activity when desuccinylated by SIRT5.[99] Through succinylation of pyruvate dehydrogenase complex (PDC) and succinate dehydrogenase (SDH), SIRT5 suppresses cellular respiration.[98] And, demalonylation of glyceraldehyde 3-phosphate dehydrogenase (GAPDH) and aldolase B, SIRT5 regulates glycolosis and gluconeogenesis.[95]
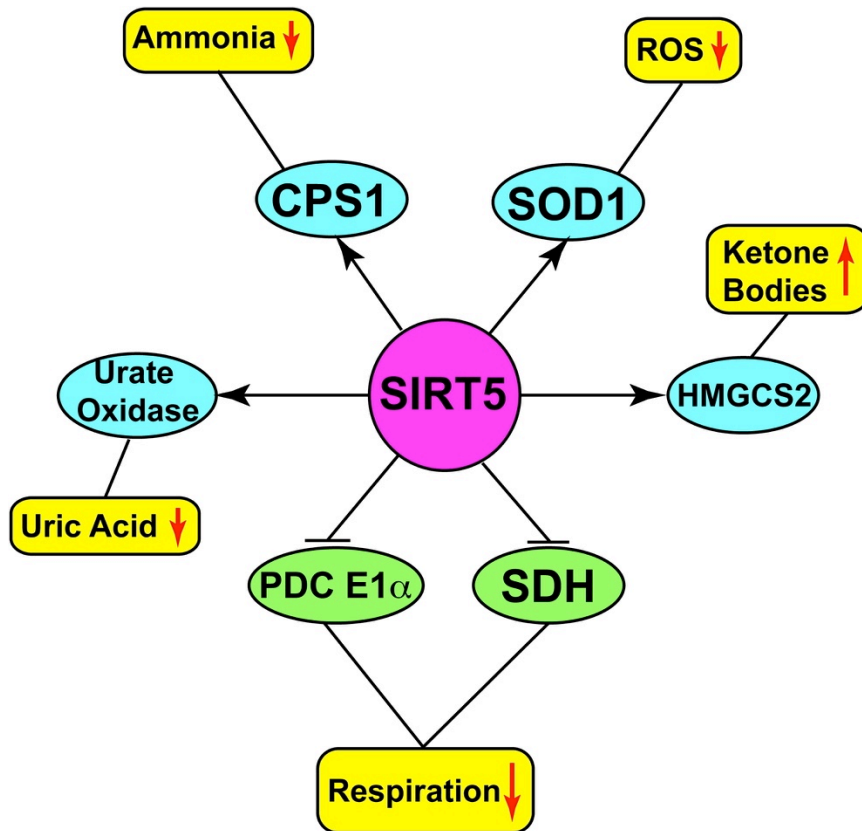
Figure 1-6. Protein targets regulated by SIRT5 *in vivo*. Through removal of acetyl, succinyl, glutaryl, or malonyl groups from target lysines, SIRT5 activates (blue ellipse) or inhibits (green ellipse) target proteins. This affects downstream targets (yellow boxes) by increasing or decreasing target levels or activity (denoted by upward or downward facing arrows).[102] Reproduced with permissions from Mary Ann Liebert, Inc.

Due to regulation of metabolic pathways important to cancer progression, SIRT5 may have an oncogenic role in specific cancers. SIRT5 activates superoxide dismutase (SOD1) *in vivo*, which plays a role in managing reactive oxygen species (ROS) within the cell.[104] SOD1 overexpression or upregulation in lung[105] and breast cancer,[106] respectively, may have a role in tumorogenesis. Because SIRT5 activates SOD1, these results suggest SIRT5 may be involved in tumor growth. In addition to these direct effects, SIRT5 is over-expressed in non-small cell lung cancer (NSCLC) and SIRT5 KD suppressed tumor formation in NSCLC.[107]

These diverse functions demonstrate the need for pharmacological modulators of SIRT5 activity. Identification of SIRT5 modulators has been limited by a lack of known *in vivo* targets; however, recent identification of the above SIRT5 targets has increased efforts in this area. Adding to the complexity is the structural similarity between sirtuins. Many modulators are non-specific by targeting the conserved NAD^+ binding pocket. To date, suramin has been most investigated as a SIRT5 inhibitor. Even though suramin possesses low micromolar potency against SIRT5,[89] its activity against SIRT1 and SIRT2 limits its efficacy *in vivo*. Several groups have reported synthetic peptide inhibitors with micromolar potency against SIRT5.[108, 109] In light of the limited number SIRT5 modulators identified to date, discovery of potent and specific modulators is necessary for basic biological and clinical applications.

Within the field of sirtuin biology, much of the drug discovery has been focused on SIRT1 using optical detection methods, such as the commercially available *Fluor-de-Lys™* assay based around a two-step reaction (Figure 1-7).[110-115] This assay utilizes a peptide-based substrate coupled to a 7-amino-4-methylcoumarin (AMC) tag via an amide bond adjacent to the terminal lysine. In the first step, SIRT1 catalyzed deacylation generates a substrate for trypsin. In the second step, trypsin releases the AMC tag through cleavage of the amide bond resulting in an increase in fluorescent signal equivalent to the sirtuin activity. These tend to be poor trypsin substrates and require high trypsin concentrations for efficient cleavage. In high-throughput settings, dispensing high viscosity solutions (i.e. concentrated trypsin solutions) can lead to large errors in sample preparation. However, the high assay sensitivity and availability of substrates for SIRT1, SIRT2, SIRT3, and SIRT5 make these assays desirable for many researchers.
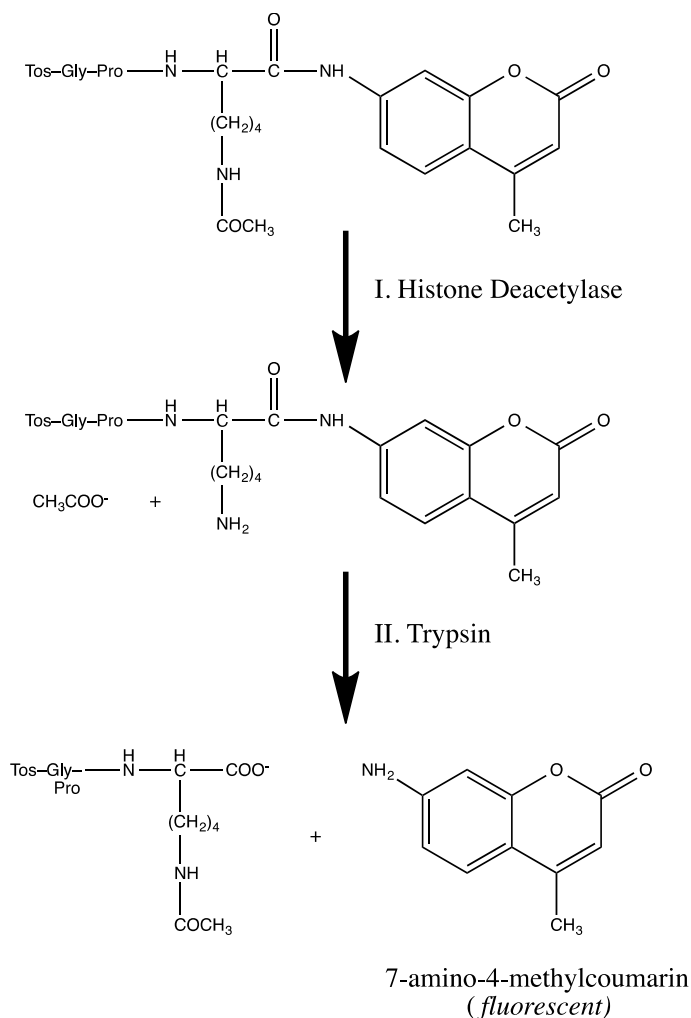
Figure 1-7. Schematic of the commercially available *Fluor-de-Lys™* assay for measuring sirtuin activity. In step 1, a sirtuin, or histone deacetylase, removes a lysine modification (i.e. acetyl group) from a peptide substrate conjugated to an AMC fluorophore generating a substrate for trypsin. In step 2, trypsin cleaves the amide bond linking AMC to the peptide releasing the fluorophore and generating and fluorescence signal.[110] Reproduced with permission from Elsevier.

In a well-known study, this assay was used to identify a number of potent SIRT1 activators based around resveratrol, a polyphenol. These compounds increased SIRT1 deacetylase activity 8-fold *in vitro* and improved yeast lifespan by 70 percent.[112] Although corroborated by *in vivo* studies in invertebrates, the SIRT1 activation could not be reproduced when using other peptide substrates.[111, 116, 117] Further investigations

revealed that SIRT1 activation was caused by interactions between the bulky AMC tag and resveratrol that enhanced SIRT1 binding affinity.

To avoid this ambiguity in screens for SIRT5 modulators, alternative SIRT5 screening assays have been developed. Among the optical detection assays, monitoring nicotinamide depletion through coupled enzyme reactions is possible and is compatible with any peptide or protein substrate.[111, 116-118] Using proteolytic cleavage by trypsin, assays based on fluorescence resonance energy transfer (FRET)[119] or internally quenched substrates have been developed.[120] However, these peptides require significant modification from natural substrate sequences, which could lead to artificial results during screening. Outside of optical assays, several assays utilizing LC-MS for analysis have been developed around natural peptides.[88, 109, 121]

Dissertation Overview

The research in this dissertation aims to continue development of electrophoresis-based high-throughput screening to develop a novel droplet-MCE platform for routine HTS. It addresses the limitations of previous platforms by achieving low sample carryover, high efficiency separations, and moderate sample throughput into a reliable analysis platform.

In Chapter 2, a novel PDMS-glass hybrid microfluidic device for analysis of droplet samples by MCE is developed. The design couples aspects of two previous group efforts into a design capable of robust droplet extraction with minimal carryover. To demonstrate the platforms utility for HTS, an electrophoretic mobility shift assay for protein kinase A (PKA) was developed around the known substrate Kemptide. A library

containing 140 test compounds was screened in 16 minutes using a 1 second MCE separation. This effort demonstrated a 2-fold improvement in sample throughput over previous MCE screening methods.

In Chapter 3, electrophoresis-based HTS as developed in Chapter 2 was applied to a novel biological target – SIRT5. Due to its implication in metabolic pathways and potential impact on cancer biology, identification of SIRT5 inhibitors is vitally important. However, existing assays generally rely on fluorescence assays known to product false positive results. Therefore, we designed a novel SIRT5 substrate based on succinate dehydrogenase that allowed ultrafast MCE analysis. The assay robustness was demonstrated using a meso-scale screen against a library containing 1280 test compounds and 128 controls. The screen was completed within 46 minutes (0.5 samples per second) and generated over 11,000 electropherograms (8 MCE injections per sample) with an excellent assay Z-factor of 0.8. Several novel SIRT5 inhibitors were identified and potency was determined using dose-response analysis. This work demonstrated a 3-fold improvement in sample throughput over the design in Chapter 2. By optimizing separation conditions, separation time was reduced to 250 ms, while efficiency was increased 2-fold. Compared to previous CE-based sirtuin screens, throughput was improved 25-fold.

Chapter 4 demonstrates the true potential of droplet-based samples for high-throughput screening performing reaction and analysis within droplet samples. In previous methods, over 99 percent of sample volume was wasted, which leads to significant extra costs and time. A microfluidic reagent addition device was developed based on work done by previous members of our group and previously reported designs.

This design achieved a simple, easy to manufacture device cable of adding sub-nanoliter reagent volumes to nanoliter volume droplets. Carryover was less than 5 percent from sample to sample and the device was able to add reagents to over 9,000 droplets continuously. Reagents could be added to droplets at up to 10 Hz reliably allowing for rapid sample preparation. The utility for HTS was demonstrated with a screen of 1280 compounds against SIRT5, which used 1,000-fold less reagent than the screen reported in Chapter 3.

Chapter 5 discusses several future directions for droplet-MCE high-throughput analysis to more broadly apply this platform. These range from coupling droplet samples to alternative separation modes, such as gel electrophoresis and microchip electrochromatography, to development of a continuous droplet generation method. Additionally, preliminary work from alternate screening targets, such as protein-protein interactions, is reported. This method, which could rely on a peristaltic pump, would allow continuous generation and analysis of droplet samples by MCE, MS, or optical assays.

CHAPTER 2: SUB-SECOND ELECTROPHORETIC SEPARATIONS FROM DROPLET SAMPLES FOR SCREENING OF ENZYME MODULATORS

Introduction

Modern high-throughput screening (HTS) technology allows for 10^4 to 10^5 automated assays to be completed in one day. HTS has emerged as a powerful tool for many applications including drug, catalyst, and chemical probe discovery. The dominant form of HTS is based on assays performed in multi-well plates (MWP) with liquid handling and plate manipulation performed by robots and detection by optical plate readers. Although this approach has been successful, it has limitations. A fluorescent or other optical indicator must be coupled to or engineered into the biochemical reaction of interest. This requirement can increase development time, reagent costs, and potential for false signals wherein test compounds affect the indicator rather than the actual reaction. Further, in such schemes only one analyte is detected per reaction and interference from buffer components or test compounds is possible.

Analysis of reaction mixtures by microchip electrophoresis (MCE) can avoid these limitations by separating substrates, products, and interfering species to eliminate the need of having a selective optical change upon reaction. Rapid separations are possible; however, reloading chips with fresh sample is a bottleneck for HTS. A commercial instrument overcomes these problems by "sipping" sample from wells and

pulling sample by vacuum into the separation channel.[25] This powerful system allows continuous operation and a reliable interface to MWP; however, it does not reach the full potential of MCE because band broadening induced by flow through the separation channel gives reduced resolution requiring longer separation times.

An alternative for screening many distinct samples by MCE is to deliver samples to the chip as droplets or segmented flow.[72] In such a method, aqueous samples encapsulated in immiscible oil are pumped into the chip where the aqueous portion is extracted for injection onto the MCE channel. A significant advantage of this approach is that it is also compatible with the emerging trend of miniaturization by performing reactions at droplet scale (pL to nL volume) rather than MWP scale (1-30 μL). Droplet strategies have been used for several novel screens.[38, 60, 62, 64, 122-124]

Although coupling droplets to MCE is an attractive prospect for HTS, most previous methods of interfacing have been developed for other applications (e.g., for two-dimensional separations[70, 125] or coupling to a sampling probe for chemical monitoring[58, 74, 126]) and have limited proven utility for screening. Extraction of droplets has relied on modified surface chemistry,[72, 74, 75] applied external fields,[77] special channel geometries,[67, 70] or the use of oleophilic films[71, 73] to remove carrier oil. In these systems the extraction and injection processes are coupled so that compromises between droplet size, injection volume, and separation speed must be made. For example, an increase in droplet flowrate will reduce separation time and separation efficiency as the time between sample droplets decreases. Likewise, injection volume is directly correlated with droplet volume, which can lead to larger injections than are typical in MCE causing a reduction in separation efficiency. An exception was a method that allowed extraction followed by

electrokinetic gated injection.[75] This approach to droplet-MCE interface yielded high efficiency (223,000 plates in 50 s separation); however, it was not shown to be compatible with screening, which requires analysis of many distinct samples and long-term unattended operation of several hundred samples. Further, this method required a complex fabrication procedure involving surface chemistry patterning.

Here we report a simplified approach to droplet-MCE interface. The method uses a minor modification of a standard MCE chip design. This method allows at least 700 MCE injections from droplet samples and sub-second separations suitable for screening. We also demonstrate a method to track samples during a screen. The system was tested using a small scale screen of protein kinase A (PKA) modulators but in principle can be applied to any assays resulting in a change in analyte charge or size, such as peptide cleavage, dephosphorylation, and deacetylation.

Materials and Methods

Chemicals and Materials. All reagents were purchased from Sigma Aldrich (St. Louis, MO) with the following exceptions. 5-carboxyfluorescein (FAM)-labeled Kemptide was purchased from AnaSpec (Fremont, CA) and the catalytic subunit of cAMP-dependent protein kinase A was purchased from New England Biolabs (Ipswich, MA). The epigenetics compound library was purchased from Cayman Chemical (Ann Arbor, MI) and the kinase inhibitor library was obtained from the Center for Chemical Genomics at University of Michigan.

PDMS Chip Fabrication. Polydimethylsiloxane (PDMS) tees were fabricated using a pour over method to align droplet tubing and microfluidic devices during operation. Briefly, a 360 μm o.d. capillary was taped in the bottom of a petri dish. A 100

o.d. capillary was glued into a 150 μm i.d x 360 o.d. sheath capillary such that ~3 mm of 100 o.d. capillary was exposed. Two of these sheathed capillaries were taped on opposite sides of the 360 μm o.d. capillary with a 2-3 mm gap between them. PDMS was poured over the mold and cured at 75 °C for 15 min. After curing the mold was flipped and PDMS was poured on the other side and cured for an additional 20 min at 75 °C. After curing, all capillaries were removed and the device was cut to size using a razor blade.

Glass Chip Fabrication. Glass chips were fabricated using photolithography and wet-etching by hydrofluoric acid (HF).[127-129] Briefly, one slide is etched to 90 μm for the capillary insertion channel and to 50 μm for the sample channel. A second slide is etched to 90 μm for the capillary insertion channel and 5 μm for all separation channels. During etching of deep channels, other features were covered with HF resistant tape (Semiconductor Equipment Corporation, Moorpark, CA). After etching, access holes were drilled with a 500 μm drill bit (Kyocera Tycom, Costa Mesa, CA). Glass slides were washed for 20 min in piranha solution (sulfuric acid:hydrogen peroxide, 4:1) and for 40 min in heated RCA solution (ammonium hydroxide:hydrogen peroxide:water, 1:1:5). Slides were rinsed with water, aligned under a microscope, and annealed at 610 °C for 8 h. Reservoirs and access ports (IDEX Heath and Science, Oak Harbor, WA) were attached at the access holes and a 40 μm i.d. x 150 μm o.d. x 2.5 mm long extraction capillary was waxed in place in the capillary insertion channel. (See Appendix A for additional modifications to glass microfabrication necessary to avoid pinholes and anisotropic etching.)

Microfluidic Chip Operation. All reservoirs and channels on the glass chip were primed with separation buffer (10 mM sodium tetraborate, pH 10, 0.9 mM

hydroxypropyl-β-cyclodextran) to remove air bubbles. Voltage for electrophoresis was applied using a CZE1000R power supply (Spellman, Hauppague, NY) and a high-voltage relay (Kilovac, Santa Barbara, CA) was used to control electrokinetic-gated injection.[130, 131] Detection was accomplished using an in-house confocal laser induced fluorescence (LIF) detector. Briefly, the 488 nm line from a solid-state laser (CrystaLaser, Reno, NV) was directed through a 488 ± 10 nm band pass filter and a 10X objective lens. Emission was filtered through a 520 ± 10 nm band pass filter and detected by a photomultiplier tube (R1477, Hamamatsu, Bridgewater, NJ). Current from the PMT was amplified by a current preamplifier (Stanford Research Systems, Sunnyvale, CA) and monitored using an in-house LabVIEW program (National Instruments, Austin, TX). Data analysis was done using Cutter 7.0,[132] Excel 2011 (Microsoft, Redmond, WA), and Igor Pro 6.32 (Wavemetrics, Inc., Lake Oswego, OR).

Droplet Generation from MWP. Droplets, segmented by perfluorinated oil (100:1, perfluorodecalin (PFD): perfluorooctanol (PFO)), were generated from a multiwell plate using a method previously described. Droplet samples were pulled into a 150 μm i.d. x 360 μm o.d. HPFA tube (IDEX Health and Science, Oak Harbor, WA) using a syringe connected to a PHD 200 syringe pump (Harvard Apparatus, Holliston TX) operating in refilling mode. After priming the syringe and tubing with 100:1 PFD:PFO, droplets were generated using a computer-controlled XYZ-positioner to move the tubing from well to well in a defined pattern. Samples were covered with carrier oil to prevent sample evaporation and aspiration of air into tubing.[37, 38]

Protein Kinase A Modulator Screen and Droplet Analysis. Each sample in the screen was prepared in 20 μL with final concentrations of 50 mM Tris, pH 7.5; 10 mM

MgCl$_2$; 200 µM ATP; 15 µM FAM-Kemptide; and, 3.75 nM protein kinase A. During screening experiments, test compounds from the kinase inhibitor library were deposited using a Caliper Sciclone (PerkinElmer, Waltham, MA) into a 384-well plate (0.1 to 12.5 µM final concentration). For the epigenetics compound library, compounds were pipetted manually into a 384-well plate (5 µM final concentration). Control samples contained dimethyl sulfoxide (DMSO) at equal volume to test compounds. Negative controls contained no inhibitor (mimicking no inhibition), and positive controls contained no enzyme (mimicking 100 percent inhibition). Reactions were incubated at room temperature for 30 min and quenched with 80 µL of 15 mM ethylenediaminetetraacetic acid (EDTA) and placed on ice. Immediately prior to droplet generation, 90 µL of each sample was transferred to a modified 384-well plate designed to allow samples to be covered by carrier oil. To extract droplets, a 50 µL syringe filled with water was attached to a 40 µm i.d. x 150 µm o.d. capillary and connected to the PDMS tee after the extraction region and the PDMS chip was primed with water. Next, tubing containing sample droplets was inserted until flush with the extraction capillary in the glass chip and connected to a 100 µL syringe on a syringe pump. Droplets were pumped into the PDMS chip at 360 nL/min and injections were made every 1 s.

Results and Discussion

Droplet extraction from segmented flow. Our strategy for high throughput electrophoresis is to introduce a series of samples to the microchip as segmented flow. A primary challenge of achieving rapid MCE analysis from segmented flow is separation of the oil phase from sample prior to MCE analysis. To simplify the process of droplet extraction, we used the native properties of glass (hydrophilic) and PDMS (hydrophobic)

29

to extract droplets through a hybrid device (Figure 2-1). An advantage of this approach is that we take advantage of the native surface chemistry of these materials to achieve extraction, this eliminating the need for surface patterning. A hybrid device has the added benefit of decoupling the extraction and analysis stages for better performance. Also, it has the practical advantage that a new extraction or analysis chip can be substituted if it stops working without the need to fabricate a new device.
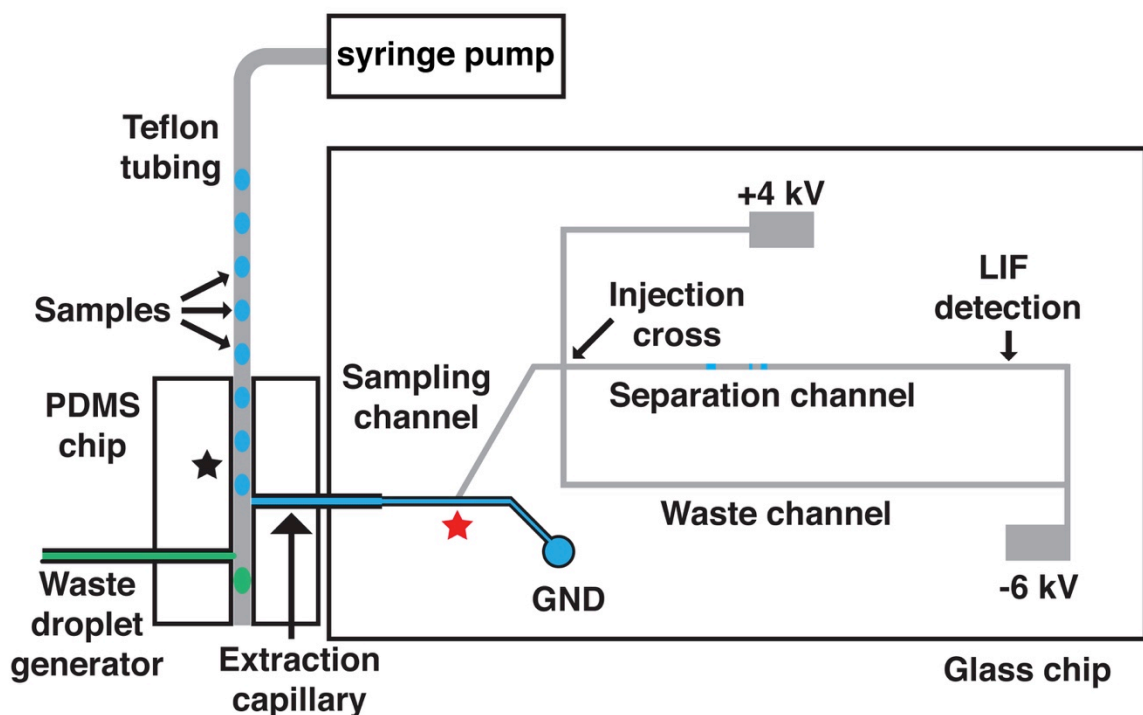
Figure 2-1. Schematic of PDMS-glass hybrid microfluidic device for analysis of segmented flow samples. Aqueous droplets (blue colored) are extracted by the extraction capillary and sampled by EOF in the sampling channel towards the injection cross. During injection, the positive high-voltage power supply is floated to allow injection of a discrete sample plug into the separation channel. The positive high-voltage is applied again during separation and excess sample is gated to the waste channel. To assist extraction waste droplets (green colored) are generated after the extraction point to provide a slight backpressure for extraction.

In this device, a length of Teflon tubing containing sample droplets is positioned orthogonal to the inlet of a fused silica extraction capillary that is interfaced to the glass

MCE chip using a tee molded from PDMS (Figure 2-1). The fused silica extraction capillary also acts as a conduit to the glass MCE chip. As droplets exit the Teflon tubing, aqueous samples are extracted into the hydrophilic fused silica extraction capillary while the oil phase continues towards the outlet of the hydrophobic PDMS device. The extracted sample droplet fills the extraction capillary and sampling channel (Figure 2-1) where it can be injected onto the MCE channel using an electrokinetic flow gate.[130, 131] Subsequent samples wash the extraction capillary and sampling channel out for serial injections.

Although the inherent surface chemistry of the extraction capillary and PDMS tee will favor droplet extraction and oil phase flow past the extraction point, it is also necessary to use proper capillary and channel dimensions so that capillary force and back pressure are balanced to favor droplet but not oil flow into the extraction capillary. In other words, with high flow rates, wide bore extraction capillaries or narrow PDMS channels, oil can be forced into the extraction capillary. In the opposite case, aqueous samples will not be fully extracted. For the flow rates and chip dimensions used here, a 40 µm i.d. fused silica capillary generated good extraction (i.e., the entire aqueous droplet) with no oil phase entering the extraction capillary. We visually observed that droplet extraction was more reliable by elevating pressure slightly at the outlet of the PDMS tee. This pressure was created by a pumping water at 150 nL/min into an inlet positioned downstream of the extraction point (Figure 2-1, waste droplet generator).

The chip was also designed to minimize carryover between samples. To reduce carryover, dead volume from the extraction point on the PDMS device to the sampling point, on the glass device was minimized through the use of narrow bore capillaries and

short capillary lengths (3.3 nL). With this small volume, we anticipated that ~10 nL of sample would be needed to washout the capillary and prevent carryover.

To evaluate the extraction efficiency and sample carryover in the extraction channel, we monitored fluorescence as alternating pairs of 8 nL droplets containing fluorescein at high (6 µM) and low (2 µM) concentration were pumped through the system. Droplets are detected as square-topped pulses within the Teflon tube (Figure 2-2) reflecting signal from fluorescence within the droplet and no signal for the oil. After extraction the droplets fill the extraction capillary and become continuous phase without pulses between droplets of the same concentration (red trace, Figure 2-2A). In the transition from high to low concentration, the signal decreases and then stabilizes. The timing of the transition suggests that the sample is 80% washed out by the first droplet and 98% washed out by the time the second droplet is extracted. In the transition from low to high concentration, the signal stabilizes more quickly. These results show that carryover should be minimized using 2 droplets. The exact volumes required may depend on the sample type being used, e.g. if surface adsorption is greater more rinses may be required.

If the back pressure was not provided by the extra flow the transitions were longer and not as reliable as shown by the increase in carryover in the red trace in Figure 2-2B starting after 60 s. This result coincides with incomplete extractions and sample buildup at the capillary inlet. By using the waste droplet to increase pressure in the extraction zone, sampling buildup was greatly reduced and carryover between samples was less than 2% (Figure 2-2A). At least 500 droplets, the most tested, could be extracted reliably with this approach.
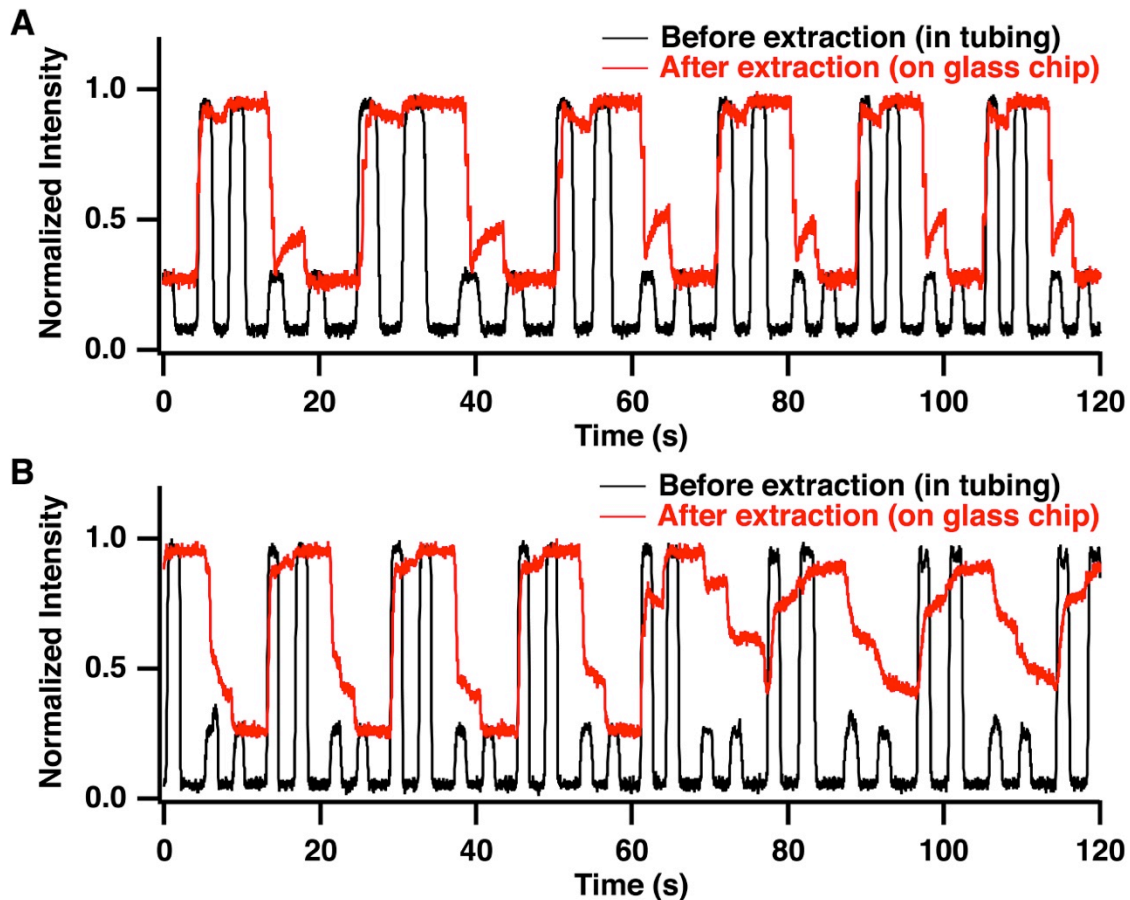
Figure 2-2. Comparison of extraction of droplet stream without (**A**) and with (**B**) waste channel droplets shows the effect of added backpressure on extraction efficiency. When waste droplets are present intensity of droplets before extraction (black trace) is nearly identical to intensity of sample after extraction (red trace) and transitions from high to low intensity occur rapidly suggesting that each droplet rapidly rinses out the previously extracted droplet from the glass chip. Without waste droplets, sample intensity is not stable over time on the MCE chip as sample droplets mix. Detection point for droplets before extraction (black star) and after extraction (red star) are marked on the schematic in Figure 1.

MCE injection from droplets. After extraction, aqueous samples fill the sample channel, which acts as the sample reservoir in a cross-style injector in MCE.[130, 131] In this way, the hybrid chip acts as a means to rapidly introduce new samples to a microfluidic device while maintaining injection geometry known to have high performance.[75, 130, 131, 133] To make an injection, sample is directed towards the injection cross by electroosmotic

flow (EOF) using applied electric fields. During separation, this sample stream is gated towards a waste reservoir on chip by a cross flow, which also provides fresh separation buffer to the electrophoresis channel. During injection, the gating flow is shut off by a high-voltage relay to allow a small plug of sample to be injected into the separation channel for analysis. Importantly, unlike many other designs used for droplet MCE, the volume and shape of the plug that is injected is controlled independently of the extraction process enabling higher efficiency for a given separation time.

Using this injection method, screening reaction samples containing substrate, product, and rhodamine were separated with good efficiency. For example, using a 10 mM sodium tetraborate buffer at pH 10 and an electric field of 2000 V/cm, separation efficiency of 16,000 plates for a 1 s separation in 0.5 cm was routinely achieved. By making a discrete injection from a larger sample droplet, injection volume is not controlled by droplet volume and multiple injections can be made from each sample droplet. Further, the separation time is not limited by droplet spacing, as is the case when an injection is made from each droplet[72, 74] or whole droplet injection is used.[70] We found that these differences were useful for HTS. Using a gated-injection scheme, coupling MCE to 2D separations or other sampling probes for chemical sensing by segmented flow should also be possible.

Mobility shift assay of enzymatic reactions. Phosphorylation of kemptide by PKA was used as a test assay for this system (Figure 2-3A). Injection of the reaction mixture results in two peaks in the electropherogram due to the unphosphorylated substrate and phosphorylated product, which migrates slower due to the addition of a negative charge through the phosphate group (Figure 2-3B). By injecting substrate alone,

34

only the first peak is present and both substrate and product migration times were verified.
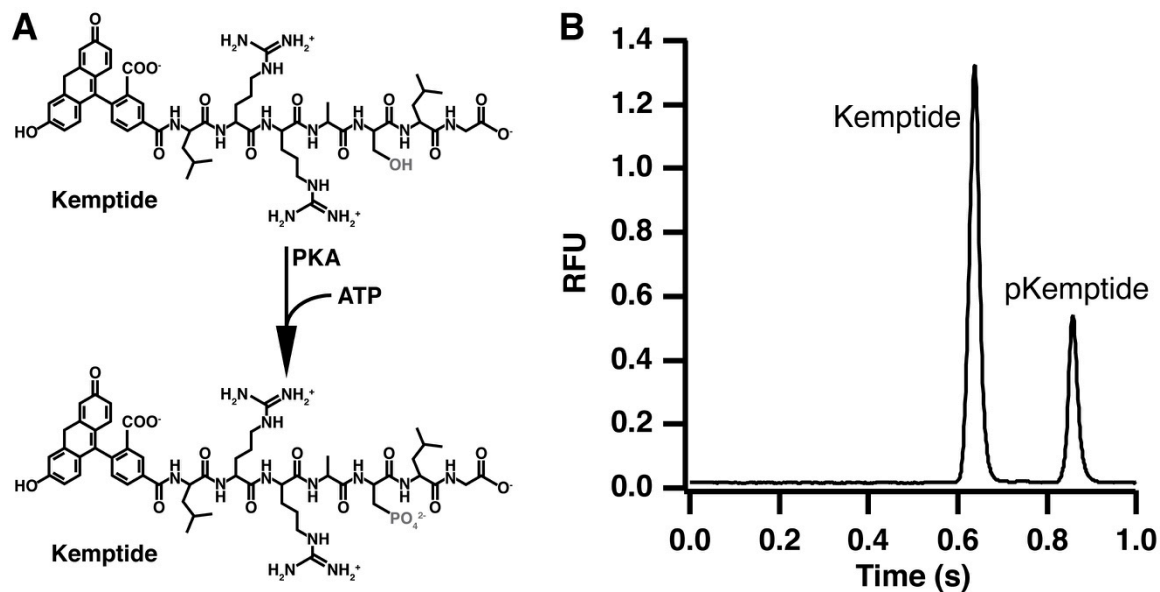
Figure 2-3. Protein kinase A catalyzed phosphorylation of kemptide (**A**) and resulting electropherogram (**B**) for the separation of the reaction mixture. Product and substrate were separated in 0.5 cm using an applied field of 2000 V/cm and a 30 ms injection.

Due to the large number of samples generated in HTS a rapid MCE separation is required. The change in charge on kemptide due to phosphorylation allowed for easy separation of the substrate and product peak. A separation in < 1 s was achieved using a high electric field (2000 V/cm) and a short separation length (0.5 cm) without sacrificing separation resolution. This separation was fast enough to allow at least three injections per droplet that entered the capillary (Figure 2-4A). Indeed, the effect of droplet clearing can be observed in the relative peak heights for each electropherogram. The first three injections shown in the trace in Figure 2-4 correspond to the second droplet for a sample and the peak heights are stable. The next four traces correspond to a new sample that has been extracted. Fluctuation in peak height for rhodamine, substrate, and product is

observed as the droplet washes out the reservoir and reaches a stable signal, similar to the continuous measurements depicted in Figure 2-2A. The last three traces correspond to the second droplet being extracted and entering the sample reservoir. By this time, the peak heights have once again stabilized for all traces. Thus, these results illustrate that use of two droplets per sample, the first to rinse the small reservoir and the second to provide a stable signal, allows for analysis of discrete samples in series. In principle, the number of injections per droplet can be varied by using different size droplets and flow rates. Likewise, the amount of rinse required could be decreased by using even lower dead volumes. Obtaining multiple injections per droplet can be valuable in achieving reliable results at the expense of throughput.

At this high of a separation speed, reproducibility was still good. For example, we performed over 700 injections in ~12 min with a migration time RSD of ~2%. Reaction yield, calculated as P/(P+S), where P and S are the product and substrate peak area respectively, had an RSD of 7% (n = 8) for negative control samples spread throughput the sample set. For a series of injections from a single sample, the RSD was generally less than 5% (n=3). As observed in the substrate peak area trace in Figure 2-4B, droplet extraction causes a slight increase in pressure on the glass device leading to an increase in substrate peak area for that injection. Using reaction yield, instead of raw peak area, for analysis combined with averaging three injections per sample mitigates this effect.

Indexing droplet data using a fluorescent dye. When analyzing a series of samples reformatted from a MWP to droplet streams it can be difficult to determine which electropherograms belong to each sample. This is especially true for the passive extraction/injection system used here. Thus, even though droplets are introduced to the

chip at a constant flow rate and injections are performed at a constant rate; we found that the exact number of injections per sample (formatted as 2 droplets of 8 nL each) can vary from 6 to 8. We attribute this primarily to slight variations in sample size, sample flow rate, and the timing of injection relative to the droplet extraction. The variability in injection number per droplet means that it is necessary to mark each droplet to register an electropherogram with test analyte or sample. Figure 2-4B illustrates the peak area for a series of electropherograms from assay samples. With the exception of a positive control, which has a low product peak area, determining which data corresponds to each sample is nearly impossible. To avoid this problem a marker compound, rhodamine 110, was added to every other sample to provide data indexing. During data analysis, every other sample (corresponding to a train of approximately 6 injections) will have a rhodamine peak in the electropherogram as can be observed in Figure 2-4A. Using changes in rhodamine intensity as a guide, the start and end point for each sample can be quickly identified across all electropherograms (black trace, Figure 2-4B). For example, from 20-100 seconds 10 samples, each containing a different test compound, are analyzed, but substrate and product peak areas remain stable because none of the compounds inhibit PKA. However, utilizing the changes in rhodamine peak area, the data can be deconvoluted to reveal each individual sample.

Droplet-based screen of protein kinase A modulators. To test our novel droplet-MCE method, we screened two small molecule libraries against PKA for inhibitory activity. The kinase inhibitor library contained 60 test compounds with known activity at various kinases and the epigenetics library contained 80 test compounds that are known to act at proteins involved in histone modification and not necessarily kinases.

A total of 168 samples were analyzed for the primary screen including positive and negative controls. Samples were prepared and reacted as outlined in the experimental section and two droplets were generated for each sample. Samples were analyzed in batches of 96 for a total of ~200 droplets per analysis. Analysis of each batch required approximately 12 min. By generating the next set of samples during analysis, near continuous analysis by MCE is possible achieving sample throughput of 0.16 samples/s.
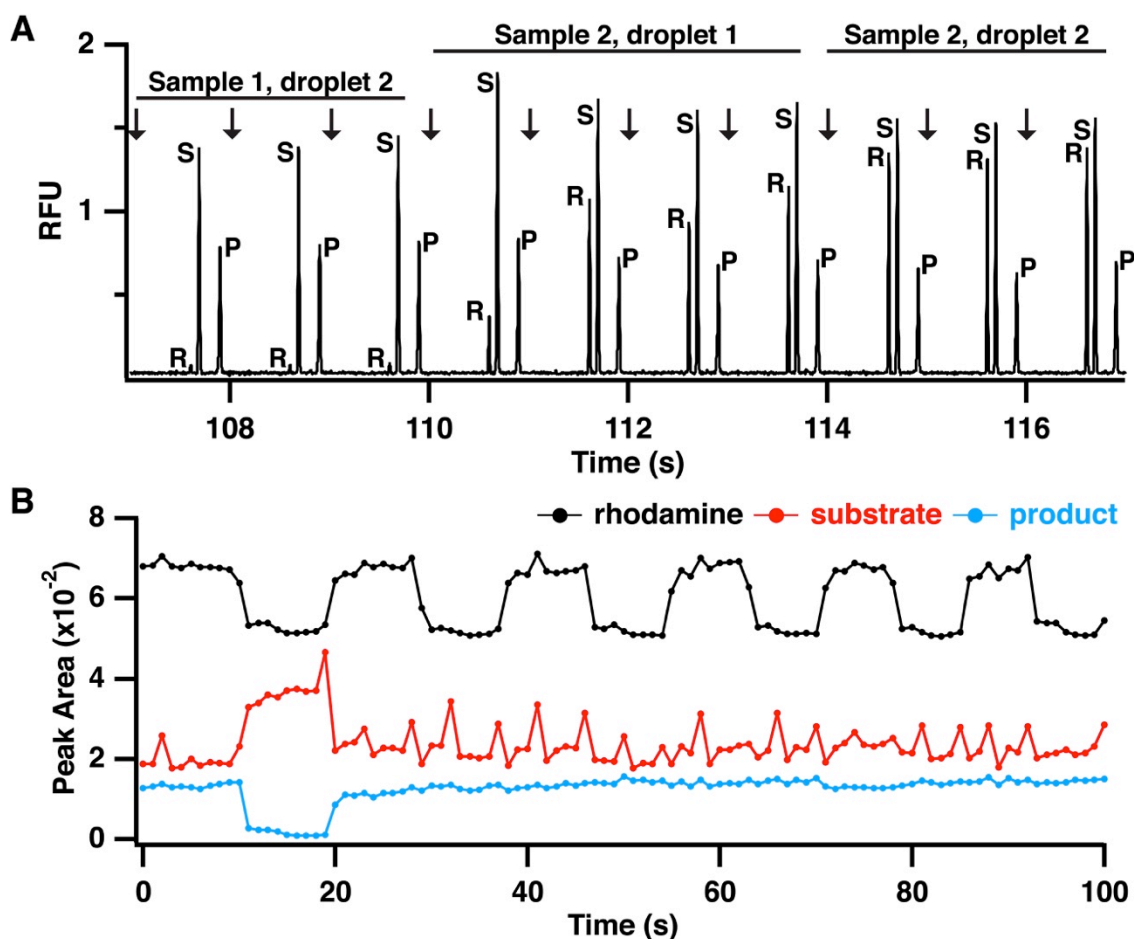
Figure 2-4. Electropherograms and raw peak area data demonstrating sample clearing and indexing for screening by MCE. (**A**) Electropherograms showing injection and separation of rhodamine (R), substrate (S), and product (P) and transition from a sample without rhodamine to a sample with rhodamine demonstrating complete sample clearing by two droplets. (**B**) Extracted peak areas for rhodamine (black trace), substrate (red trace), and product (blue trace) for analysis of 12 samples – two controls and ten test

compounds. Changes in rhodamine peak height were used to determine start and end points for each compound to calculate reaction yield.

Reaction yields were calculated for each sample and normalized to the average positive control reaction yield (Figure 2-5). An inhibition threshold was set at 80%, which corresponds to three standard deviations below the normalized positive control yield across all experiments (n = 40). Any compounds with reaction yields below this threshold were identified as inhibitors of PKA with lower reaction yields denoting stronger inhibitors. In total, 25 test compounds (7 from the epigentics library and 18 from the kinase library) were identified as potential hits during the primary screen and all of these compounds showed a dose-dependent inhibition of protein kinase A during follow up screening experiments. Two false negatives were identified during the screen. One compound, H-89 – showed no inhibition at 12.5 μM, but was active at three lower concentrations. The second compound, piceattanol, was present in both compound libraries but was only active in the kinase library. However, a dose-dependent response was observed suggesting this is a true hit compound and was likely degraded in the epigentics compound library. Overall the assays had a high Z'-factor of 0.8 making identification of both strong and weak inhibitors possible.

Follow up dose-response curves for H-89 and ellagic acid (Figure 2-6), two known protein kinase A inhibitors, showed good agreement with accepted IC_{50} values. For H-89, the experimental IC_{50} value was 89 ± 1 nM and the IC_{50} value for ellagic acid was 1.00 ± 0.01 μM. Previous results using filter based assays with $[\gamma^{-32}P]ATP$ were 135 nM for H-89,[134] and 3.5 μM for ellagic.[135]
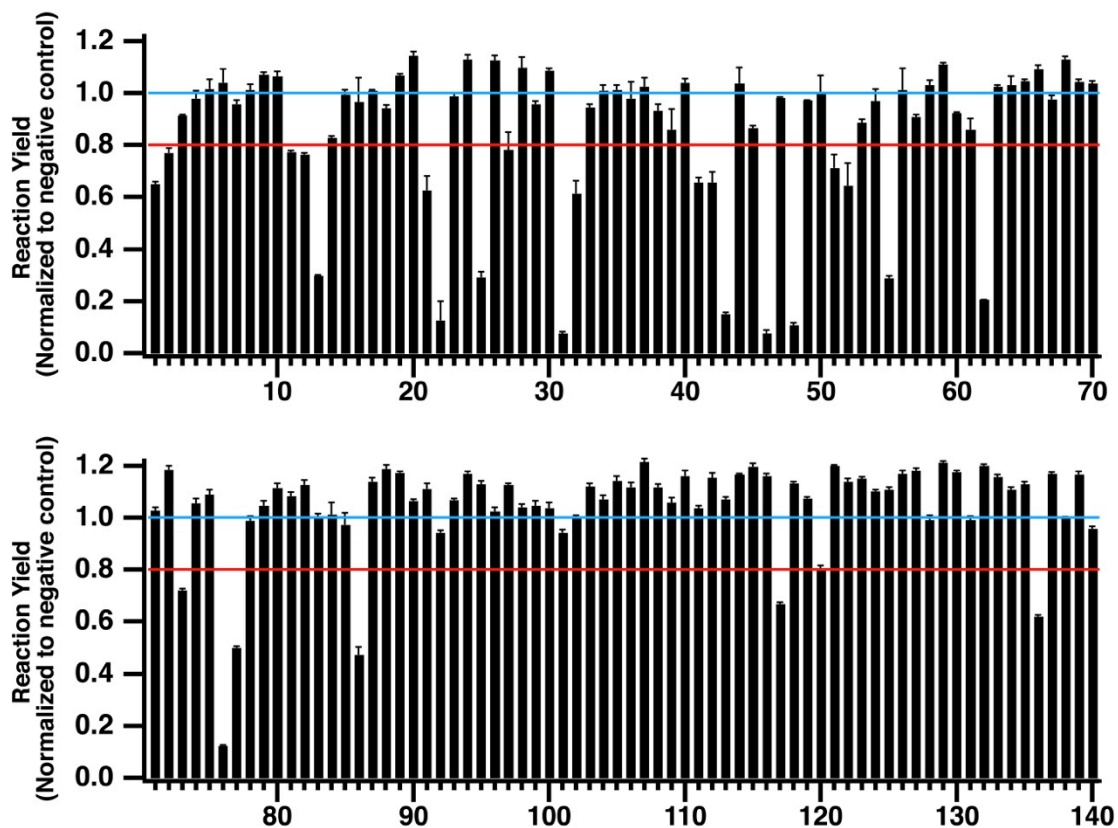
Figure 2-5. Screening 140 small molecules against protein kinase A reveals 25 hit compounds based on the inhibitor threshold (red line). All reaction yields are normalized to the average negative control yield (blue line). With the exception of compound 25, which is plotted at 2.5 µM, compounds 1-60 were tested at 12.5 µM and compounds 61-140 were tested at 5 µM.

Comparison to Other Systems. It is interesting to consider the potential of this system relative to the commercial MCE screening system described in the introduction. Using a comparable peptide substrate and product, the Caliper instrument was able to analyze samples from multiwell plates using a 42 s separation in a single channel corresponding to 0.02 samples/s.[25] In a previous report, we used a droplet extraction method to achieve 0.07 samples/s for 1-channel. The efficiency was much lower because the droplet volume and flow rate determined the injection volume. In a previous report, the same extraction geometry achieved an average separation efficiency of 53,500 plates

for a 12 s separation of three amino acid neurotransmitters.[74] The droplet MCE system achieves about ten-fold higher rates per channel even though replicate injections are performed and some replicates are wasted on carryover. This increase in throughput is due to the higher efficiency enabled by combination of droplet introduction and electrokinetic injection. A further potential advantage of droplet-based sample introduction is a substantial reduction in reagent consumption by utilizing an all-droplet format, i.e. reactions performed in droplets,[38, 63] which could achieve over a 1000-fold reduction in reagents. While these observations demonstrate a significant potential advantage of the droplet MCE approach, further testing and development is required before a droplet system could compete in terms of robustness and routine use for screening 10^4 to 10^5 samples and continuous operation.
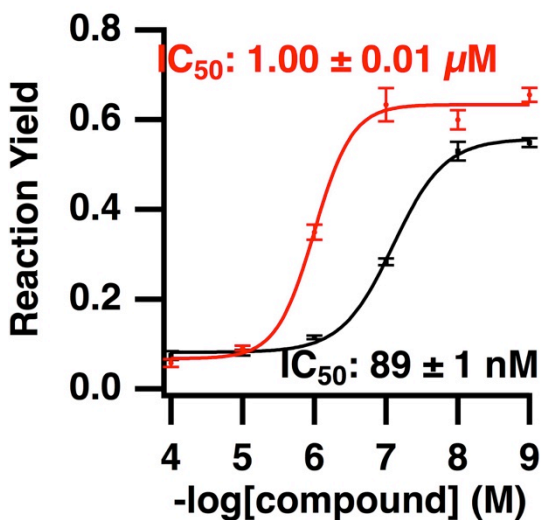
Figure 2-6. Dose-response curves for H-89 (black trace) and ellagic acid (red trace) generated from protein kinase A screening data. The measured IC_{50} values agree with literature values of 150 nM[134] and 3 µM[135] for H-89 and ellagic acid, respectively.

Conclusion

This work has demonstrated a novel droplet extraction method for coupling segmented flow to MCE that uses the native properties of PDMS and glass to separate the two phases in segmented flow. We demonstrated the utility of this sample introduction method combined with MCE for HTS by performing a proof-of-concept screen with PKA and a set 140 small molecules. Each sample consisted of two droplets and approximately 6 injections were made per sample. This equates to an injection throughput of 1 Hz and a sample throughput of 0.16 Hz, which would allow for analysis of >10,000 samples per day. In order to increase sample throughput without sacrificing separation resolution or data quality, parallel analysis would be required and could be achieved by fabricated multiple separation channels per device. Additionally, this platform is applicable to other screening assays and other droplet-MCE applications, such as coupling stages of a 2D separation or chemical sensing from sampling probes.

CHAPTER 3: IDENTIFICATION OF SIRTUIN 5 INHIBITORS BY ULTRAFAST MICROCHIP ELECTROPHORESIS USING NANOLITER VOLUME SAMPLES

Introduction

Sirtuins are an evolutionarily conserved class of nicotinamide adenine dinucleotide (NAD^+)–dependent deacylases comprised of seven members (SIRT1-SIRT7).[80, 81] The SIRT mediated deacylase reaction consumes NAD^+ generating a deacylated product, 2'-O-acetyl-ADP-ribose, and nicotinamide. Recent research has revealed novel catalytic functions for sirtuins, such as deacylation,[90, 91] desuccinylation,[88, 92, 94] deglutarylation,[93] demalonylation,[94, 95] and decrotonylation[96, 97], with SIRT5 preferentially targeting succinyl, glutaryl, and malonyl moieties.[88, 92-95, 98, 99] Through removal of these modifications, SIRT5 regulates the activity of many metabolic enzymes, such as carbamoyl phosphate synthetase 1 (CPS1),[100, 103] superoxide dismutase 1 (SOD1),[104] succinate dehydrogenase (SDH),[98] pyruvate dehydrogenase complex (PDC),[98] and 3-hydroxyl-3-methylglutaryl-CoA synthase 2 (HMGCS2).[99] SIRT5 regulates glycolysis through demalonylation of glyceraldehyde 3-phosphate dehydrogenase (GAPDH) and aldolase B, among other targets.[95] SIRT5 knockout cells show extensive hypersuccinylation. Although no striking biological phenotype or abnormality is observed for SIRT5 knockout cell lines,[101] SIRT5 may play a role in cancer biology[102, 136]

as suggested by its overexpression and reported pro-proliferative role in lung cancer.[104, 107]

Because of the diverse roles that SIRT5 plays within cells, identification of small molecule modulators of SIRT5 activity could have biological and clinical applications. Development of robust HTS assays for SIRT5 is necessary to enable rapid testing and identification of modulators. To date, much work has been done screening other members of the sirtuin family through optical assays, such as the commercially available *Fluor-de-Lys*™ assay based on 7-amino-4-methylcoumarin (AMC).[111-115] After catalytic removal of the lysine modification by a sirtuin, the AMC probe is accessible to cleavage by trypsin leading to an increase in fluorescent signal.[110] This type of assay was used for the identification of Sirtuin 1 activators reported to increase lifespan in invertebrates.[112] While these assays are amenable to HTS, the close proximity of dye molecule and lysine residue has resulted in artifactual results during screening.[111, 116, 117] To avoid these limitations, groups have developed alternative assays for SIRT5 screening based on optical detection of nicotinamide formation,[118] inclusion of fluorophore-quencher pairs in the substrate,[120] high-performance liquid chromatrography-mass spectrometry (HPLC-MS),[88, 109, 121] and fluorescence-resonance energy transfer.[119] However, the number of compounds screened has been limited and the throughput required for large-scale screening has not been demonstrated.

Previously, electrophoresis assays have been used for screening of sirtuins,[23-25, 137-139] GTPase,[72] and other enzymes.[140, 141] Although these assays typically use fluorescent substrates, the label is often located remote from the target residue reducing the likelihood of false positives due to non-specific interactions. Conventional capillary

(CE) or microchip electrophoresis (MCE) methods use auto-samplers or manual sample loading leading to a maximum throughput of a few samples per minute.

Droplet-based sample introduction for CE and MCE has recently been demonstrated for screening[72, 142] and other assays[70, 71, 74-76] as a way to improve sample introduction to microfluidic devices. Indeed, we previously developed a droplet-MCE assay for protein kinase A (PKA) capable of analyzing 8 samples per minute.[142] Due to the small number of compounds tested in these screens, the method robustness required for routine high-throughput analysis has not been demonstrated. Herein we report the use of droplet-MCE with 3-fold improved throughput over prior studies for a screen of 1280 compounds against SIRT5.

Materials and Methods

Chemicals and Materials. Unless otherwise specified all reagents were purchased from Sigma Aldrich (St. Louis, MO). SDHA-derived peptide was synthesized by GenicBio Limited (Shanghai, China). All test compounds were from the Prestwick Chemical Library (Prestwick Chemical, Washington DC) and were supplied by the Center for Chemical Genomics at the University of Michigan or from the Epigenetics Screening Library (Cayman Chemical, Ann Arbor, MI).

Microfluidic Device Fabrication. Polydimethylsiloxane (PDMS) droplet extraction devices were prepared using a pour over method as previous described.[142] Glass microfluidic devices were fabricated using photolithography and wet chemical etching by hydrofluoric acid.[127-129] Each device is fabricated from two etched pieces of glass that are aligned prior to bonding. One slide was etched to 80 μm for the capillary insertion channel and sample channel. The second slide was etched to 80 μm for capillary

insertion and 3 μm for separation channels. During etching of deep channels, other features were covered with HF resistant tape (Semiconductor Equipment Corporation, Moorpark, CA). After etching, fluidic access holes were made with a 0.5 mm drill bit (Kyocera Tycom, Costa Mesa, CA). Glass slides were washed for 20 min in piranha solution (sulfuric acid:hydrogen peroxide, 4:1) and for 40 min in heated RCA solution (ammonium hydroxide:hydrogen peroxide:water, 1:1:5). Slides were rinsed with water, channels were aligned under a microscope, and bonded at 610 °C for 8 h. Reservoirs (IDEX Health and Science, Oak Harbor, WA) were attached at the access holes using epoxy and a 30 μm i.d. x 150 μm o.d. x 1 mm long extraction capillary was waxed in place in the capillary insertion channel.

Droplet Generation from Multiwell Plate. Droplet formation followed the procedure previously published.[35] Droplets segmented by perfluorodecalin (PFD) were generated from modified polypropylene 384-well plates (Nunc ShallowWell, Thermo Scientific, Waltham, MA) and collected into 150 μm i.d. x 360 μm o.d. HPFA+ tubing (IDEX Health and Science, Oak Harbor, WA). Well height across the entire plate was reduced by 1.5 mm using a CNC milling machine allowing samples to be covered by carrier oil to prevent evaporation and aspiration of air bubbles. For droplet formation, multiwell plate (MWP) and tubing were mounted onto a computer controlled XYZ-positioner so that the tubing inlet could move freely above the wells. The tubing outlet was connected to a 100 μL syringe mounted in a PHD 200 syringe pump (Harvard Apparatus, Holliston, TX) and both were primed with PFD to remove any air bubbles.[37] With the syringe pump operating in refilling mode (1000 nL/min), the tubing inlet was moved from well to well in programmed pattern to generate droplets at 0.75 droplets per

second. Briefly, the computer was programmed to move at 2000 mm/s, which was the maximum rate of linear motion. For each sample droplet, the tubing would dwell in the aqueous phase (420 ms) and in the oil layer (150 ms). Addition oil phase would be aspirated as the tubing moved from well to well. The final droplet volume was 8.2 ± 0.3 nL and each oil spacer was 10.0 ± 0.4 nL. After formation of droplets a short oil plug (~10 mm) is aspirated into the tube to prevent sample loss caused by flow induce when making connections.

Microchip Electrophoresis Analysis with Droplet Samples. Prior to each experiment, all fluidic channels were filled with separation buffer (10 mM sodium tetraborate, pH 10) ensuring no air bubbles remained. Positive (+2 kV) and negative (-3 kV) high voltage (CZE1000R, Spellman, Hauppague, NY) was applied to the microfluidic device via platinum electrodes at the fluid reservoirs. Sample was electrokinetically injected[130, 131] for 15 ms using a high-voltage relay (Kilovac, Santa Barbara, CA) controlled by an in-house LabVIEW program (National Instruments, Austin, TX). Detection was accomplished using a confocal laser-induced fluorescence detector. Briefly, a 488 nm line from a solid state laser (CrystaLaser, Reno, NV) was directed through a 488 ± 10 nm band pass filter and reflected by a 500 nm dichroic mirror into a 40X objective lens. Emitted light was collected by the same objective and passed through the dichroic mirror. The emitted light filtered through a 520 ± 10 nm band pass filter and 400 μm pinhole prior to being detected by a photomultiplier tube (R1477, Hamamatsu, Bridgewater, NJ). Current from the PMT was amplified (SR570 current preamplifier, Stanford Research Systems, Sunnyvale, CA) and monitored using in-house LabVIEW control software. Data were sampled at 1000 Hz using a 16-bit data

acquisition card (PCI-6036E, National Instruments Corp., Austin, TX). Electropherograms were analyzed with Cutter 7.0 [132]. Statistical analysis and plotting was done in Excel 2011 (Microsoft, Redmond, WA), and Igor Pro 6.32 (Wavemetrics, Inc., Lake Oswego, OR).

Droplet samples were introduced as outlined previously. A length of tubing containing sample droplets connected to a 100 µL syringe via a union and the outlet was inserted in to the PDMS extraction device at a 90° angle to the extraction capillary inlet. Downstream of the extraction region, a 40 µm i.d. x 150 µm o.d. fused silica capillary connected to a 100 µL syringe is inserted into the device to generate waste droplets that promote extraction by increasing backpressure at the extraction point. Droplets were pumped into the extraction device at 700 nL/min and electrokinetic injections were made at 4 Hz.

In Vitro PDC Desuccinylation Assay. Porcine heart PDC (Sigma Aldrich, St. Louis, MO) was purified by centrifugation at 135,000xg for 2 hours in 100 mM potassium phosphate, pH 7.5, 0.05% lauryl maltoside, 2.5 mM EDTA, and 30% glycerol. Desuccinylation reactions were carried out on 30 μg of purified porcine heart PDC in a final reaction volume of 60 μl in presence of 25 mM Tris-Cl, pH 8.0, 200 mM NaCl, 5 mM KCl, 1 mM MgCl2, 0.1% PEG 8000, and 3.125 mM NAD^+ at 37°C for 2 hours. Where indicated, 10 μg of SIRT5 or SIRT5^{H158Y} (expressed and purified in house) was added. During incubation, tubes were occasionally agitated. Following desuccinylation, 15 μl each reaction was analyzed by immunoblotting with a succinyl-lysine antibody (PTM Biolabs, Inc, Chicago, IL). After analysis, the membrane was stripped and re-

probed for PDHA1 (Abcam, Cambridge, MA) and SIRT5 (Cell Signaling Technology, Danvers, MA).

Peptide-based SIRT5 Assay. Assay conditions were developed using a novel succinyl-lysine peptide derived from succinate dehydrogenase.[98] The substrate peptide (GGQSLK[succ]FGKG) was labeled at the N-terminus with 5-carboxyfluorescein (5-FAM) and yielded a desuccinylated peptide (GGQSLKFGKG) as a product. Reactions were performed in 10 mM Tris, pH 8 containing 1 mM dithiothreitol (DTT) with enzyme concentration fixed at 10 nM. Reactions were stopped by dilution with 1.5 volumes of 10 mM sodium tetraborate, pH 10. Kinetic parameters were determined using substrate concentrations ranging from 0 to 50 µM at time points from 0 to 30 minutes. Kinetics data was fitted using the Michaelis-Menton model in GraphPad Prism 6. Assay conditions were validated using a small-scale screen of the Epigenetics Screening Library.

High-throughput SIRT5 Screening. All screens were performed at 10 µL final volume in a modified low volume MWP and were prepared using a MultiDrop Combi (Thermo Scientific, Waltham, MA). A Caliper Life Science Sciclone ALH300 (PerkinElmer, Waltham, MA) was used to deposit 50 nL of 2 mM test compounds into MWPs containing 5 µL of 2X reaction buffer (20 mM Tris, pH 8, 2 mM DTT). To index samples during analysis, 1 µL of 1 µM rhodamine 110 was added to even number columns and 1 µL of water was added to odd number columns. Next, 1 µL of 10 µM peptide was added to all wells and 3 µL of 33 nM SIRT5 was added to initiate reactions. Final reaction conditions were 1 µM peptide, 10 nM SIRT5, and 10 µM test compound with 0.5% DMSO. Reactions were quenched by addition of 15 µL of 10 mM sodium

49

tetraborate, pH 10 after 30 minutes incubation at room temperature. Each plate contained 16 negative (0.5% DMSO) and 16 positive (10 µM anacardic acid) controls for a total of 352 samples per plate. Each sample was reformatted into a single droplet as detailed above. Reaction yield based on substrate and product peak area was used for data analysis and normalized to positive and negative controls within each row to account for variation in reaction yield. Hit compounds were verified by dose-response analysis from 0.1 to 100 µM (unless otherwise noted on individual plots) and IC_{50} values were calculated from best fit curves using GraphPad Prism 6.

Results and Discussion

Development of a SIRT5 Screening Substrate. Several research groups have developed assays for SIRT5, since it was first reported to remove novel protein post-translational modifications, such as succinyl, malonyl, and glutaryl moieties.[88, 92, 94] Based around fluorogenic substrates,[111, 112, 114] these assays are amenable to HTS; but, the engineered assay substrates may not always mimic natural substrates well due to their short length and the presence of a bulky fluorescent probe near target residues. To avoid these limitations, assays based on high-pressure liquid chromatography (HPLC),[88] mass spectrometry (MS),[121] or fluorescence resonance energy transfer (FRET)[119] have been developed that use short peptides based on natural SIRT5 substrates.

In developing our electrophoresis assay, we wanted our peptide substrate to have the fluorescent tag remote from the succinyl lysine to reduce potential for false positive results, have a total charge suitable for rapid electrophoretic separation of substrate and product, and be based on a known SIRT5 target to mimic *in vivo* substrates. Known SIRT5 targets, such as CPS1,[99, 100, 103] PDC,[98] SDH,[98] and HMGCS2,[99] as well as

hypersuccinylated proteins, such as hydroxyacyl-Coenzyme A dehydrogenase (HADH),[98] acetyl-Coenzyme A acetyltransferase (ACAT),[98] and malate dehydrogenase (MDH)[99] were identified as templates for substrate development. We selected a peptide based on SDHA K179 due to the favorable peptide charge (-2 for substrate, 0 for product) under basic pH used for analysis; although in principle another target could be used for substrates if desired. The length was sufficient to provide distance (five amino acids) between the 5-FAM tag and the target lysine while providing several amino acids on either side of K179 for substrate recognition as demonstrated by other groups.[88, 109, 143] Additionally, total peptide charge was only slightly negative and allowed for short migration times and good separation from the product peptide formed after SIRT5 desuccinylation.

Separation of the substrate and product peptides was achieved in 250 ms due to favorable charge-to-size ratio, high electric field, and short separation distance (see below). Injection of SIRT5 reaction mixture resulted in two peaks in the electropherogram associated with the succinylated substrate and desuccinylated product peptides (Figure 3-1A). Removal of the succinyl moiety caused a +2 change in peptide charge resulting in a faster migration time.

To evaluate the quality of our SDHA-derive peptide substrate, we compared the activity of SIRT5 and SIRT5[H158Y] – catalytically inactive SIRT5 – with the peptide substrate and full PDC. For the peptide substrate, robust activity, as quantified by product peak area, was observed for SIRT5 with only slight activity observed for SIRT5[H158Y] (Figure 3-1A). Likewise incubation of PDC with SIRT5, but not SIRT5[H158Y], resulted in decreased succinylation of PDHA1 – the catalytic subunit of PDC (Figure 3-1B).

Therefore, in terms of SIRT5 activity, our SDHA-derived peptide substrate behaved similarly to full PDC.
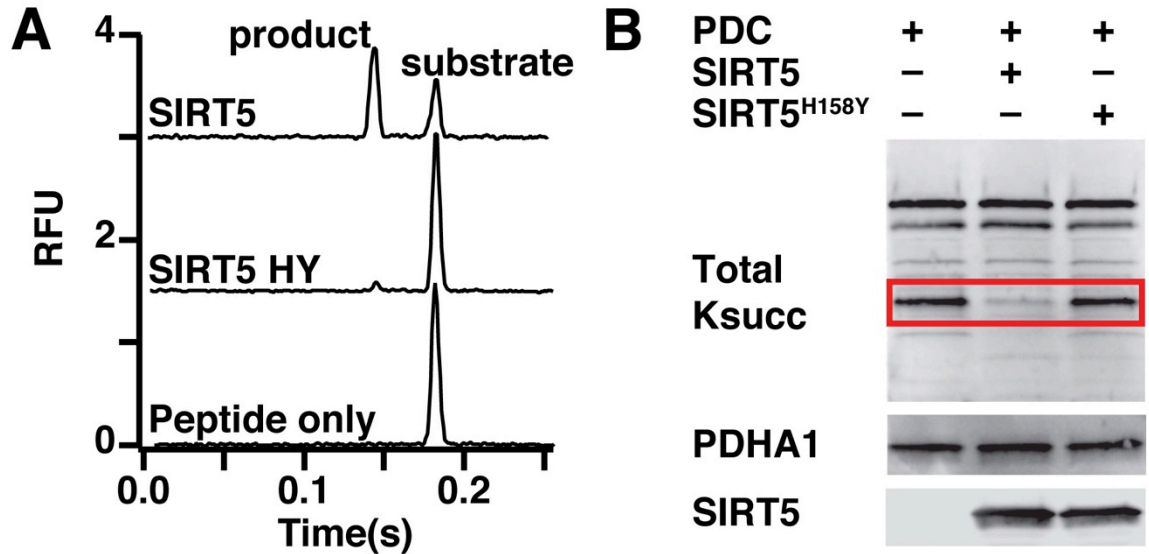
Figure 3-1. SIRT5 and SIRT5[H158Y] have similar activity against SDHA-derived peptide and PDC holoenzyme. (a) Electropherograms demonstrating that SIRT5 desuccinylates target peptide forming a product with shorter migration time and that SIRT5[H158Y] has reduced enzymatic activity. (b) Succinylation of porcine heart PDC is reduced following incubation with SIRT5 but not SIRT5[H158Y]. Upper blot: total lysine succinylation; PDHA1 band highlighted in red. Middle and lower blots: PDHA1 and SIRT5, respectively.

Improvements to Sample Throughput for Microchip Electrophoresis. Analysis of droplet samples by MCE was done using a hybrid PDMS-glass microfluidic device modified from that described previously (Figure 3-2).[142] In this system, samples stored in a length of Teflon tubing are flowed past the inlet of a fused silica extraction capillary inserted into the glass MCE device. As the droplets exit the Teflon tubing, they are wicked into the extraction capillary. Once on the microfluidic device they were pulled by EOF toward the voltage-gated injector for MCE analysis. A combination dead volume

in the extraction capillary and separation speed limited the system throughput. In this work, we examined improving the throughput to enable larger scale screens.
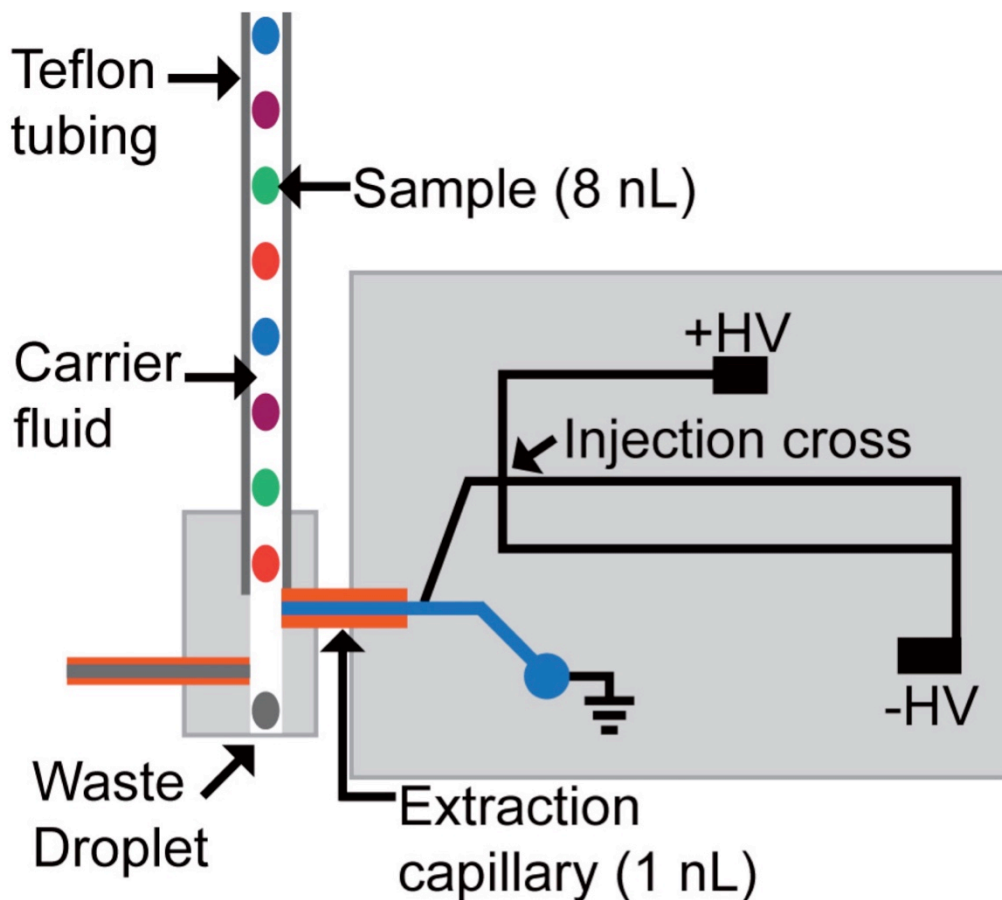
Figure 3-2. Schematic of microfluidic device for analysis of droplet samples by MCE showing positioning of droplet samples orthogonally to the 1 mm fused silica extraction capillary.

In the original system, the extraction capillary had a 3.1 nL volume (2.5 mm length x 40 μm i.d.). To effectively clear this dead volume, 16 nL of sample (2 droplets of 8 nL each) was required. The time required to perform this rinse limited assay throughput to 0.16 samples per second. For these experiments, the device was redesigned to accommodate a 1 nL extraction capillary (1 mm length x 30 μm i.d.). We found that

with this volume a single 8 nL droplet provided a sufficient rinse of the extraction capillary allowing throughput to be increased 2-fold relative to the previous implementation.

Although reduced dead volume increased sample throughput, separation speed remained a bottleneck. In previous work, separation distance was 5 mm and electric field was 2000 V/cm. Using these conditions, rhodamine, substrate, and product for SIRT5 assays were resolved within 1 s (Figure 3-3A). Resolution could be maintained at shorter times by reducing detection length and increasing the field (Figure 3-3A). The fastest separation achieved was 250 ms at 3500 V/cm and 2 mm separation distance.

At the high field and short separation length, over injection led to poor resolution. To determine the best injection time, peak variance for substrate and product peptide was measured for injection widths of 10 ms to 35 ms (Figure 3-3B). A minimum peak variance was observed at 15 ms injection width for both substrate and product peptides and was used for all future separations. Under these conditions, the average separation efficiency for three analytes was 7,000 ± 1,000 plates. When corrected for analyte migration time, the separation generated 41,000 ± 8,000 theoretical plates/s. These conditions allowed 4 injections/s so that 8 injections were obtained per droplet and sample throughput was 0.5 Hz. This result is a 3-fold increase in sample throughput compared to the previous design.[142]
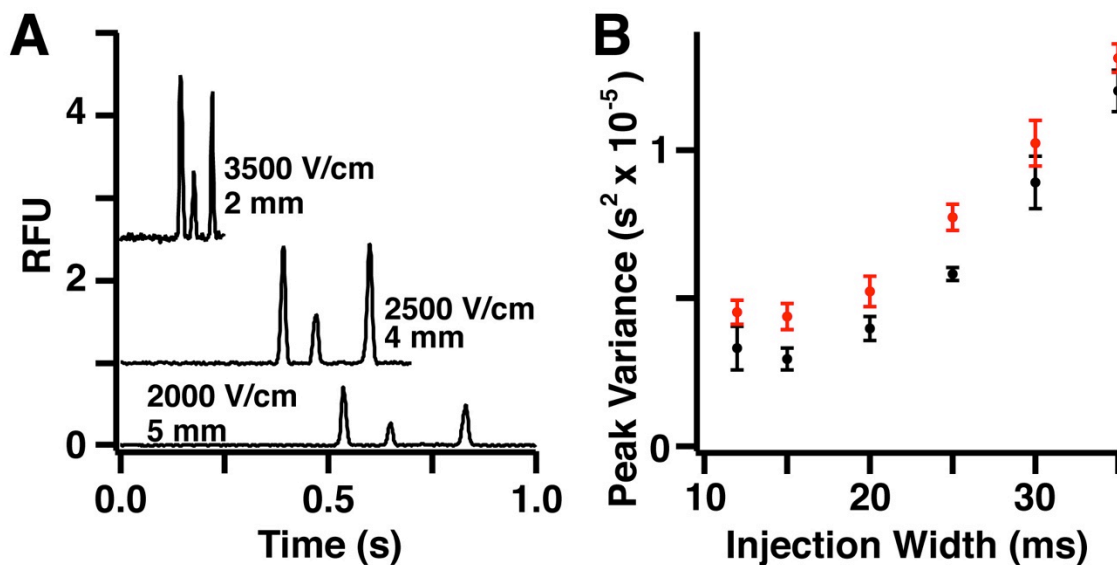
Figure 3-3. Separation throughput was increased 4-fold for SIRT5 assay through improvement of separation and injection conditions. (a) Electropherograms for initial separation conditions based on previous work and improved conditions capable of baseline separation in as little as 250 ms. (b) Optimum injection width is 15 ms based substrate (black) and product (red) peak variance.

The high rate of injections allowed monitoring of when carryover was eliminated (typically 3 injections) and collection of at least 3 replicate assays per droplet. Carryover was determined by monitoring the presence or absence of a rhodamine signal (rhodamine was present in every other droplet) and stability of peak height for substrate and product peaks in the electropherogram.

An important consideration is whether the electropherograms are stable over many injections. Migration time RSD for rhodamine, substrate, and product were 1.3%, 0.7%, and 0.6%, respectively (n = 1400). Additionally, peak areas were stable over many injections. For samples containing rhodamine, peak area RSD was less than 5% for replicate injections of the same sample (n = 3) and average rhodamine peak area RSD was 6% over 88 samples (n = 264 injections). This corresponds to one batch of samples (e.g. 88 samples with rhodamine and 88 without). Slight changes in peak magnitude were

observed from batch to batch, but this did not affect data quality because peak area ratios were used for analysis (Figure 3-4). Substrate and product peak area fluctuated from sample to sample due to slight variation in enzyme efficiency; however, peak area RSD was less than 5% for replicate injections of the same sample (n = 3).
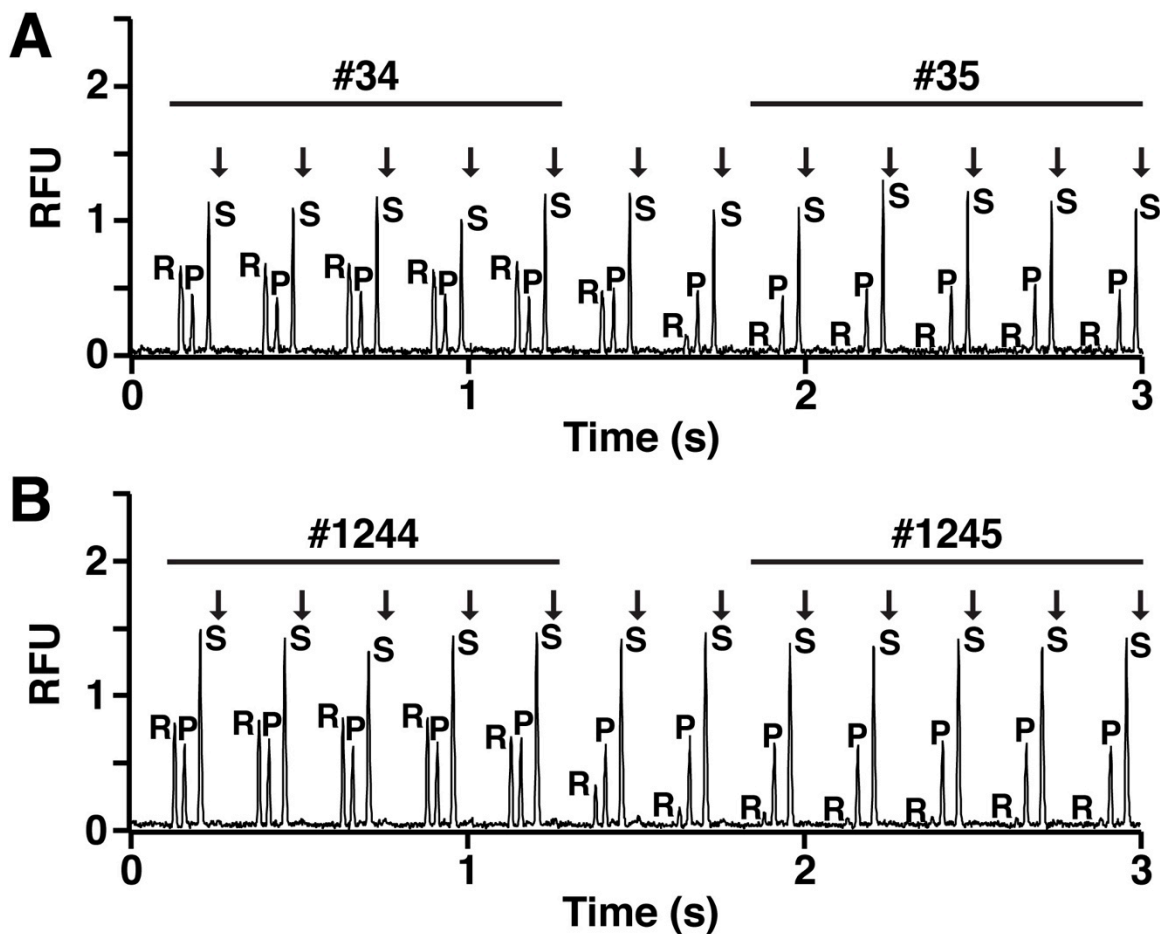
Figure 3-4. Representative electropherograms from injections made at the beginning (a) and end (b) of SIRT5 screening. The compound number is labeled above injections, which are denoted by an arrow. Individual peaks corresponding to rhodamine (R), product (P), and substrate (S) are labeled.

SIRT5 Inhibitor Screening. The assay for SIRT5 monitored the depletion of substrate peptide (5-FAM-GGQSLK[succ]FGKG) and formation of product peptide (5-

56

FAM-GGQSLKFGKG) simultaneously (Figure 3-5A). Reaction yield was normalized to positive and negative controls within each row of the well plate and plotted as normalized SIRT5 activity for each sample. Monitoring two analytes and normalizing to row controls mitigated the effect of variation in sample preparation, injection, or separation efficiency over the course of screening. Samples were indexed by addition of rhodamine 110 to even number samples and monitoring changes in rhodamine peak area to identify samples as previously demonstrated.[142] Prior to screening, substrate concentration for screening was determined from kinetics data. Based on Michaelis-Menton kinetics, the K_m (1.6 ± 0.4 µM) and K_{cat}/K_m (5.8 x 10^4 $M^{-1}s^{-1}$) values were determined (Figure 3-5B). These match well with reported values for SIRT5 substrate peptides of similar length based on Histone H3 (K_m = 5.8 ± 2.7 and K_{cat}/K_m = 4.3 x 10^3 $M^{-1}s^{-1}$)[88] and CPS1 (K_m = 3.8 ± 0.6 and K_{cat}/K_m = 1.4 x 10^4 $M^{-1}s^{-1}$).[109] Reaction progress was linear up to 50 minutes, the longest point tested (Figure 3-5C). Addition of 1.5 volumes of 10 mM sodium tetraborate, pH 10 completely inactivates SIRT5 (Figure 3-5D). To satisfy screening assay requirements[2, 144] substrate concentration was fixed at 1 µM, below the K_m, and reactions were quenched after 30 minutes.
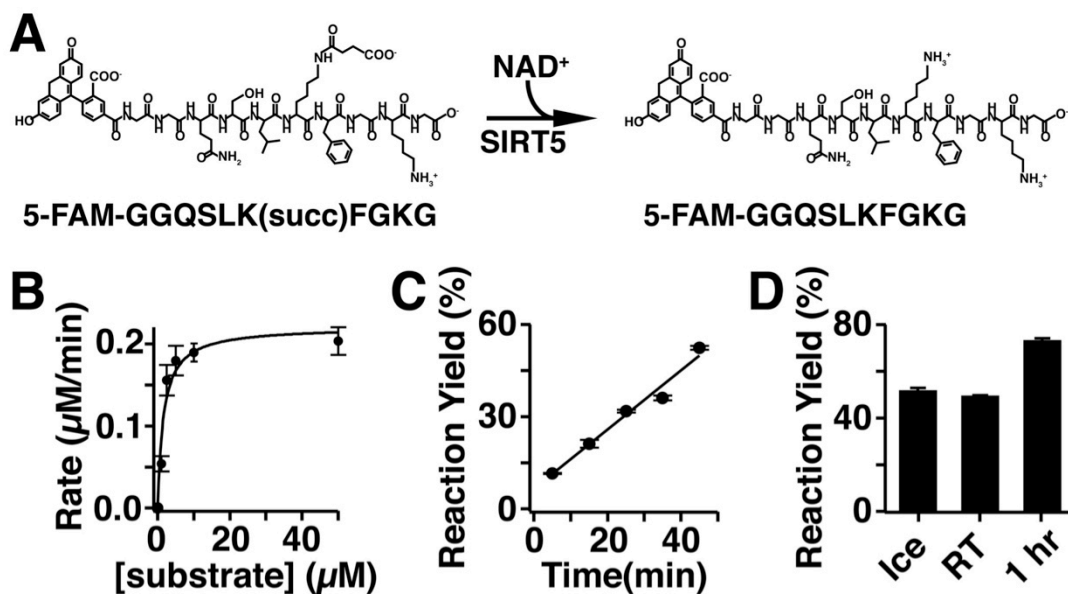
Figure 3-5. A) SIRT5 catalyzes the removal of succinyl moieties from lysine side chains in the presence of NAD^+ causing a +2 change in peptide charge. **B**) Michaelis-Menton kinetics data for SIRT5 with excess NAD^+. K_m is 1.6 ± 0.4 μM, K_{cat} is 0.092 ± 0.008 s^{-1}, and K_{cat}/K_m is 5.8×10^4 $M^{-1}s^{-1}$. **C**) Reaction progress for 1 μM substrate and 10 nM SIRT5 demonstrating reaction linearity up to ~50 minutes. **D**) SIRT5 reaction can be quenched by addition of 1.5 volumes of 10 mM sodium tetraborate, pH 10. Ice sample was quenched after 30 minutes and stored at -80 °C, RT sample was quenched after 30 minutes and stored at room temperature, and 1 hr sample was allowed to react for 1 hr before quenching. (n = 3 for all samples).

To validate reaction conditions for high throughput screening, SIRT5 activity was screened against a library of 80 compounds from an epigenetics focus library known to inhibit other members of the sirtuin family (Figure 3-6A). Each test compound was screened at 10 μM. Seven compounds were identified as SIRT5 inhibitors, based on a 50 percent inhibition of SIRT5 activity. These hits were verified with dose-response curves and IC_{50} values ranged from 60 nM to 8 μM (Figure 3-6B). Of the compounds, suramin has previously been reported as a SIRT5 inhibitor in NAD^+-nicotinamide exchange assays (IC_{50} = 22 μM)[89] and fluorogenic assays (IC_{50} = 47 μM).[145] AGK-2 has been reported as a SIRT5 inhibitor with an IC_{50} value above 100 μM.[108] The difference in IC_{50} values may be due to these assays focusing on SIRT5 deacetylase activity, which is much

lower than SIRT5 desuccinylase activity, or differences in assay conditions. The potent

inhibitor anacardic acid was chosen as a positive control for future screens based on the

results of pilot screening.
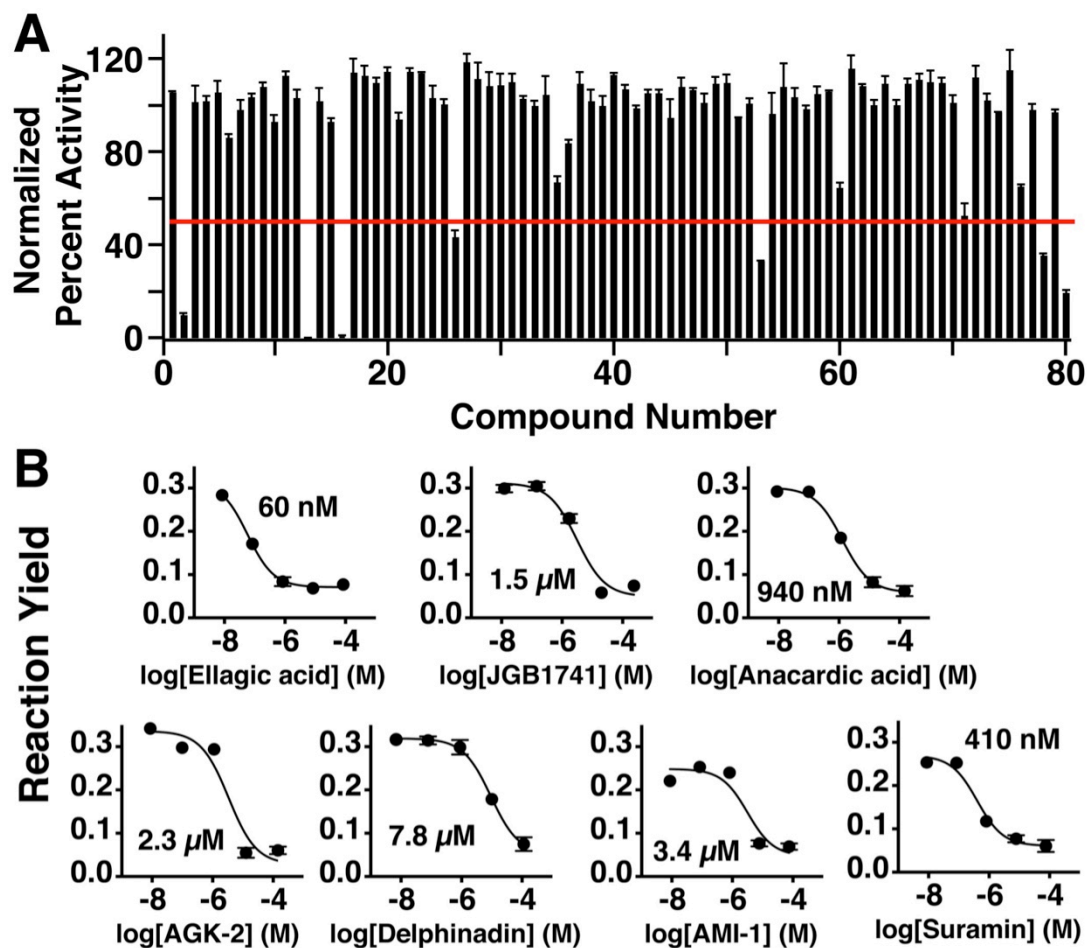
Figure 3-6. A) Data from SIRT5 assay validation screen using 80 compounds from the Epigenetics Screening Library. Inhibition threshold is denoted by red line. **B)** Dose-response curves for compounds reducing SIRT5 activity by 50 percent.

These validated conditions were used to screen the Prestwick Chemical Library,

which contains 1280 approved drug compounds, against SIRT5 (Figure 3-7A). Reactions

were prepared in 384-well plates using high-throughput sample preparation

instrumentation for incorporation into existing HTS workflows. Each of the 1408 samples

(1280 compounds, 64 positive controls, and 64 negative controls) were reformatted into a single droplet with an average volume of 8.2 ± 0.3 nL (n = 352) at 0.75 Hz (although faster reformatting is possible[146]). Analysis was done in batches of 176 samples, corresponding to one-half of a plate, with a sample throughput of 0.5 Hz. Total analysis time was 46 minutes and generated over 11,000 electropherograms at 8 injections per sample (Figure 3-7B). The assay Z'-factor, when corrected for row effects caused by sample preparation, was 0.8.

Figure 3-7. Screen of Prestwick Collection Library against SIRT5. A). Normalized SIRT5 activity with each of the 1280 compounds. Each point represents the average

60

enzyme activity with a test compound and the red line denotes the inhibition threshold. B) Top plot: Electropherograms corresponding to the 160 compounds in the grey region of Panel A. Bottom plot: Enlarged view of red highlight region (338-342 s) showing separation of rhodamine (R), product peptide (P), and substrate peptide (S) for three compounds. #1117 is an inhibitor. Injections are denoted with an arrow and 6-8 injections are made from each sample droplet.

Among the compounds, 10 reduced SIRT5 activity by 70 percent and were selected for further study. At the time of initial screening, all reactions containing SIRT5 inhibitors were re-formatted as duplicate droplets and analyzed by MCE to confirm results (Figure 3-8). These compounds were evaluated for dose-dependent SIRT5 inhibition and 8 were confirmed as SIRT5 inhibitors. The remaining two compounds did not exhibit dose-dependent inhibition of SIRT5 and were identified as false positives caused by sample preparation.
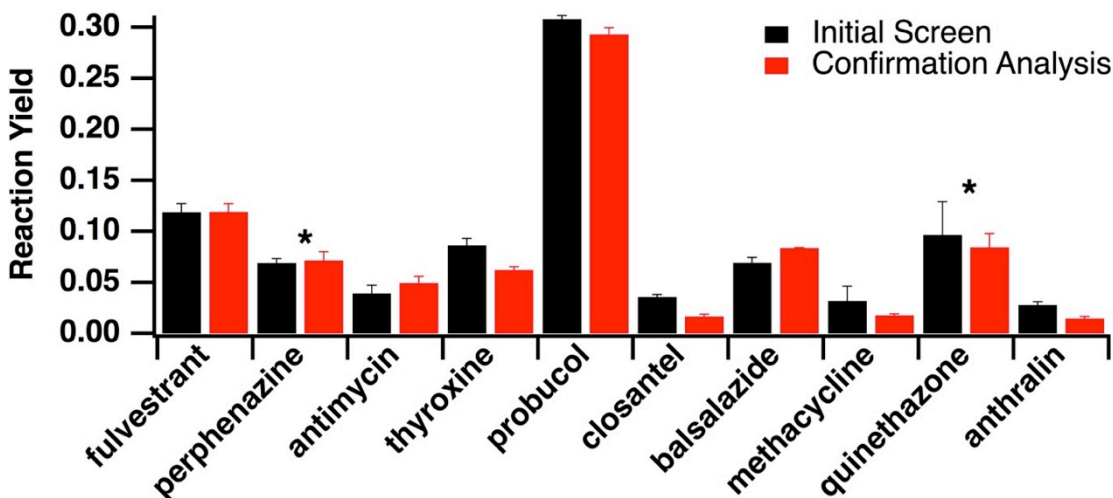
Figure 3-8. Confirmation of SIRT5 inhibitors during initial screening and demonstration of analysis reproducibility. All compounds identified as reducing SIRT5 activity by 70 percent were formatted into two sample droplets each and re-analyzed by MCE. In all cases, the data from re-testing (red bars) matches well with initial screening (black bars) data demonstrating reproducibility of analysis and confirming SIRT5 inhibitors for follow up studies. Compounds labeled with an asterisks (*) were identified as false-positives by dose-response analysis (i.e. dose-dependent inhibition was not observed).

61

All dose-response curves had good fit ($R^2 > 0.90$) except antimycin A, which had

an IC_{50} value near the maximum tested dose (Figure 3-9). (See Appendix B for dose-

response fit values and structures of confirmed inhibitors.) The calculated IC_{50} values are

in the low micromolar range matching the most potent reported SIRT5 inhibitors.[108, 109,]

[147] None of the compounds have previously been reported as SIRT5 inhibitors; however,

SIRT5 was reported as a potential target of probucol based on molecular targeting and

docking studies.[148]
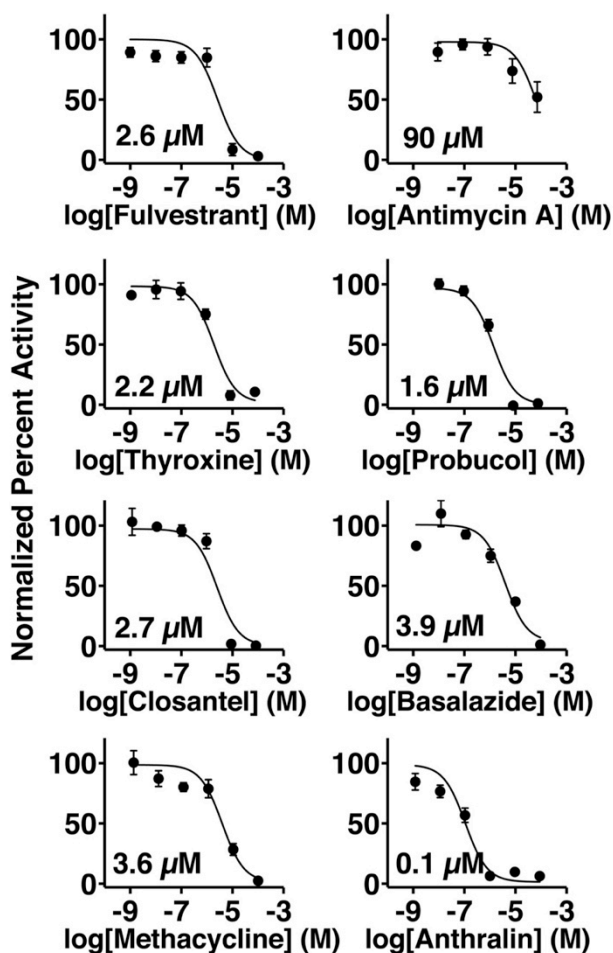
Figure 3-9. Dose-response analysis for compounds reducing SIRT5 activity by 70 percent. Ten compounds were identified during screening and 8 were confirmed as inhibitors with IC_{50} values denoted on each plot.

Future Improvements to sample throughput and robustness. If run continuously, the current system could analyze over 14,000 samples in 8 hours; however, even higher throughput may be possible with further improvement. For example, the current separation speed was limited by peak resolution between rhodamine and product peptide, while the resolution between product and substrate is 2.5. If rhodamine – used for sample indexing – was replaced by a more positively charged analyte with faster migration velocity, then separation time could be further reduced without loss of baseline resolution. For example, reducing separation time to 125 ms (half of the current separation time) could increase sample throughput to 1 Hz (>28,000 samples in 8 hours). Additional throughput could be achieved by testing multiple compounds simultaneously.[149] While additional assays would be needed to de-convolute any inhibitors or synergistic inhibition effects, throughput would increase linearly with the number of compounds per reaction.

Although we have demonstrated an assay for SIRT5 capable of screening a meso-scale compound library, several factors limit using droplet samples for routine analysis. Several steps during sample analysis require making zero dead volume connections with small flexible tubing, which can be difficult and is labor intensive. During droplet formation, the number of droplets that can be formed reproducibly is limited by back pressure from droplet samples within the collection tubing. This limits read length to several hundred samples requiring batch analysis for large libraries. Although generating droplets in parallel is possible, it increases complexity and requires additional low dead volume connections.[146] If droplets could be generated and analyzed continuously, then

analysis limits imposed by low dead volume connections and droplet read length could be mitigated.

Conclusion

In this work, we have described a SIRT5 screening assay based on ultrafast electrophoresis using nanoliter volume samples suitable for meso-scale library screening. A novel SIRT5 substrate derived from SDHA was developed to achieve rapid separation of substrate and product, while avoiding several limitations associated with commercially available fluorogenic substrates. Using this assay, 1408 samples (1280 compounds, 128 controls) were screened against SIRT5 and 8 previously unknown SIRT5 inhibitors were identified. Analysis was completed within 46 minutes (0.5 Hz) and over 11,000 MCE injections were made demonstrating method speed, robustness, and reliability. Under these conditions, throughput was increased 3-fold relative to previous MCE-based screening and 25-fold compared to previous sirtuin screens by MCE or CE.

CHAPTER 4: TOWARD AN ALL-DROPLET MICROCHIP ELECTROPHORESIS SCREENING PLATFORM

Introduction

Over the past few decades, high-throughput screening (HTS) has become a vital tool for drug discovery within the pharmaceutical industry.[1, 2] As it has gained popularity, the scale of HTS has increased to encompass libraries containing hundreds of thousands of compounds. To mitigate the rising cost of screening such large libraries,[61, 150] plate densities have increased and assay volumes have decreased. Although assay volume can be as low as several microliters, a typical assay of 10^6 compounds requires several liters of each reagent. These volume requirements are prohibitive when screening rare, difficult to express, or expensive enzymes. Further increasing the plate density (i.e. 6144-well plates) requires sub-microliter sample volumes; however, customized liquid dispensing methods are necessary and sample evaporation is common.[151, 152] Therefore, alternate strategies for miniaturizing HTS assays are necessary.

Droplet microfluidics has emerged as a powerful tool for handling and manipulating low volume samples and provides an interesting solution for decreasing sample volume in high-throughput screening.[53, 60, 62-64] In droplet microfluidics, aqueous samples, typically picoliter to nanoliter in volume, are encapsulated within an immiscible phase and manipulated within microfluidic devices.[27] Because carrier fluid, typically air

or fluorinated oil, surrounds sample droplets, evaporation is significantly reduced. A range of droplet transformations are possible, such as mixing,[48-52] reagent addition,[27, 38, 50, 52, 57, 58] dilution,[59, 60] splitting,[39-42] and sorting,[35, 53, 54, 56] to achieve complete analysis within a miniaturized format. In one example, the authors deposited nanoliter volume droplets in a 2D array on a flat surface and covered them with an oil layer.[153] In this manner, they could add reagents and sample from nanoliter volume droplets without sample evaporation.[154, 155] Using these methods sample consumption could be reduced by more than 1,000-fold relative to conventional assays.[53]

Accurate reagent dispensing is necessary to reduce sample-to-sample variability and to achieve high-quality screening results. Several reagent addition systems for droplet microfluidics have been developed based on active and passive methods. Active methods, such as electrocoalescence[156-159] or the thermocapillary effect,[160] provide robust operation and are able to selectively add reagents to some droplets but not others. However, they require external input to control reagent addition and have more complicated operation. Passive devices, on the other hand, afford simpler operation but are unable to add reagents on only certain droplets (e.g. cell sorting applications) and performance is dependent on reagent composition (e.g. organic content and surfactants).[38, 52, 57, 58] One group reported the use of PDMS reagent addition devices with hydrophilic reagent channels to achieve robust operation for blood coagulation assays, but droplets were entirely manipulated within the device and carryover was not detailed.[52] Another group built upon this design, using PVDF and HFPA+ tubing, and demonstrated low carryover reagent addition to droplets from *in vivo* sample probes and screening assays.[38, 58]

Although robust operation was reported, a single reagent inlet and complicated fabrication procedure limit widespread use.

In this work we demonstrate a simple and robust PDMS device for passive reagent addition was developed using single layer SU-8 fabrication. The high sample throughput, simple operation, and low carryover are demonstrated in several fundamental experiments. Samples prepared using the reagent addition device were analyzed using microchip electrophoresis to demonstrate progress toward all-droplet screening assays.

Materials and Methods

Chemicals and Materials. Unless otherwise specified all reagents were purchased from Sigma Aldrich (St. Louis, MO). PDMS devices were fabricated from degassed RTV-615 (Momentive, Inc., Waterford, NY) using a base to curing agent ratio of 10:1. Fluorescent peptide (5-FAM-GGQSLK[succ]FGKG) was purchased from GenicBio Ltd (Shanghai, China).

Microfluidic Device Fabrication. Reagent addition devices were fabricated in PDMS using standard soft lithography.[42, 161] Briefly, HMDS was spun onto a 3-inch silicon wafer (University Wafer, Boston, MA) to promote photoresist adhesion. SU-8 2075 photoresist (MicroChem, Corp., Newton, MA) was spun onto the wafer to achieve a 110-μm deep layer. Wafers were baked (5 min at 65 °C and 15 min at 95 °C) prior to UV light exposure (Optical Associates, Inc., Malpitas, CA) through a photomask to cross-link features. After exposure, wafers were baked (3 min at 65 °C and 8 min at 95 °C) prior to developing in SU-8 photoresist developer (MicroChem, Corp., Newton, MA). After fabrication, droplet channels were 110 μm wide and reagent inlets were 100 μm wide. After casting PDMS over the molds, devices were trimmed to size and bonded to

unpatterned PDMS using plasma oxidation. Sealed devices were placed on a hot plate (75 °C) for 5 minutes to enhance bonding prior to surface functionalization. After functionalization, reagent capillaries (40 μm i.d. x 150 μm o.d.) were inserted into reagent inlet channels to be flush with the droplet channel. Derivatized transfer capillaries (100 μm i.d. x 150 μm o.d.) were inserted as needed to facilitate sample transfer. Capillaries were adapted to 360 μm fittings by gluing a 1 cm length of 180 μm i.d. x 360 μm o.d. capillary or 150 μm i.d. x 360 μm o.d. HFPA+ tubing at one end.

Fluorophilic derivatization of PDMS and fused silica. For PDMS devices, channels were derivatized by filling with 1H,1H,2H,2H-perfluorooctyltrichlorosilane (4% v/v in anhydrous hexadecane) for 10 min.[42] Devices were rinsed by sequential perfusion with hexadecane and hexane prior to baking at 80 °C overnight. Fused silica capillary was derivatized based on a previously reported method.[22] Briefly, the fused silica capillary was flushed with 1 M sodium hydroxide (10 min) and water (10 min) at 25 μL/min to activate surface silanols. Capillaries were purged with nitrogen (30 psi) at 90 °C for 1 hr to remove any remaining water. The surface was derivatized by perfusion with 1H,1H,2H,2H-perfluorooctyltrichlorosilane (5% v/v in toluene) at 90 °C for 2 hr at 25 μL/min. Capillaries were rinsed with toluene and methanol (30 min at 25 μL/min) before drying under nitrogen (30 psi) for 3 hr at 90 °C.

Droplet Reagent Addition. Prior to experiments, reagent addition devices were primed with carrier fluid (200:1 perfluorodecalin:perfluorooctanol) to coat PDMS surfaces. At the beginning of experiments, transfer capillaries were primed for 5 min under experimental conditions to remove any air bubbles and ensure stable flow. Sample droplets were generated via tee junction (throughput experiments)[32-34] or sipping from a

multiwell plate (carryover and electrophoresis experiments).[35-38, 142, 146] Reagents could be added at 10 to 30 percent of parent droplet volume by controlling relative flow rates via a syringe pump (Chemyx Inc, Stafford, TX). Droplet signal was monitored by laser-induced fluorescence or extracted from movies using frame-by-frame analysis in ImageJ.

Droplet Analysis by Microchip Electrophoresis. For demonstration of coupling reagent addition to MCE analysis, sets of droplet samples containing either fluorescent dye or water were analyzed as previously described.[142] All parameters were identical except for droplet flow rate during extraction, which was increased to 1000 nL/min to account for two droplets per sample. Sample droplets with average volume of 3.6 ± 0.3 nL (n = 60) were generated from a multiwell plate to consist of alternating sets of two droplets containing either rhodamine or water in 0.5% DMSO (i.e. R-R-W-W, etc.). A fluorescent peptide (8 μM in 80 mM Tris, pH 8) was added to mimic reagent addition conditions during HTS. Flow rates were controlled so that 0.6 nL of reagent was added to each droplet.

Results and Discussion

To significantly reduce sample consumption for HTS and to enable screening of rare or hard to purify enzymes, this work proposes to perform all aspects of sample preparation within nanoliter volume samples. The workflow for analysis consists of three steps: droplet generation, reagent addition, and analysis (Figure 4-1). In most high-throughput analysis facilities, test compounds are arrayed in 96- or 384-well plates for rapid dispensing. Therefore, starting droplets will be formed from compound libraries into a series of test compound droplets. After formation, test compound droplets will be pumped through a microfluidic device to inject picoliter volumes of assay reagents into

69

each droplet and allow reaction incubation. Finally, sample droplets can be analyzed by MCE to determine test compound efficacy. Several groups have reported methods for generating droplets. Therefore, this work will focus on addition of assay reagents and analysis by MCE.
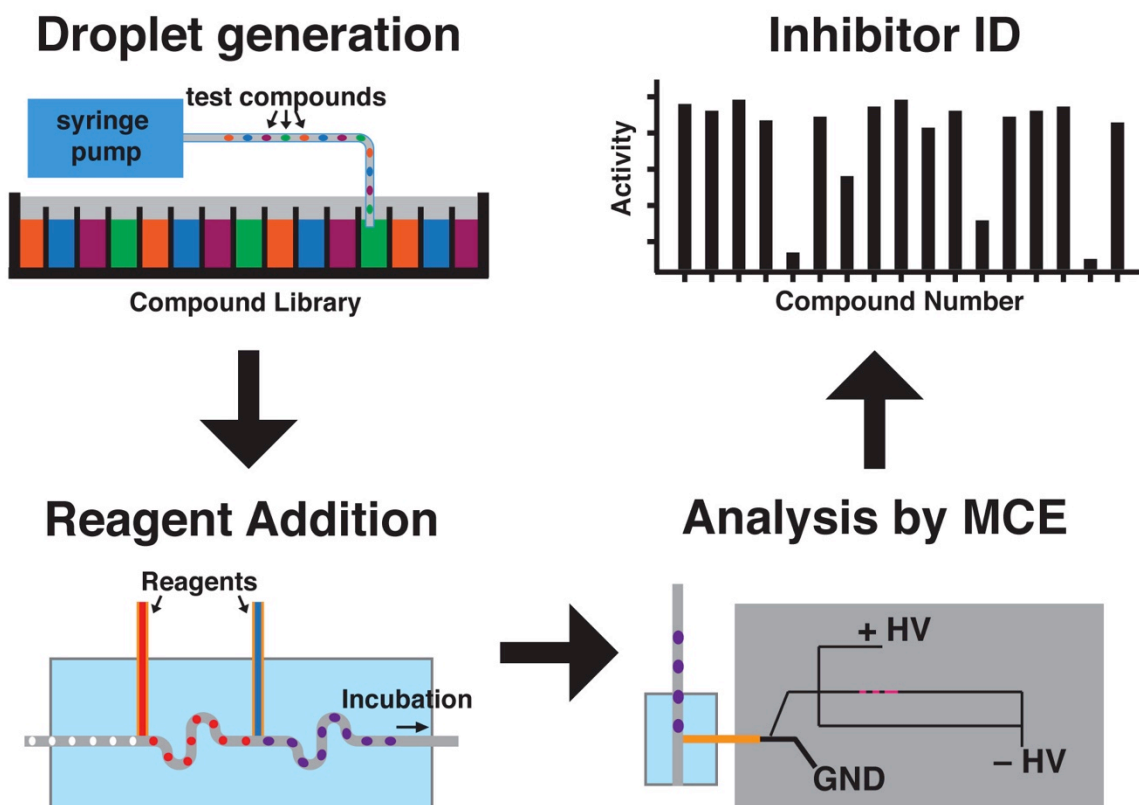
Figure 4-1. Overview of all-droplet high-throughput screening with microchip electrophoresis for detection. Droplets containing test compounds are generated by sipping from an MWP. Reagents (e.g. substrate and enzyme) are directly injected into droplets using a PDMS microfluidic device and collected for incubation. Completed reactions are analyzed by MCE and inhibitors are identified based on amount of substrate and product present in each sample.

Reagent Addition Device Design and Operation. To perform HTS entirely within droplet format, reliable addition of reagents to each droplet is necessary. Several methods exist for adding reagents, but the simplest utilize direct injection of reagents into

passing droplets at tee junction. Several groups have developed these devices in various formats with the common attribute being the use of hydrophilic channels for reagent delivery.[52, 57] Although these devices demonstrated reliable operation within the parameters necessary for HTS, they were either difficult to fabricate[38, 58] or were demonstrated to be compatible with sample droplets formed off of the device.[52, 57]

To address these limitations, we developed a single layer PDMS device for reagent addition using these existing devices as a design guide. The device consists of a tee junction in which the outlet of a fused silica capillary can be oriented flush with the PDMS droplet channel (Figure 4-2). The design is scalable so that several reagents can be added sequentially within a single device by incorporating additional reagent channels similar to existing PDMS reagent addition devices. Additionally, serpentine channels were integrated to facilitate rapid mixing of reagents. We found that using narrow bore reagent capillaries, typically 40 µm i.d. x 150 µm o.d., reduced sample carryover due to lower diffusional mixing as a result of high linear flow rate at the outlet. At smaller inner diameter (e.g. 20 µm i.d. x 150 µm o.d.), the increased surface area of fused silica, due to thicker capillary walls, caused droplet sticking and increased carryover. This effect could be mitigated by either derivatizing the tip of the reagent capillary or using a capillary with smaller outer diameter, such as 20 µm i.d. x 90 µm o.d., which would reduce the hydrophilic surface area of the capillary.
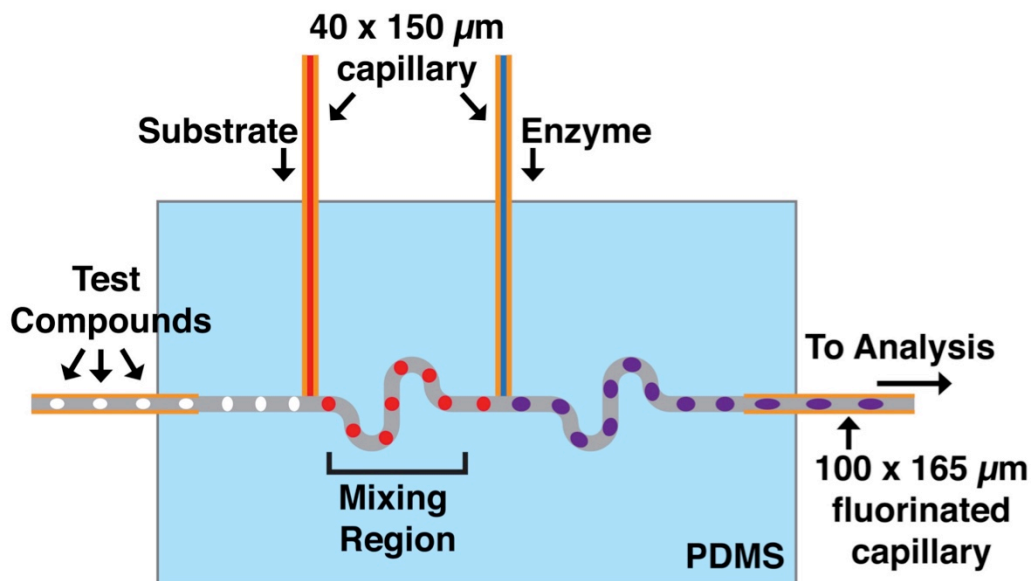
Figure 4-2. Schematic of PDMS droplet reagent addition device. Sample droplets containing test compounds are pumped onto the chip through a fluorinated capillary while reagents are injected via hydrophilic capillaries. Serpentine mixing regions on the device rapidly distribute reagent throughout the droplet. Droplets are collected via another fluorinated capillary for incubation or analysis.

One of the biggest challenges for reagent addition into preformed droplets is transferring sample droplets onto the device without droplet breakup. We chose to use a fluorinated fused silica capillary (100 µm i.d. x 165 µm o.d.) to transfer droplets onto the device (Figure 4-2). Due to the larger cross section, the capillary stretches the PDMS channel forming a tight seal to prevent leaking. Droplet samples transition from capillary to chip without sticking due to he similar dimensions for the capillary and channel. Because most fittings are designed around 360 µm tubing, the transfer capillary was adapted by inserting one end into a length of HFPA+ tubing (150 µm i.d. x 360 µm o.d.). This allowed for zero dead volume connections to droplet storage tubing using a Teflon connector (Figure 4-3).
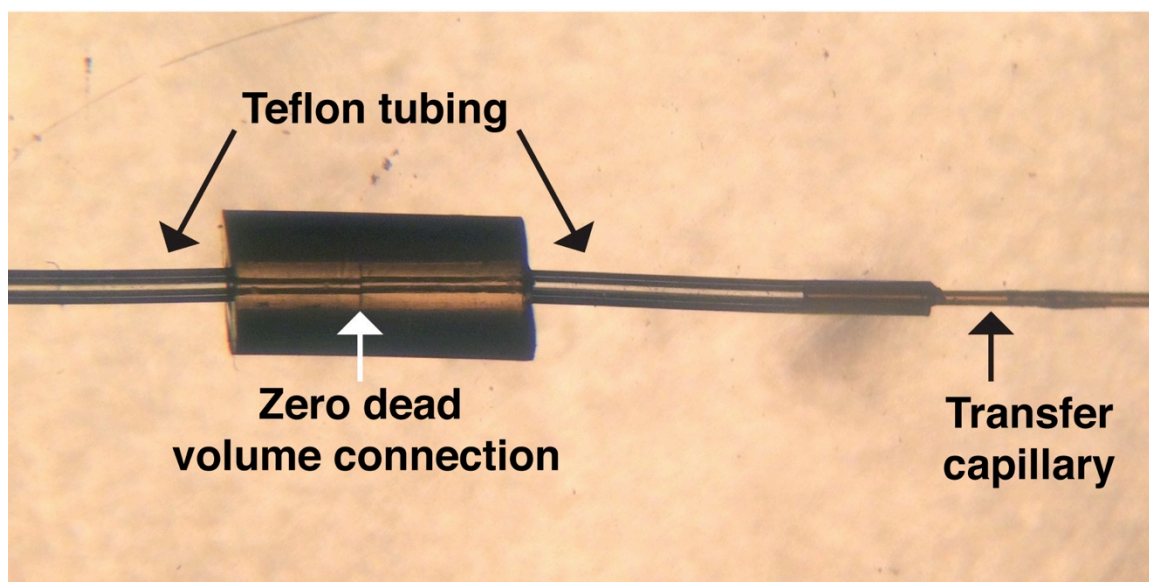
Figure 4-3. Image of zero dead volume Teflon union used to connect Teflon tubing containing sample droplets (left side of image) to the fluorinated transfer capillary. Droplets seamlessly transfer from Teflon-Teflon and from Teflon-capillary with minimal carryover.

Oil phase surfactant (e.g. perfluorooctanol) plays an important role in reagent addition by stabilizing droplets to reduce carryover. However, high surfactant concentrations will overly stabilize droplets and prevent reagents from being added. To determine an acceptable surfactant concentration, reagent addition stability was monitored for experiments using 0-1 % perfluorooctanol as a surfactant. When surfactant concentration was greater than 1 %, coalescence of the reagent stream into the droplet did not occur and reagent only droplets were formed (Figure 4-4A). When the surfactant concentration lowered to 0.5 %, successful reagent addition was observed for every droplet (Figure 4-4B). As the concentration was further reduced to 0 %, reagent addition was successful, but carryover was increased (Figure 4-4B). We hypothesize that at low surfactant concentrations, diffusional mixing between the reagent stream and passing droplet leads to increased carryover. Conversely, at high surfactant concentration the

droplet interface is stabilized and merging with reagent streams does not occur leading to formation of reagent only droplets. Therefore, surfactant concentration was fixed at 0.5 % v/v to provide low carryover and robust reagent addition. Under different conditions, for example high organic content, increased surfactant concentration may be necessary to stabilize droplets and reduce carryover.
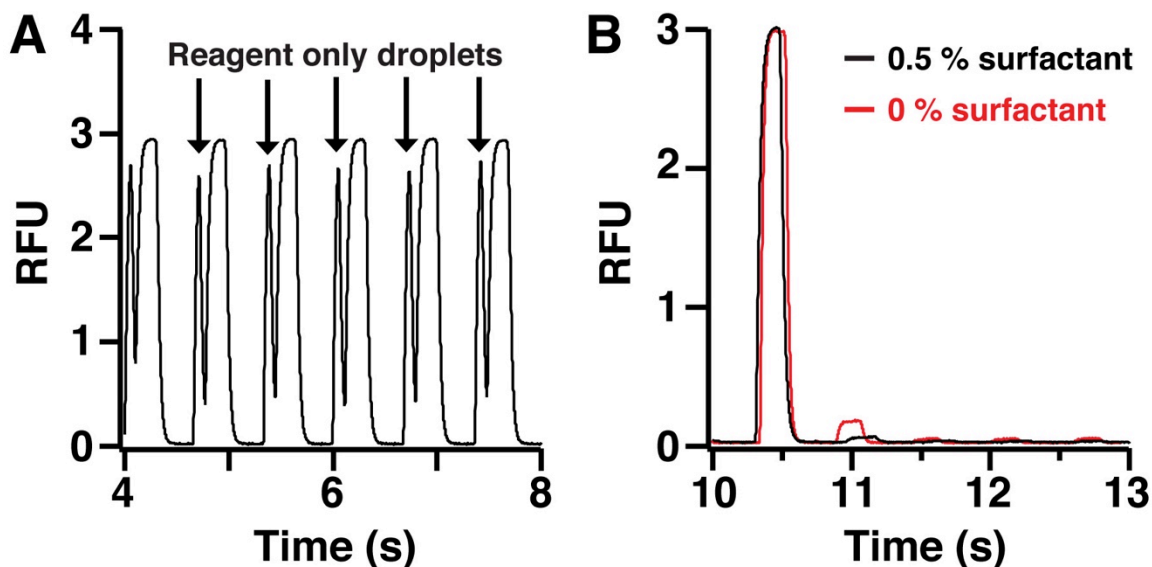
Figure 4-4. Effect of oil phase surfactant concentration on reagent addition and carryover. **A)** At high surfactant concentration (1 %), reagent droplets do not completely merge with passing droplets leading to formation of reagent only droplets. **B)** At low surfactant concentrations, reagent droplets readily merger with passing droplets. However, carryover increases, slightly, as surfactant concentration approaches 0 %.

Characterization of Reagent Addition Throughput and Stability. In HTS, the sample throughput directly correlates to total analysis time and operating at maximum sustainable throughput is beneficial. For compatibility with various analysis methods, our reagent addition device should operate across a range of sample throughputs. To test speed and reproducibility of reagent addition, a dual tee device was fabricated, which allowed formation of and reagent addition into droplets on a single device. The size

droplets and rate of reagent addition was extracted from high-speed video and reagent flow rate was maintained so that 10 percent of the parent droplet volume was added regardless of the droplet flow rate.

As expected, the rate of reagent addition increases linearly with droplet flow rate (Figure 4-5). At a droplet flow rate of 1 µL/min, reagent addition occurs at approximately 1 Hz and increases linearly up to the fastest flow rate tested. However, at high flow rates, reagent addition become unstable and reagent was not added to every droplet. This is likely due to the low dwell time at the reagent capillary and imprecision in flow rate caused by the syringe pumps. Droplet intensity was measured to ensure a similar amount of reagent was added regardless of sample throughput. Based on analysis of 1 min videos at each flow rate, normalized droplet intensity RSD was less than 5 percent across all flow rates (Figure 4-5).
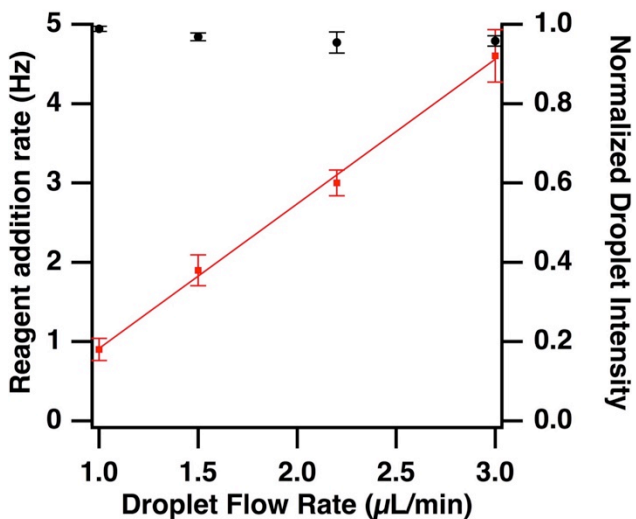
Figure 4-5. Reagent addition throughput increases linearly with droplet flow rate up to 3 µL/min (the fastest flow rate tested). At each flow rate, reagent flow rate was adjusted to achieve 10 percent addition into the parent droplet. Normalized droplet intensity, a measure of reagent addition reliability, is consistent across the flow rates tested.

Measurement of Carryover During Transfer and Addition. Whereas previous demonstrations of reagent addition utilized continuous signal changes (i.e. *in vivo* perfusate[58] or continuous blood perfusion[52]), HTS often has discrete signal changes from sample to sample. Therefore, carryover must be minimized at each step of reagent addition to maintain a high assay quality. Device carryover was monitored a three points during reagent addition to quantify where carryover occurs: transfer of droplets onto the device, first reagent addition, and second reagent addition. To quantify carryover, sets of droplets containing a signal droplet (rhodamine) and four blank droplets were generated. At the first reagent inlet, assay buffer was added (80 mM Tris, pH 8, 8 mM DTT) and enzyme buffer (10 mM sodium phosphate, pH 8, 100 mM sodium chloride, 0.01% Tween 20, 15% glycerol) was added at the second reagent inlet. If carryover is zero percent, one expect no signal from blank droplets and any signal in blank droplets can be considered carryover caused by reagent addition.

During the transfer step, sample droplets are transferred from the collection tubing into a transfer capillary and then onto the PDMS device with minimal carryover (Figure 4-6). The first blank droplet had 0.12 ± 0.04 percent carryover and subsequent blank droplets had 0.01 ± 0.05 percent carryover. This low carryover is made possible by the use of zero dead volume connections and the similar size of the transfer capillary and PDMS channel. More significant carryover is observed after the first reagent is added. However, the cumulative carryover is sequestered in the first blank droplet (2 ± 1 percent) whereas the second blank had negligible carryover (0.03 ± 0.1 percent). After the second reagent addition, cumulative carryover in the first droplet had increased to 5.5

76

± 0.3 percent, but carryover remained low in the second blank droplet (0.5 ± 0.3 percent).

These data suggest that for best results, two droplets should be used per sample.
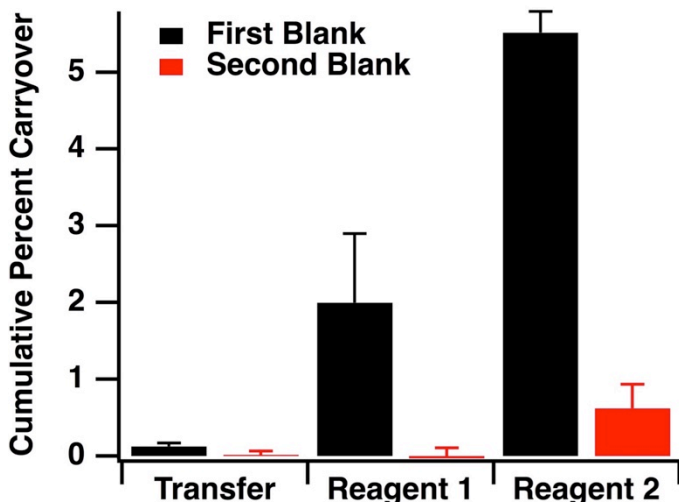
Figure 4-6. Plot of reagent addition carryover in the first and second blank sample at each step of reagent addition. Most carryover is contributed by addition of reagents with reagents containing glycerol and Tween leading to higher carryover. At all steps, carryover is less than 1 percent in the second blank sample suggesting that two droplet per sample should be sufficient to avoid carryover during analysis. The droplet train consisted of alternating sets of a signal droplet followed by four blank droplets (e.g. S-W-W-W-W). In all cases, the last two blank droplets had no carryover.

The increased carryover observed for the second reagent could be due to the presence of 15 % glycerol and 0.01 % Tween 20 in the reagent. Both of these buffer components are necessary to prevent enzyme adsorption, but increase the wettability of the PDMS surfaces leading to increased carryover. However, these values match well with reported carryover for a device fabricated from HFPA+/PVDF in which carryover in the first droplet was ~5 percent and was reduced to less than 1 percent in subsequent droplets.[38]

In addition to carryover caused by reagent addition carryover could occur if analytes partition from the droplet into the oil phase. Once in the oil phase, the analyte

could then partition into adjacent droplets leading to artificial results.[162] Although it is generally accepted that fluorinated oil phases prevent sample-to-sample contamination, the use of non-fluorinated oils (e.g. mineral oil) or inclusion of oil phase surfactants (e.g. RainDance EA-surfactant) results in formation of reverse micelles that can transport analyte from one droplet to another through the carrier fluid.[163, 164] In most cases, this migration occurred over the course of several hours or when using fluorescent dyes. For HTS, many substrates are peptide-based and the peptide sequence can be optimized ot sequester analytes within droplets (i.e. many hydrophilic residues). Additionally, in droplet incubation times are typically much less than 1 hr for HTS and analyte migration should be minimal. However, further investigation is required to quantify this effect when using perfluorodecalin:pefluorooctanol as an oil:surfactant phase.

Coupling Reagent Addition Samples to MCE Analysis. To demonstrate the utility of all-droplet sample preparation for high-throughput analysis, sample droplets were coupled to microchip electrophoresis for analysis. Preformed droplets contained either water or rhodamine and fluorescent peptide was directly injected using the reagent addition device. In order to mimic assay conditions, samples were collected into HFPA+ tubing and allowed to 'incubate' for 30 min before being analyzed by MCE as described previously.[142]

Due to the on chip dead volume and carryover within the first droplet of each sample, peak heights for rhodamine and peptide do not stabilize until the second droplet as observed by MCE (Figure 4-7A). Because each sample is comprised of 2 droplets, 8 replicate injections are made from each droplet and sample throughput is 0.33 Hz. This approach, which lowers throughput from the maximal possible, is necessary to ensure at

least 3 replicate injections are made from the second sample droplet where carry-over is low.

During HTS, raw data is converted to a reaction yield to quantitate test compound efficacy and quickly identify compounds that inhibit enzyme activity. To mimic this data transformation and demonstrate that reagent addition does not affect data quality, the peak area ratio between rhodamine and fluorescent peptide was used for analysis. Furthermore, the average peak area ratio for water and rhodamine containing droplets was used to normalize data. For droplets containing only water, the normalized peak area ratio is 0, because only a peptide peak is observed in the electropherogram. For rhodamine containing samples, both rhodamine and peptide peaks are observed in the electropherogram resulting in a normalized peak area ratio of 1. If significant carryover were observed for either sample type, the peak area ratio would begin to deviate significantly from these values and a rhodamine peak would be observed in electropherograms from water droplets (Figure 4-7B).
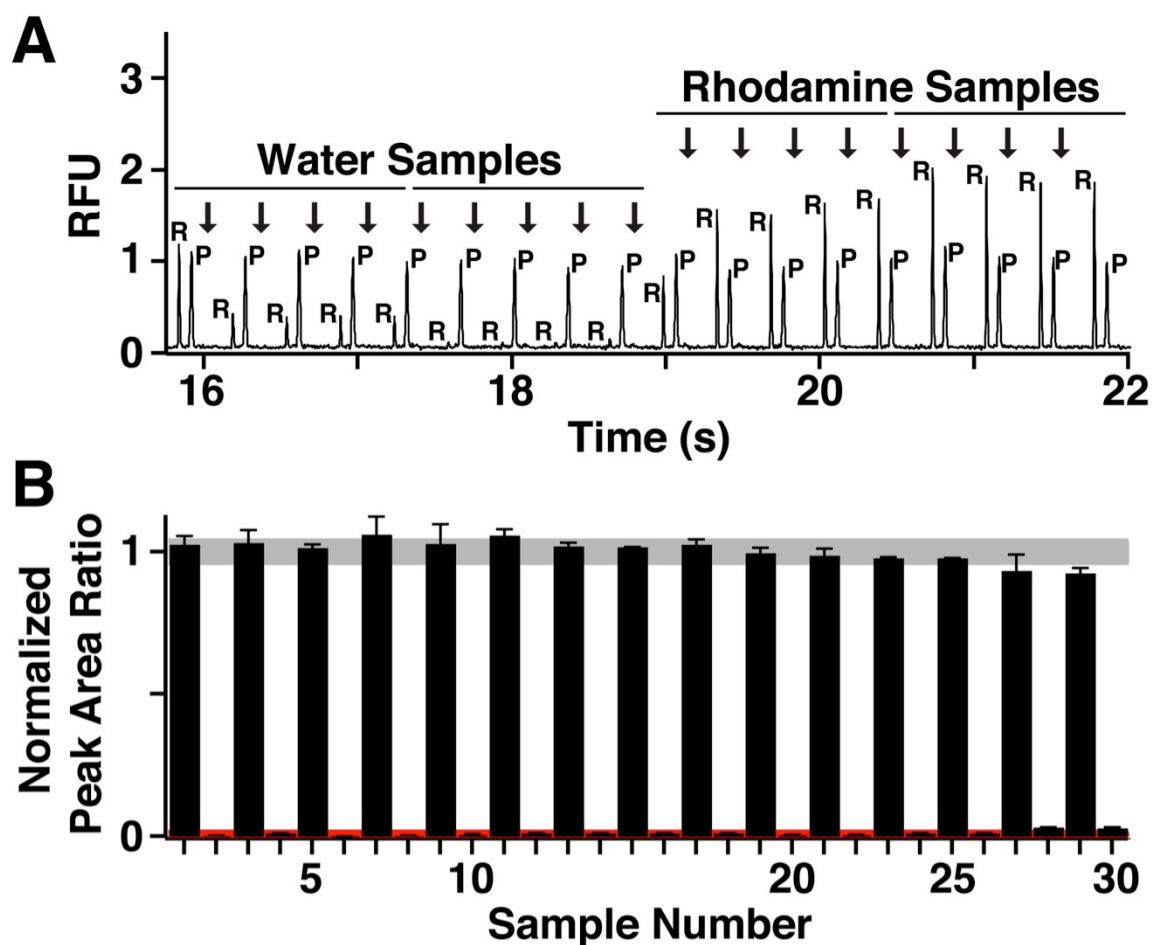
Figure 4-7. Demonstration of coupling reagent addition sample preparation to microchip electrophoresis for analysis. (**A**) Selected raw electropherograms from the analysis of alternating sample sets (two droplets each) demonstrating that carryover is present in the first droplet but is not present in the second sample droplet. Arrows denote MCE injections and the rhodamine (R) and peptide (P) peaks are labeled in each separation. (**B**) Plot of normalized peak area ratio (rhodamine:peptide) from samples containing either rhodamine or water. The shaded regions denote ± 1 standard deviation for the average peak area ratio of each sample type.

Conclusion

We have demonstrated the several aspects of an all-droplet high-throughput screening platform using microchip electrophoresis for biochemical assay screening. We designed a simple PDMS device to allow direct injection of reagents into preformed nanoliter volume droplets. Carryover during the reagent addition steps matches closely to

previously published results for a more complicated device. Sample throughput was 0.33 Hz allowing at least 3 replicate MCE injections from the second droplet with negligible carryover during analysis. This platform should allow for routine sample preparation in droplet format allowing a 1,000-fold reduction in reagent consumption. Although this project demonstrates technological improvements toward all-droplet assays, the lack of widespread adoption is likely due to a number of factors. These factors range from the need to optimize conditions (i.e. oil phase and surfactant concentration) for each sample type, the inability to retest samples without repeating the assay, and the inability to perform continuous operation due to limitations on the number of droplets that can be reliably formed.

Another limitation to widespread adoption is the challenge of forming distinct droplets containing test compounds of interest. This work couples droplets to existing MWP libraries to achieve this task; however, it is relatively low throughput and requires libraries be organized in well plates. An alternative strategy would be to use bead-based chemistry to sequester test compounds and dispense them into droplets as a suspension.[165] The authors demonstrated dispensing beads loaded with a small molecule at up to 10 Hz and exposure to UV radiation disperses the molecule into the droplet. Using this method, a barcoded, bead-based library containing small molecules could be rapidly formatted into droplets to significantly increase the speed of library formation for droplet-based HTS.

CHAPTER 5: FUTURE DIRECTIONS

In this dissertation, the utility of ultrafast electrophoresis coupled to droplet samples for HTS has been described. Although these efforts have demonstrated the throughput necessary for HTS, batch analysis and manual connections limit widespread use. Therefore, automated droplet formation and continuous device operation are desirable. The general principle of mobility shift assays for screening could be applied to other pharmacological targets, such as protein-protein interactions. Lastly, nanoliter volume sample introduction has to potential to greatly reduce sample requirements for other separations based analyses, such as electrochromatography or gel electrophoresis.

Automated and Continuous Droplet Generation

One of the limitations for widespread adoption of droplet-based HTS is the difficulty with continuous operation. Due to back pressure issues, only several hundred droplets can be formed reliably requiring large compound libraries to be analyzed in small sections. In batch analysis mode, continuous operation is only possible if one set of droplets is analyzed while the next is being formed. Inherent to this type of analysis is the requirement for making repeated low dead volume connections, which can be difficult and time consuming. To reduce the number of necessary connections and to achieve the

maximum analysis throughput, droplets should be continuously generated on-line. This could be achieved through a pressure or magnetic driven peristaltic pump.

Peristaltic pumps are used routinely for liquid dispensing in continuous phase systems. In these pumps, two to six 'rollers' are attached to a rotor and compress a flexible tubing cause liquid to flow. As the rollers rotate, the tubing is alternately compressed and released generating a consistent flow rate correlated to the rotor speed. Commercially, this has been developed as the HyperCyt autosampler (IntelliCyt Corp., Albuquerque, NM) used for rapid sample introduction to flow cytometers (Figure 5-1).[166] In the design, samples are arranged in a MWP and reformatted into air-segmented droplets for serial analysis. The sample tubing passes through a peristaltic pump allowing continuous operation by generating suction at the inlet and pressure at the outlet. The system is capable of 0.67 samples per second (2 µL samples) with less than 2 percent carryover. Continuous sample analysis should be possible, with very little modification, by coupling a HyperCyt autosampler directly to the inlet of an MCE device or mass spectrometer. Under these conditions, the operator would simply need to switch out 384 well plates every 10 minutes or a robotic plate handler could be used to achieve complete automation.
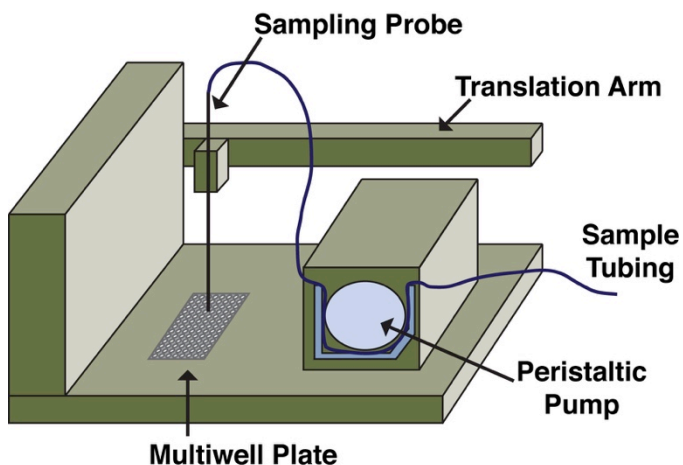
Figure 5-1. Schematic of the HyperCyt platform for high-throughput flow cytometry. A sample probe is translated around an MWP using a computer controlled positioner while air segmented droplets are generated using a peristaltic pump to generate flow.[166] Reproduced with permissions from Nature Publishing Group.

Alternatively, the carrier phase could be replaced with a magnetic ionic liquid (MILs).[167-169] MILs are a sub-class of ionic liquids – room temperature molten salts – that incorporate high spin transition metals making them susceptible to external magnetic fields. If the oil or air carrier phase was replaced with an MIL, an external magnetic field could be used to generate flow within the tubing.[170] For example, several ring-shaped electromagnets could be placed in a series along the droplet tubing. By energizing them in a wave pattern, a traveling magnetic wave could be generated within the droplet tubing creating bulk flow of the magnetic ionic liquid. Because the aqueous samples are dispersed in series within the ionic liquid, they would be dragged along. Assuming sufficient force could be generated, this electromagnetic pump could be used to generate samples from a well plate and push them toward the MCE device for analysis (Figure 5-2). Preliminary work would need to be done to determine the number, placement, and current needed to create sufficient pumping force. However, in a similar method using a ferrofluid, linear flow rates as high up to 7.4 mm/s (40 mL/min) within a PVC pipe (15.4

mm i.d. x 21 mm o.d.) were achieved using 12 A current at 1 kHz when using a 16 electromagnet array.[170] The primary advantage over the HyperCyt method is that droplets would not be compressed in the pump, which may cause coalescence or break up. Additionally, through use of microfabrication strategies a miniaturized pump could be developed allowing integration with existing droplet generation workflows.
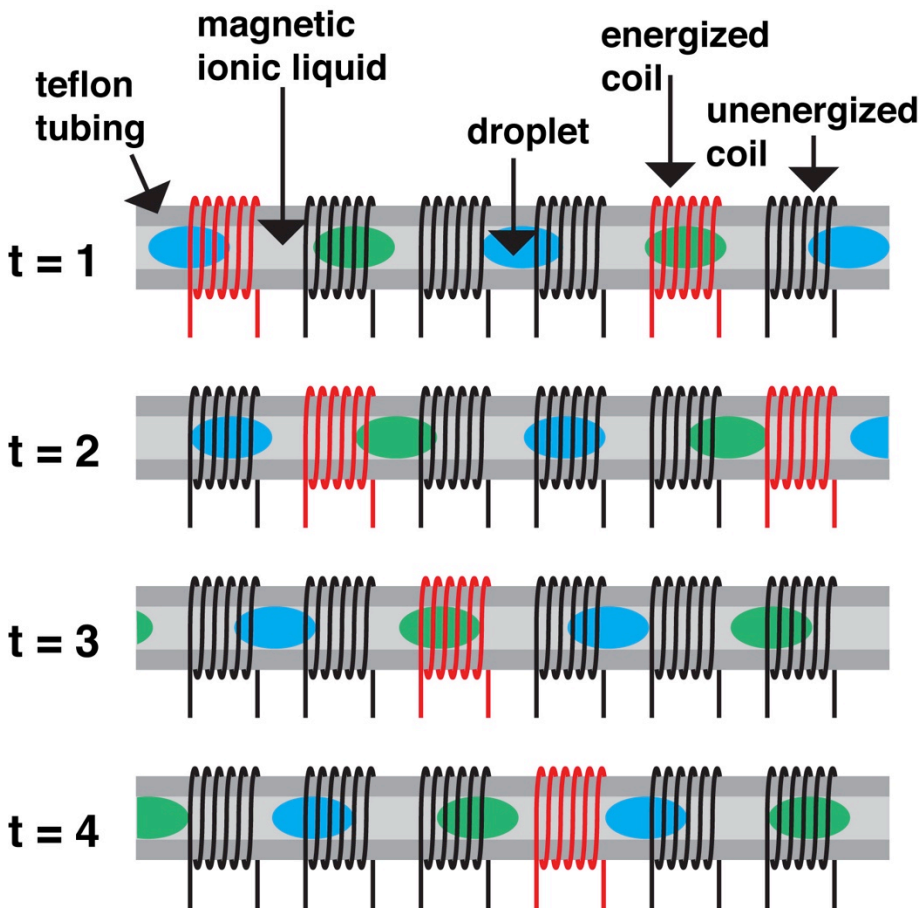
Figure 5-2. Schematic of electromagnetic fluid pump for segmented flow using magnetic ionic liquids (MIL) as the carrier fluid. Several coils of wire would be placed in a series along the Teflon tubing (i.e. electromagnets) and energized sequentially to generate a traveling magnetic wave. This magnetic wave would drive the MIL and droplets through the tubing.

Protein-Protein Interaction Screening by Microchip Electrophoresis

Although the major focus of this thesis was development of analytical methods for screening biochemical assays, the general principles (i.e. mobility shift between substrate and product) could be applied to alternative screening targets. Within the cell, few proteins act independently. Instead, proteins interact as part of large protein complexes held together by non-covalent interactions based on intermolecular forces, such as hydrostatic or hydrophobic interactions. Through these large interactions, collections of proteins can work synergistically to achieve complex cellular functions, such as DNA replication, transcription, or metabolism. Therefore, protein-protein interactions (PPIs) provide useful targets for disease intervention and drug discovery.[171, 172]

Previously in our group, PPI screening based on electrophoresis has been developed for Hsp70-Bag3 interactions.[22] Using affinity probe capillary electrophoresis, a library of over 3000 molecules was screened against this non-covalent complex (Figure 5-3). However, throughput was limited to ~220 samples per day and separation efficiency was poor due to additional pressure driven flow. The long separation time was due to a combination of long detection length and suppression of EOF caused by derivatized capillaries (necessary to prevent protein adsorption). To increase the utility, faster separations and higher throughput are necessary.
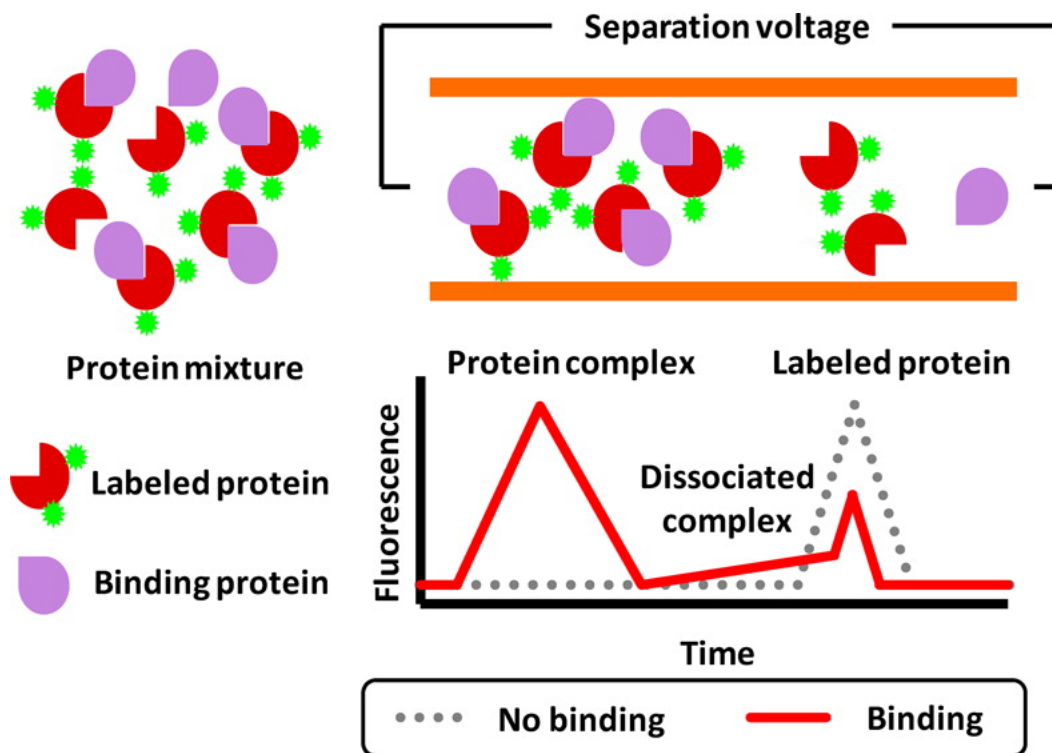
Figure 5-3. Affinity probe capillary electrophoresis for monitoring protein-protein interactions. One protein (affinity probe) is labeled with a fluorescent tag while the other protein is unlabeled. Two peaks are observed in the electropherogram corresponding to the labeled protein and the protein complex (labeled protein bound to unlabeled target).[22] Reproduced with permissions from American Chemical Society.

By adapting the separation to microchip format, shorter separation lengths and high voltages could be used to significantly reduce separation time. Additionally, through the use of high pH buffer (i.e. 10 mM borate at pH 10) and short separation lengths, protein adsorption to channel surfaces could be significantly reduced. Using a glass MCE device with 3 cm separation length, a 15 s separation of the free Hsp70 and Hsp70-Bag3 complex is possible (Figure 5-4A). When injected alone, Alexa Fluor 488-labeled Hsp70 is detected at 12 s, whereas the migration time shifts to 10 s when Hsp70 complexes with Bag3. The addition of unlabeled Hsp70 competes for Bag3 binding resulting in observation of both complex and free Hps70 peaks in the electropherogram. To ensure

that basic separation conditions do not greatly impact complex formation, Hsp70 was

incubated with increasing concentrations of Bag3 to determine the binding constant

(Figure 5-4B). Under these conditions a binding constant of 140 ± 20 nM was calculated

for Hsp70. Using flow cytometry protein interaction assays (FCPIA), the binding

constant was reported to be 14 nM. Although the large difference could be caused by use

of high pH buffers, a binding study with lower Hsp70 concentration is necessary to

accurately determine the binding constant for on chip analysis.
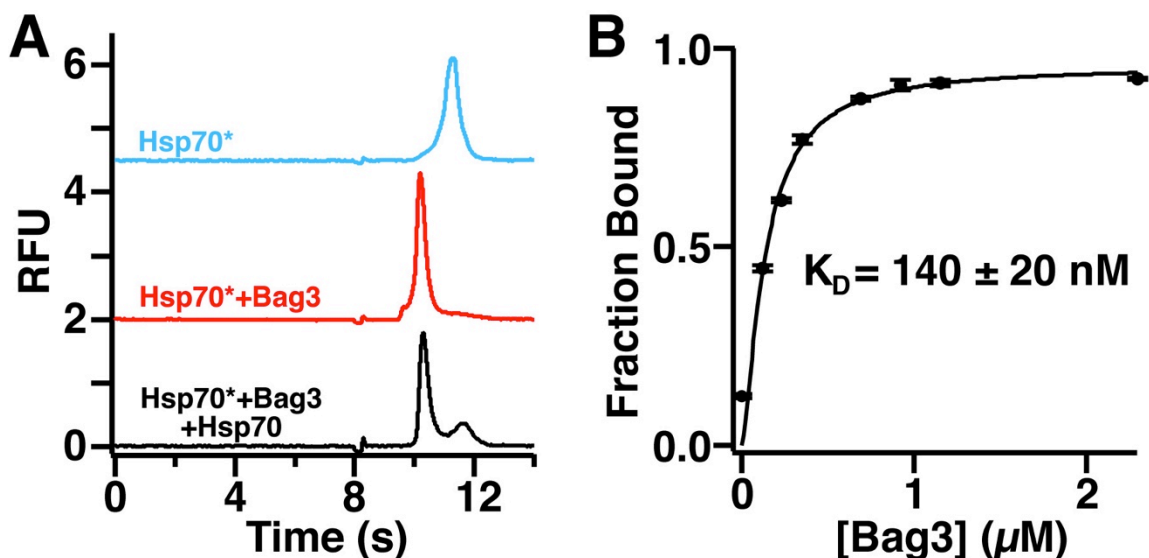
Figure 5-4. Protein-protein interaction monitoring using affinity probe microchip electrophoresis. A) Unbound Hsp70 (blue trace) can be separated from the protein complex (red trace) using a 14 second separation. Competition between labeled and unlabeled Hsp70 for Bag3 binding leads to both peaks in the electropherogram (black trace). B) Binding assay plot for 0.5 µM Hsp70 with Bag3. Binding constant is 140 nM.

Reducing separation time from 6.5 min to 15 s increased throughput 26-fold

relative to the initial CE assay. Additionally, complicated derivatization methods are not

required, as protein adsorption was not observed in a glass MCE device when using basic

buffers. Preliminary droplet experiments suggest that sample introduction is not affected by protein-rich samples though more work is needed to determine long-term stability.

Coupling Droplet Samples to Microchip Electrochromatography

Although zone electrophoresis represents a powerful separation technique for many applications, coupling droplet samples to separation techniques (e.g. LC) would reduce sample requirements for an even broader range of analytes. However, desegmentation of samples prior to analysis by LC, for example, and injection of nanoliter aliquots can be difficult. To address this, other separation modes could be integrated into the existing microchip system to allow routine analysis of droplet samples. In the existing droplet-MCE device, electroosmotic flow is used to move samples around the microchip without the need for valves or external pressure pumps. By maintaining EOF pumping and incorporating a packed chromatographic bed or entangled polymer solution on-chip, electrochromatography or gel electrophoresis separations could be possible (Figure 5-5).

For microchip electrochromatography (MEC), replacing the existing separation channel (3 μm x 36 μm) with a deeper and wider channel (50 μm x 100 μm) would allow for packing with 5-10 μm stationary phase. The bed could be packed through the chip outlet with the narrow channels for sample handling serving as a weir to constrain the particle bed. After packing, a UV curable frit could be formed near the channel outlet to prevent bed movement during analysis. Coupling droplet samples to MEC opens of a number of potential applications. For the analysis of *in vivo* neurochemical samples, our group has previously reported using LC-MS with benzoyl chloride sample derivatization or MCE with naphthalene-2,3-dicarboxaldehyde derivatization for analysis of dialysate samples.[173] Analysis by LC-MS typically requires several microliters of sample, limiting temporal resolution. Analysis by CE is much faster, but is limited to analysis of amino

acid neurotransmitters due to detection limits. (See Appendix C for improvements to neurotransmitter separations by MCE by controlling separation channel parameters.) To improve temporal resolution, samples could be segmented as nanoliter volume droplets and analyzed on chip by CEC to increase the number of analytes that could be monitored relative to previous CE-based separations.[75, 126]

A similar modification of the microchip could be used to analyze protein samples by gel electrophoresis with greatly reduced sample requirements. Using a UV-cured gel phase, an entangled polymer bed could be formed selectively within the separation channel. With the other solutions operating under free solution conditions, sample could be quickly directed toward the flow gated injection cross and injected onto the bed for separation. Our group has pioneered work in microscale western blotting using capillary and microchip electrophoresis.[174, 175] Although each electrokinetic injection requires only a few hundred picoliters of sample, filling the sample reservoir typically requires at least 5-10 μL of sample. Additionally, manually filling sample reservoirs is time consuming and limits sample throughput. To address these challenges, samples could be introduced to the microchip as a series of droplets and sequentially injected onto the gel bed for separation, reducing sample requirements to several nanoliters and allowing higher throughput.
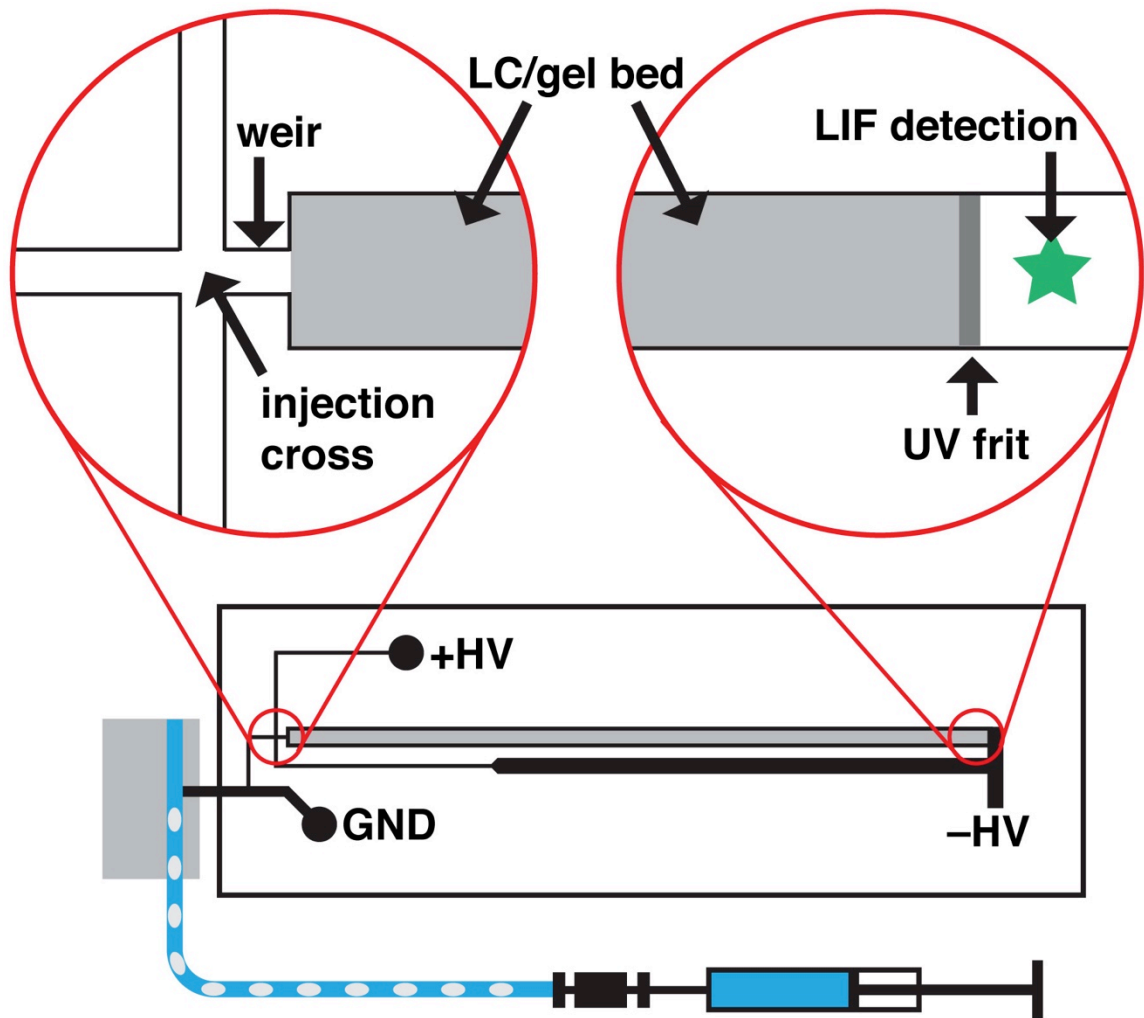
Figure 5-5. Microfluidic device for capillary electrochromatography (CEC) or gel electrophoresis (CGE) from droplet samples. A larger bore channel to accommodate entangled polymer beds or stationary phase replaces the narrow bore electrophoresis channel. The injection cross, with physical weir, and detection point with UV frit are shown in enlarged regions.

APPENDICES

Appendix A

Fabrication Strategies for Deep Etching of Glass Substrates

Fabrication of droplet analysis devices requires deep etching (>75 μm) of capillary insertion channels to facilitate sample transfer. In order to maintain feature fidelity, several substrate optimizations were required. The standard substrate used for glass devices consists of a 0.7-1.1 mm glass slide coated with 530 nm of low reflectivity chromium and 500 nm of AZ1505 photoresist. During etching both coatings are required to prevent wholesale etching of the substrate. Without chrome present, photoresist adhesion to glass is poor and delamination occurs within several minutes of etching. Likewise, without photoresist present to protect the chrome layer, hydrofluoric acid will rapidly etch away the chrome layer leaving a pitted and uneven surface on the substrate.

When etching very deep channels using substrates with both coatings prepared by our glass supplier (Telic Company), some devices would come out with rough channel features that were highly anisotropic in etching pattern (i.e. more horizontally etched than vertically etched) making them unusable (Figure A-1A). This phenomenon was dubbed 'rough etching' and occurred in 25 to 40 percent of devices and varied greatly from batch to batch. The high random occurrence and etching anisotropy suggested that chrome adhesion was poor leading to flaking during long etches. Cleaning and polishing glass

93

substrates prior to sputter chrome was tested, but proved unsuccessful at mitigating the issue.

After much experimentation and step-by-step investigation of the substrates, chrome layer stress induced by sputter coating was identified as the issue. To relive the stress and improve etching, glass slides were coated with chrome and annealed at 310 °C for 3 hr prior to spinning AZ1505 photoresist. Under these conditions, etching up to 200 μm deep features was possible without issues related to chrome layer adhesion (Figure A-1B). Using the same substrate (prior to annealing), rough etching is observed. Although the effect is most noticeable when etching deep features, significantly surface roughness was observed even for shallow features (<10 μm). Therefore, it is recommended to anneal any glass slides used for deep features or in cases when high feature fidelity is required.
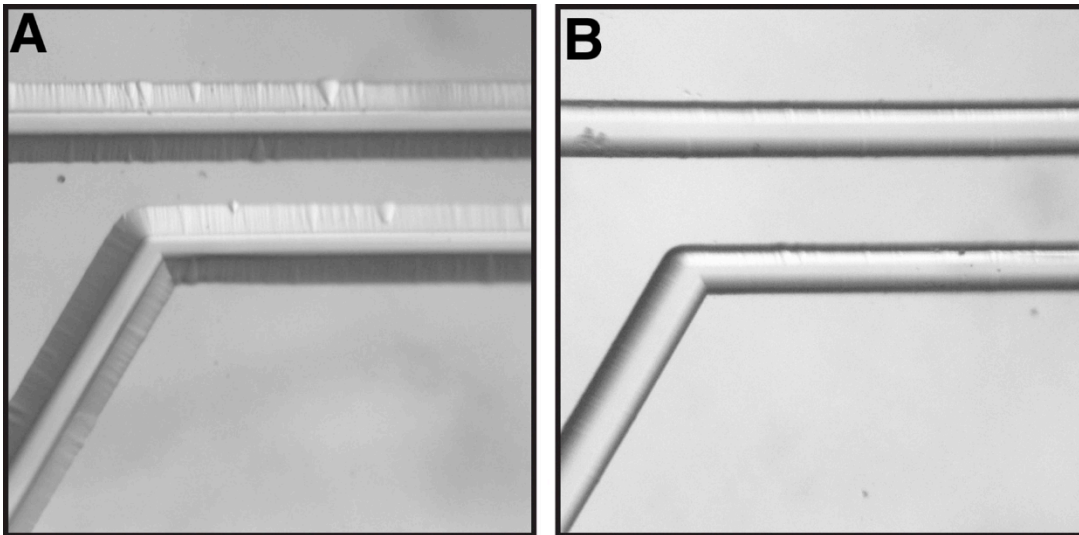
Figure A-1. Images of rough (A) and smooth (B) etching of glass slides. In the rough etched image, the channel is much wider due to anisotropic etching and the walls are not smooth. After annealing, isotropic etching occurs and channels have smooth surfaces.
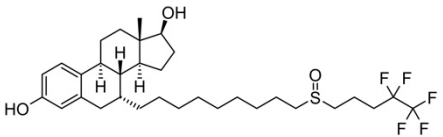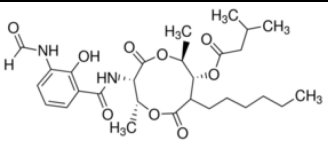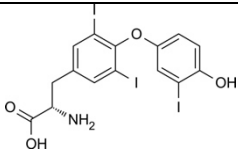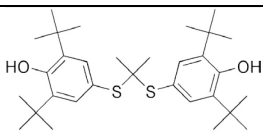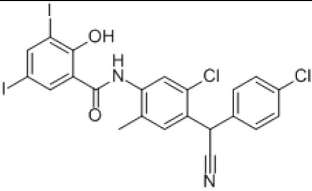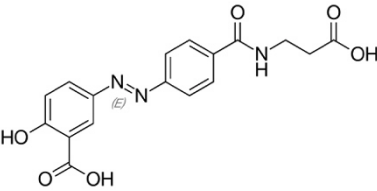
Because the manufacturer is unable to anneal the chrome layer prior to shipment, substrates should be ordered without photoresist and annealed in lab. After annealing the chrome layer, photoresist must be applied using the following procedure (Figure A-2). Hexamethyldisilazane, an adhesion promoter, is applied to the substrate using a spin coater at 500 RPM for 15 s. AZ1505 photoresist is dispensed to evenly cover the entire substrate and a 500 nm layer is formed by spinning at 4000 RPM for 45 s. After spinning, substrates are placed on a hot plate at 100 °C for 50 s to soft-bake the photoresist. (Note: It is crucial that a hot plate be used for all baking steps, as contact heat is required for even solvent evaporation.) If an oven will be used, optimization is necessary. After cooling, substrates are exposed through a photomask for ~9 s and photoresist is developed (AZ726 developer) for 40 s with gentle shaking. Uncovered chrome is etched in CR1A chrome etching for 2 min to expose glass for HF etching. Substrates should be rinsed in deionized water, dried under nitrogen, and placed on a hot plate at 115 °C for 1 min to set photoresist. At this point, taping and HF etching can proceed as normal.
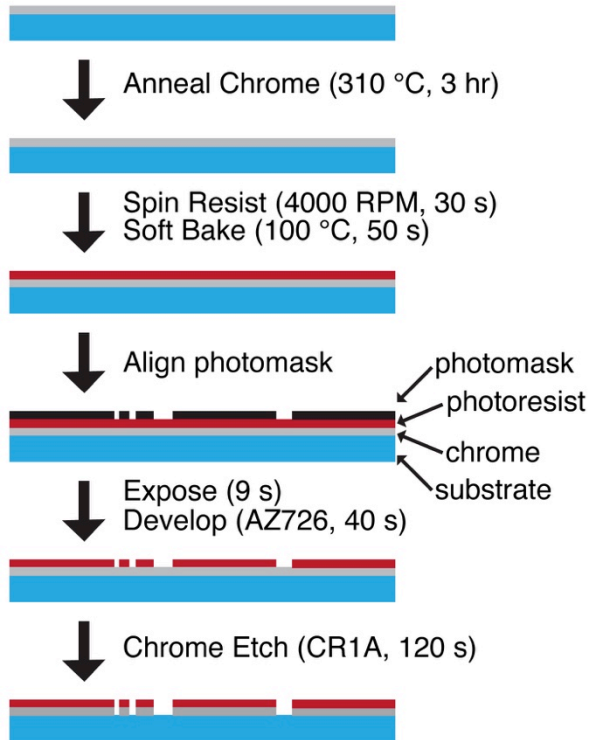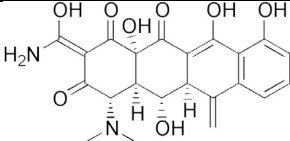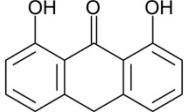
Figure A-2. Overview of fabrication process for deep feature etching with high fidelity. Chrome coated substrates are annealed at 310 °C for 3 hr prior to spin coating 500 nm of AZ1505 resist. After soft baking, photomask pattern is transferred by UV exposure. Photoresist is developed and exposed chrome is etched to reveal glass substrate for HF etching.

Appendix B

Inhibitor Structure and Potency from SIRT5 Screening

Compound	Structure	IC$_{50}$ (μM)	Curve Fit
Fulvestrant		2.6	0.9055
Antimycin A		90	0.6418
Thyroxine		2.2	0.9569
Probucol		1.6	0.9685
Closantel		2.7	0.9350
Balsalazide		3.9	0.9214

Methacylcine		3.6	0.9281
Anthralin		0.1	0.9176

Appendix C

Effect of Channel Geometry on Separation Speed and Efficiency

In electrophoretic separations, efficiency is a measure of separation quality and can be determined from the following equation:

$$N = \frac{t_{mig}^2}{\sigma_{tot}^2}$$

in which t_{mig} is analyte migration time and σ_{tot} is the total zone variance from all sources of band broadening. Of these, Joule heating can significantly reduce separation efficiency through the formation of temperature gradients caused by resistive heating of the separation buffer under high electric field. These temperature gradients lead to differences in mobility within the analytes zone causing broader peaks. To mitigate these effects, narrow bore capillaries are used to improve heat dissipation due to increased surface area-to-volume ratio. Within microchips, heat dissipation primarily occurs through the top and bottom of the microchannel where the substrate is thinnest and to a lesser extend out the sides of the channel. Historically, capillary-based separations have higher efficiency (>500,000 theoretical plates) due to more efficient heat dissipation allowing application of higher electric fields. On the other hand, microchip separations, have separation efficiency less than 250,000 theoretical plates.

To investigate the effect of channel cross section, which impacts surface area-to-volume ratio, devices with channel depths of 6 μm and 3 μm were used to separate a set of derivatized amino acids. In both cases, the channels are thin and wide to provide more surface area on the top and bottom of the channel for heat dissipation. For a 6 μm x 42 μm channel, the surface area-to-volume ratio is 0.37 and a 3 μm x 36 μm channel has a ratio of 0.72 allowing for better heat dissipation. When the same electric field is applied –

1,100 V/cm – the current is 40 percent lower on a 3 μm chip significantly reducing joule heating. This is evidenced in the electropherograms for each condition. With 6 μm channels, separation efficiency is 200,000 theoretical plates and plate height is 550 nm. Baseline resolution is not achieved between all analytes and only moderate separation is observed between D- and L-aspartate (Figure C-1A). In contrast, when channel height is reduced to 3 μm, efficiency improves to ~400,000 plates with a plate height of 275 nm. Baseline resolution is observed between all analytes, including chiral separation of D- and L-aspartate (Figure C-1B). Qualitatively, this can be observed as much sharper peaks for all analytes compared to deep channels. Further reduction in channel cross-section (2 μm x 34 μm) resulted in reduced current but separation efficiency was not improved and microchannels were easily clogged.
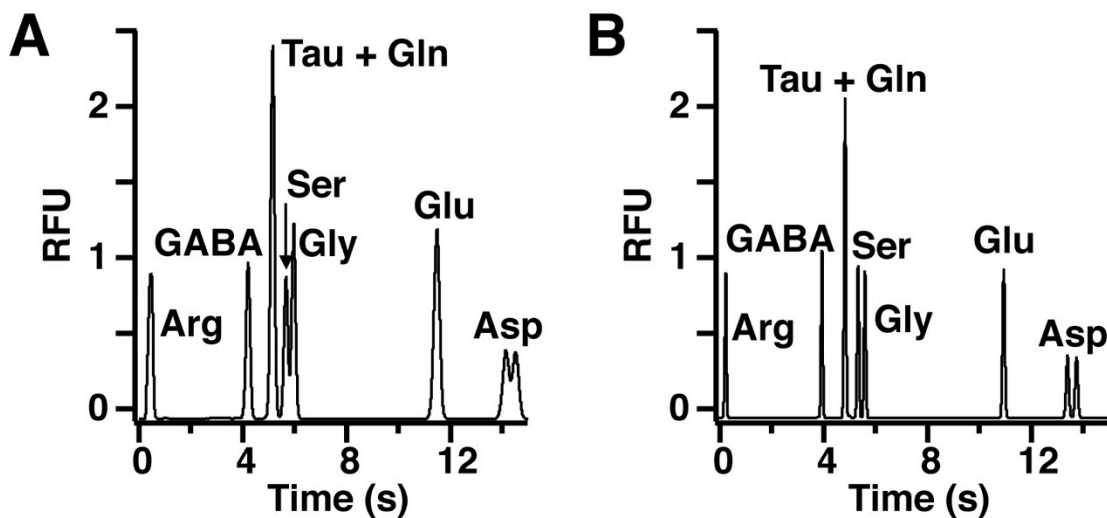
Figure C-1. Reduction in channel depth from 6 μm (A) to 3 μm (B) results in 2-fold improvement to separation efficiency as measured by theoretical plates. For both devices, applied electric field was 1,100 V/cm, LIF detection occurred at 11.1 cm, and background electrolyte was 10 mM sodium tetraborate, pH 10 with 0.9 mM hydroxyproply-β-cylcodextran.

Although separation efficiency is greatly improved, separation time remains relatively long (15 seconds with overlapping injections) limiting analysis throughput. CE theory states that separation length can be reduced, under the same applied voltage, without sacrificing separation efficiency and resulting in faster separations. To test this, devices with 3 μm deep channels were fabricated with 12 cm and 4 cm separation lengths. The same voltage was applied resulting in higher electric field on the 4 cm device (2,800 V/cm). On the shorter chip, separation time was reduced to 2 seconds using an overlapped injection (Figure C-2). Separation efficiency, measured in theoretical plates, was reduced to 130,000; however, plate height was 230 nm, which is similar to chips with longer channels. The reduced efficiency could be attributed to over-injection caused by the high electric field and software limit of 10 ms injections. With independent control of injection voltage, it is anticipated that separation efficiency could be further improved by reducing injection volume.
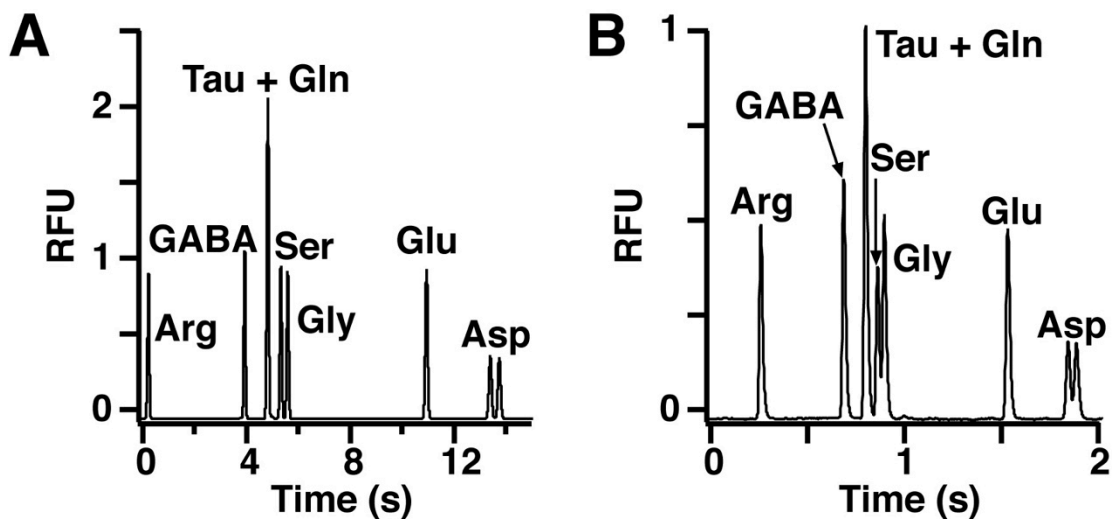
Figure C-2. Reduction in channel length from 12 cm (**A**) to 4 cm (**B**) while maintaining the same applied voltage results in short separation times with similar separation

efficiency. Electric field was 1,100 V/cm for A and 2,800 V/cm for B with the same background electrolyte as in Figure B-1.

These improvements move microchip electrophoresis significantly closer to traditional capillary separations in terms of efficiency, when comparing relatively long channels. By reducing separation length, a fast and efficient separation of labeled neurotransmitters is possible. This opens up a number of possibilities for *in vivo* chemical monitoring by allowing multi-analyte detection without sacrificing temporal resolution. Several challenges remain with using these separations. Injection control software to allow shorter injections or lower field during injection is necessary to improve efficiency. Additionally, achieving high electric field on chip requires application of very high voltages (-12 kV and + 8 kV) and arcing is common. To improve long-term operation at high voltages, an improved electrode design with better insulation is necessary.

REFERENCES

(1)   Gómez-Hens, A.; Aguilar-Caballos, M. P. *TrAC, Trends Anal Chem* **2007**, *26*, 171-182.

(2)   Inglese, J.; Johnson, R. L.; Simeonov, A.; Xia, M.; Zheng, W.; Austin, C. P.; Auld, D. S. *Nat Chem Biol* **2007**, *3*, 466-479.

(3)   Hodder, P.; Mull, R.; Cassaday, J.; Berry, K.; Strulovici, B. *J Biomol Screen* **2004**, *9*, 417-426.

(4)   Hodgson, L. *ACS Chem Biol* **2008**, *3*, 335-337.

(5)   Miraglia, S.; Swartzman, E. E.; Mellentin-Michelotti, J.; Evangelista, L.; Smith, C.; Gunawan, I.; Lohman, K.; Goldberg, E. M.; Manian, B.; Yuan, P.-M. *J Biomol Screen* **1999**, *4*, 193-204.

(6)   Hopkins, A. L.; Groom, C. R. *Nat Rev Drug Discov* **2002**, *1*, 727-730.

(7)   Zheng, C. J.; Han, L. Y.; Yap, C. W.; Ji, Z. L.; Cao, Z. W.; Chen, Y. Z. *Pharmacol Rev* **2006**, *58*, 259-279.

(8)   Rotman, B.; Zderic, J. A.; Edelstein, M. *Proc Natl Acad Sci U S A* **1963**, *50*, 1-6.

(9)   Shiau, A. K.; Massari, M. E.; Ozbal, C. C. *Comb Chem High T Scr* **2008**, *11*, 231-372.

(10)   Ackermann, B. L.; Berna, M. J.; Eckstein, J. A.; Ott, L. W.; Chaudhary, A. K. *Annu Rev Anal Chem* **2008**, *1*, 357-396.

(11)   Comess, K. M.; Schurdak, M. E.; Voorbach, M. J.; Coen, M.; Trumbull, J. D.; Yang, H.; Gao, L.; Tang, H.; Cheng, X.; Lerner, C. G.; McCall, J. O.; Burns, D. J.; Beutel, B. A. *J Biomol Screen* **2006**, *11*, 743-754.

(12)   Fuhrer, T.; Heer, D.; Begemann, B.; Zamboni, N. *Anal Chem* **2011**, *83*, 7074-7080.

(13)   Hsieh, F.; Keshishian, H.; Muir, C. *J Biomol Screen* **1998**, *3*, 189-198.

(14)   Leveridge, M.; Buxton, R.; Argyrou, A.; Francis, P.; Leavens, B.; West, A.; Rees, M.; Hardwicke, P.; Bridges, A.; Ratcliffe, S.; Chung, C.-w. *J Biomol Screen* **2013**.

(15)   Pavlic, M.; Schubert, B.; Libiseller, K.; Oberacher, H. *Forensic Sci Int* **2010**, *197*, 40-47.

(16)   Roddy, T. P.; Horvath, C. R.; Stout, S. J.; Kenney, K. L.; Ho, P.-I.; Zhang, J.-H.; Vickers, C.; Kaushik, V.; Hubbard, B.; Wang, Y. K. *Anal Chem* **2007**, *79*, 8207-8213.

(17)   Jorgenson, J. W.; Lukacs, K. D. *Anal Chem* **1981**, *53*, 1298-1302.

(18)   Harrison, D. J.; Manz, A.; Fan, Z.; Luedi, H.; Widmer, H. M. *Anal Chem* **1992**, *64*, 1926-1932.

(19)   Manz, A.; Fettinger, J. C.; Verpoorte, E.; Lüdi, H.; Widmer, H. M.; Harrison, D. J. *TrAC, Trends Anal Chem* **1991**, *10*, 144-149.

(20)   Kennedy, R. T.; German, I.; Thompson, J. E.; Witowski, S. R. *Chem Rev* **1999**, *99*, 3081-3132.

(21)   Cheng, Y. F.; Dovichi, N. J. *Science* **1988**, *242*, 562-564.

(22)   Rauch, J. N.; Nie, J.; Buchholz, T. J.; Gestwicki, J. E.; Kennedy, R. T. *Anal Chem* **2013**, *85*, 9824-9831.

(23)   Fan, Y.; Ludewig, R.; Imhof, D.; Scriba, G. K. E. *Electrophoresis* **2008**, *29*, 3717-3723.

(24)   Fan, Y.; Ludewig, R.; Scriba, G. K. E. *Anal Biochem* **2009**, *387*, 243-248.

(25)   Liu, Y.; Gerber, R.; Wu, J.; Tsuruda, T.; McCarter, J. D. *Anal Biochem* **2008**, *378*, 53-59.

(26)   PerkinElmer. LabChip EZ Reader MSA assays. http://www.perkinelmer.com/Resources/TechnicalResources/ApplicationSupport Knowledgebase/LabChip/labchip_ezreader.xhtml (accessed Sep 20, 2015)

(27)   Trivedi, V.; Doshi, A.; Kurup, G. K.; Ereifej, E.; Vandevord, P. J.; Basu, A. S. *Lab Chip* **2010**, *10*, 2433-2442.

(28)   Skeggs, L. *Am J Clin Pathol* **1957**, *28*, 311-322.

(29)   Skeggs, L. T.; Hochstrasser, H. *Clin Chem* **1964**, *10*, 918-936.

(30)   Baret, J.-C. *Lab Chip* **2012**, *12*, 422-433.

(31)   Anna, S. L.; Bontoux, N.; Stone, H. A. *Appl Phys Lett* **2003**, *82*, 364.

(32)   Song, H.; Tice, J. D.; Ismagilov, R. F. *Angew Chem Int Ed* **2003**, *42*, 768-772.

(33)   Garstecki, P.; Fuerstman, M. J.; Stone, H. A.; Whitesides, G. M. *Lab Chip* **2006**, *6*, 437-446.

(34)   Ward, T.; Faivre, M.; Abkarian, M.; Stone, H. A. *Electrophoresis* **2005**, *26*, 3716-3724.

(35)   Chabert, M.; Dorfman, K. D.; de Cremoux, P.; Roeraade, J.; Viovy, J.-L. *Anal Chem* **2006**, *78*, 7722-7728.

(36)   Pei, J.; Li, Q.; Kennedy, R. *J Am Soc Mass Spectrom* **2010**, *21*, 1107-1113.

(37)   Pei, J.; Li, Q.; Lee, M. S.; Valaskovic, G. A.; Kennedy, R. T. *Anal Chem* **2009**, *81*, 6558-6561.

(38)   Sun, S.; Slaney, T. R.; Kennedy, R. T. *Anal Chem* **2012**, *84*, 5794-5800.

(39)   Adamson, D. N.; Mustafi, D.; Zhang, J. X. J.; Zheng, B.; Ismagilov, R. F. *Lab Chip* **2006**, *6*, 1178-1186.

(40)   Choi, J.-H.; Lee, S.-K.; Lim, J.-M.; Yang, S.-M.; Yi, G.-R. *Lab Chip* **2010**, *10*, 456-461.

(41)   Link, D. R.; Anna, S. L.; Weitz, D. A.; Stone, H. A. *Phys Rev Lett* **2004**, *92*, 054503.

(42)   Nie, J.; Kennedy, R. T. *Anal Chem* **2010**, *82*, 7852-7856.

(43)   Christopher, G. F.; Bergstein, J.; End, N. B.; Poon, M.; Nguyen, C.; Anna, S. L. *Lab Chip* **2009**, *9*, 1102-1109.

(44)   Fidalgo, L. M.; Abell, C.; Huck, W. T. S. *Lab Chip* **2007**, *7*, 984-986.

(45)   Mazutis, L.; Baret, J.-C.; Griffiths, A. D. *Lab Chip* **2009**, *9*, 2665-2672.

(46)   Niu, X.; Gulati, S.; Edel, J. B.; deMello, A. J. *Lab Chip* **2008**, *8*, 1837-1841.

(47)   Zagnoni, M.; Cooper, J. M. *Lab Chip* **2009**, *9*, 2652-2658.

(48)   Casadevall i Solvas, X.; Srisa-Art, M.; deMello, A. J.; Edel, J. B. *Anal Chem*
         2010, *82*, 3950-3956.

(49)   Liau, A.; Karnik, R.; Majumdar, A.; Cate, J. H. D. *Anal Chem* **2005**, *77*, 7618-
         7625.

(50)   Shestopalov, I.; Tice, J. D.; Ismagilov, R. F. *Lab Chip* **2004**, *4*, 316-321.

(51)   Song, H.; Bringer, M. R.; Tice, J. D.; Gerdts, C. J.; Ismagilov, R. F. *Appl Phys
         Lett* **2003**, *83*, 4664.

(52)   Song, H.; Li, H.-W.; Munson, M. S.; Van Ha, T. G.; Ismagilov, R. F. *Anal Chem*
         2006, *78*, 4839-4849.

(53)   Agresti, J. J.; Antipov, E.; Abate, A. R.; Ahn, K.; Rowat, A. C.; Baret, J.-C.;
         Marquez, M.; Klibanov, A. M.; Griffiths, A. D.; Weitz, D. A. *Proc Natl Acad Sci*
         2010, *107*, 4004-4009.

(54)   Baret, J.-C.; Miller, O. J.; Taly, V.; Ryckelynck, M.; El-Harrak, A.; Frenz, L.;
         Rick, C.; Samuels, M. L.; Hutchison, J. B.; Agresti, J. J.; Link, D. R.; Weitz, D.
         A.; Griffiths, A. D. *Lab Chip* **2009**, *9*, 1850-1858.

(55)   Chabert, M.; Viovy, J.-L. *Proc Natl Acad Sci* **2008**, *105*, 3191-3196.

(56)   Zhang, K.; Liang, Q.; Ma, S.; Mu, X.; Hu, P.; Wang, Y.; Luo, G. *Lab Chip* **2009**,
         9, 2992-2999.

(57)   Li, L.; Boedicker, J. Q.; Ismagilov, R. F. *Anal Chem* **2007**, *79*, 2756-2761.

(58)   Slaney, T. R.; Nie, J.; Hershey, N. D.; Thwar, P. K.; Linderman, J.; Burns, M. A.;
         Kennedy, R. T. *Anal Chem* **2011**, *83*, 5207-5213.

(59)   Niu, X.; Gielen, F.; Edel, J. B.; deMello, A. J. *Nat Chem* **2011**, *3*, 437-442.

(60)   Song, H.; Ismagilov, R. F. *J Am Chem Soc* **2003**, *125*, 14613-14619.

(61)   Macarrón, R.; Hertzberg, R. *Mol Biotechnol* **2011**, *47*, 270-285.

(62)   Zheng, B.; Roach, L. S.; Ismagilov, R. F. *J Am Chem Soc* **2003**, *125*, 11170-
         11171.

(63)   Miller, O. J.; Harrak, A. E.; Mangeat, T.; Baret, J.-C.; Frenz, L.; Debs, B. E.;
         Mayot, E.; Samuels, M. L.; Rooney, E. K.; Dieu, P.; Galvan, M.; Link, D. R.;
         Griffiths, A. D. *Proc Natl Acad Sci* **2012**, *109*, 378-383.

(64)   Brouzes, E.; Medkova, M.; Savenelli, N.; Marran, D.; Twardowski, M.;
         Hutchison, J. B.; Rothberg, J. M.; Link, D. R.; Perrimon, N.; Samuels, M. L. *Proc
         Natl Acad Sci* **2009**, *106*, 14195-14200.

(65)   Zec, H.; Rane, T. D.; Wang, T.-H. *Lab Chip* **2012**, *12*, 3055-3062.

(66)   Boedicker, J. Q.; Li, L.; Kline, T. R.; Ismagilov, R. F. *Lab Chip* **2008**, *8*, 1265-
         1272.

(67)   Angelescu, D. E.; Mercier, B.; Siess, D.; Schroeder, R. *Anal Chem* **2010**, *82*,
         2412-2420.

(68)   Edgar, J. S.; Pabbati, C. P.; Lorenz, R. M.; He, M.; Fiorini, G. S.; Chiu, D. T.
         Anal Chem **2006**, *78*, 6948-6954.

(69)   Kelly, R. T.; Page, J. S.; Marginean, I.; Tang, K.; Smith, R. D. *Angew Chem Int
         Ed* **2009**, *48*, 6832-6835.

(70)   Niu, X. Z.; Zhang, B.; Marszalek, R. T.; Ces, O.; Edel, J. B.; Klug, D. R.;
         deMello, A. J. *Chem Commun* **2009**, 6159-6161.

(71)   Niu, X.; Pereira, F.; Edel, J. B.; de Mello, A. J. *Anal Chem* **2013**, *85*, 8654-8660.

(72)   Pei, J.; Nie, J.; Kennedy, R. T. *Anal Chem* **2010**, *82*, 9261-9267.

(73)   Pereira, F.; Niu, X.; deMello, A. J. *PLoS ONE* **2013**, *8*, e63087.

(74)   Roman, G. T.; Wang, M.; Shultz, K. N.; Jennings, C.; Kennedy, R. T. *Anal Chem*
         2008, *80*, 8231-8238.

(75)   Wang, M.; Roman, G. T.; Perry, M. L.; Kennedy, R. T. *Anal Chem* **2009**, *81*,
         9072-9078.

(76)   DeLaMarre, M. F.; Shippy, S. A. *Anal Chem* **2014**, *86*, 10193-10200.

(77)   Fidalgo, L. M.; Whyte, G.; Ruotolo, B. T.; Benesch, J. L. P.; Stengel, F.; Abell,
         C.; Robinson, C. V.; Huck, W. T. S. *Angew Chem Int Ed* **2009**, *48*, 3665-3668.

(78)   Filla, L. A.; Kirkpatrick, D. C.; Martin, R. S. *Anal Chem* **2011**, *83*, 5996-6003.

(79)   Wang, M.; Slaney, T.; Mabrouk, O.; Kennedy, R. T. *J Neurosci Methods* **2010**,
         190, 39-48.

(80)   Imai, S.-i.; Armstrong, C. M.; Kaeberlein, M.; Guarente, L. *Nature* **2000**, *403*,
         795-800.

(81)   Imai, S.-i.; Guarente, L. *Trends Pharmacol Sci* **2010**, *31*, 212-220.

(82)   Michan, S.; Sinclair, D. *Biochem J* **2007**, *404*, 1-13.

(83)   Landry, J.; Sutton, A.; Tafrov, S. T.; Heller, R. C.; Stebbins, J.; Pillus, L.; Sternglanz, R. *Proc Natl Acad Sci* **2000**, *97*, 5807-5811.

(84)   Michishita, E.; Park, J. Y.; Burneskis, J. M.; Barrett, J. C.; Horikawa, I. *Mol Biol Cell* **2005**, *16*, 4623-4635.

(85)   Chang, H.-C.; Guarente, L. *Trends Endocrin Met* **2014**, *25*, 138-145.

(86)   Hall, J. A.; Dominy, J. E.; Lee, Y.; Puigserver, P. *J Clin Invest* **2013**, *123*, 973-979.

(87)   Guarente, L. *Nature* **2006**, *444*, 868-874.

(88)   Du, J.; Zhou, Y.; Su, X.; Yu, J. J.; Khan, S.; Jiang, H.; Kim, J.; Woo, J.; Kim, J. H.; Choi, B. H.; He, B.; Chen, W.; Zhang, S.; Cerione, R. A.; Auwerx, J.; Hao, Q.; Lin, H. *Science* **2011**, *334*, 806-809.

(89)   Schuetz, A.; Min, J.; Antoshenko, T.; Wang, C.-L.; Allali-Hassani, A.; Dong, A.; Loppnau, P.; Vedadi, M.; Bochkarev, A.; Sternglanz, R.; Plotnikov, A. N. *Structure* **2007**, *15*, 377-389.

(90)   Jiang, H.; Khan, S.; Wang, Y.; Charron, G.; He, B.; Sebastian, C.; Du, J.; Kim, R.; Ge, E.; Mostoslavsky, R.; Hang, H. C.; Hao, Q.; Lin, H. *Nature* **2013**, *496*, 110-113.

(91)   Feldman, J. L.; Baeza, J.; Denu, J. M. *J Biol Chem* **2013**, *288*, 31350-31356.

(92)   Zhang, Z.; Tan, M.; Xie, Z.; Dai, L.; Chen, Y.; Zhao, Y. *Nat Chem Biol* **2011**, *7*, 58-63.

(93)   Tan, M.; Peng, C.; Anderson, Kristin A.; Chhoy, P.; Xie, Z.; Dai, L.; Park, J.; Chen, Y.; Huang, H.; Zhang, Y.; Ro, J.; Wagner, Gregory R.; Green, Michelle F.; Madsen, Andreas S.; Schmiesing, J.; Peterson, Brett S.; Xu, G.; Ilkayeva, Olga R.; Muehlbauer, Michael J.; Braulke, T.; Mühlhausen, C.; Backos, Donald S.; Olsen, Christian A.; McGuire, Peter J.; Pletcher, Scott D.; Lombard, David B.; Hirschey, Matthew D.; Zhao, Y. *Cell Metab* **2014**, *19*, 605-617.

(94)   Peng, C.; Lu, Z.; Xie, Z.; Cheng, Z.; Chen, Y.; Tan, M.; Luo, H.; Zhang, Y.; He, W.; Yang, K.; Zwaans, B. M. M.; Tishkoff, D.; Ho, L.; Lombard, D.; He, T.-C.; Dai, J.; Verdin, E.; Ye, Y.; Zhao, Y. *Mol Cell Proteomics* **2011**, *10*, M111.012658.

(95) Nishida, Y.; Rardin, Matthew J.; Carrico, C.; He, W.; Sahu, Alexandria K.; Gut, P.; Najjar, R.; Fitch, M.; Hellerstein, M.; Gibson, Bradford W.; Verdin, E. *Mol Cell* **2015**, *59*, 321-332.

(96) Tan, M.; Luo, H.; Lee, S.; Jin, F.; Yang, Jeong S.; Montellier, E.; Buchou, T.; Cheng, Z.; Rousseaux, S.; Rajagopal, N.; Lu, Z.; Ye, Z.; Zhu, Q.; Wysocka, J.; Ye, Y.; Khochbin, S.; Ren, B.; Zhao, Y. *Cell* **2011**, *146*, 1016-1028.

(97) Bao, X.; Wang, Y.; Li, X.; Li, X.-M.; Liu, Z.; Yang, T.; Wong, C. F.; Zhang, J.; Hao, Q.; Li, X. D. *eLife* **2014**, *3*, e02999.

(98) Park, J.; Chen, Y.; Tishkoff, Daniel X.; Peng, C.; Tan, M.; Dai, L.; Xie, Z.; Zhang, Y.; Zwaans, Bernadette M. M.; Skinner, Mary E.; Lombard, David B.; Zhao, Y. *Mol Cell* **2013**, *50*, 919-930.

(99) Rardin, Matthew J.; He, W.; Nishida, Y.; Newman, John C.; Carrico, C.; Danielson, Steven R.; Guo, A.; Gut, P.; Sahu, Alexandria K.; Li, B.; Uppala, R.; Fitch, M.; Riiff, T.; Zhu, L.; Zhou, J.; Mulhern, D.; Stevens, Robert D.; Ilkayeva, Olga R.; Newgard, Christopher B.; Jacobson, Matthew P.; Hellerstein, M.; Goetzman, Eric S.; Gibson, Bradford W.; Verdin, E. *Cell Metab* **2013**, *18*, 920-933.

(100) Nakagawa, T.; Lomb, D. J.; Haigis, M. C.; Guarente, L. *Cell* **2009**, *137*, 560-570.

(101) Yu, J.; Sadhukhan, S.; Noriega, L. G.; Moullan, N.; He, B.; Weiss, R. S.; Lin, H.; Schoonjans, K.; Auwerx, J. *Sci Rep* **2013**, *3*, 2806.

(102) Kumar, S.; Lombard, D. B. *Antioxid Redox Sign* **2014**, *22*, 1060-1077.

(103) Ogura, M.; Nakamura, Y.; Tanaka, D.; Zhuang, X.; Fujita, Y.; Obara, A.; Hamasaki, A.; Hosokawa, M.; Inagaki, N. *Biochem Biophys Res Commun* **2010**, *393*, 73-78.

(104) Lin, Z.-F.; Xu, H.-B.; Wang, J.-Y.; Lin, Q.; Ruan, Z.; Liu, F.-B.; Jin, W.; Huang, H.-H.; Chen, X. *Biochem Biophys Res Commun* **2013**, *441*, 191-195.

(105) Somwar, R.; Erdjument-Bromage, H.; Larsson, E.; Shum, D.; Lockwood, W. W.; Yang, G.; Sander, C.; Ouerfelli, O.; Tempst, P. J.; Djaballah, H.; Varmus, H. E. *Proc Natl Acad Sci* **2011**, *108*, 16375-16380.

(106) Papa, L.; Hahn, M.; Marsh, E. L.; Evans, B. S.; Germain, D. *J Biol Chem* **2014**, *289*, 5412-5416.

(107) Lu, W.; Zuo, Y.; Feng, Y.; Zhang, M. *Tumor Biol* **2014**, *35*, 10699-10705.

(108) He, B.; Du, J.; Lin, H. *J Am Chem Soc* **2012**, *134*, 1922-1925.

(109)   Roessler, C.; Nowak, T.; Pannek, M.; Gertz, M.; Nguyen, G. T. T.; Scharfe, M.; Born, I.; Sippl, W.; Steegborn, C.; Schutkowski, M. *Angew Chem Int Ed* **2014**, *53*, 10728-10732.

(110)   Wegener, D.; Hildmann, C.; Riester, D.; Schwienhorst, A. *Anal Biochem* **2003**, *321*, 202-208.

(111)   Borra, M. T.; Smith, B. C.; Denu, J. M. *J Biol Chem* **2005**, *280*, 17187-17195.

(112)   Howitz, K. T.; Bitterman, K. J.; Cohen, H. Y.; Lamming, D. W.; Lavu, S.; Wood, J. G.; Zipkin, R. E.; Chung, P.; Kisielewski, A.; Zhang, L.-L.; Scherer, B.; Sinclair, D. A. *Nature* **2003**, *425*, 191-196.

(113)   Kokkonen, P.; Rahnasto-Rilla, M.; Mellini, P.; Jarho, E.; Lahtela-Kakkonen, M.; Kokkola, T. *Eur J Pharm Sci* **2014**, *63*, 71-76.

(114)   Madsen, A. S.; Olsen, C. A. *J Med Chem* **2012**, *55*, 5582-5590.

(115)   Parenti, M. D.; Grozio, A.; Bauer, I.; Galeno, L.; Damonte, P.; Millo, E.; Sociali, G.; Franceschi, C.; Ballestrero, A.; Bruzzone, S.; Rio, A. D.; Nencioni, A. *J Med Chem* **2014**, *57*, 4796-4804.

(116)   Beher, D.; Wu, J.; Cumine, S.; Kim, K. W.; Lu, S.-C.; Atangan, L.; Wang, M. *Chem Biol Drug Des* **2009**, *74*, 619-624.

(117)   Pacholec, M.; Bleasdale, J. E.; Chrunyk, B.; Cunningham, D.; Flynn, D.; Garofalo, R. S.; Griffith, D.; Griffor, M.; Loulakis, P.; Pabst, B.; Qiu, X.; Stockman, B.; Thanabal, V.; Varghese, A.; Ward, J.; Withka, J.; Ahn, K. *J Biol Chem* **2010**, *285*, 8340-8351.

(118)   Smith, B. C.; Hallows, W. C.; Denu, J. M. *Anal Biochem* **2009**, *394*, 101-109.

(119)   Li, Y.; Huang, W.; You, L.; Xie, T.; He, B. *Bioorg Med Chem Lett* **2015**, *25*, 1671-1674.

(120)   Roessler, C.; Tüting, C.; Meleshin, M.; Steegborn, C.; Schutkowski, M. *J Med Chem* **2015**, *58*, 7217-7223.

(121)   Fischer, F.; Gertz, M.; Suenkel, B.; Lakshminarasimhan, M.; Schutkowski, M.; Steegborn, C. *PLoS ONE* **2012**, *7*, e45098.

(122)   Küster, S. K.; Fagerer, S. R.; Verboket, P. E.; Eyer, K.; Jefimovs, K.; Zenobi, R.; Dittrich, P. S. *Anal Chem* **2013**, *85*, 1285-1289.

(123)   He, M.; Edgar, J. S.; Jeffries, G. D. M.; Lorenz, R. M.; Shelby, J. P.; Chiu, D. T. *Anal Chem* **2005**, *77*, 1539-1544.

(124)   Sun, M.; Fang, Q. *Lab Chip* **2010**, *10*, 2864-2868.

(125)   Edgar, J. S.; Milne, G.; Zhao, Y.; Pabbati, C. P.; Lim, D. S. W.; Chiu, D. T. *Angew Chem Int Ed* **2009**, *48*, 2719-2722.

(126)   Wang, M.; Roman, G. T.; Schultz, K.; Jennings, C.; Kennedy, R. T. *Anal Chem* **2008**, *80*, 5607-5615.

(127)   Harrison, D. J.; Fluri, K.; Seiler, K.; Fan, Z.; Effenhauser, C. S.; Manz, A. *Science* **1993**, *261*, 895-897.

(128)   Roper, M. G.; Shackman, J. G.; Dahlgren, G. M.; Kennedy, R. T. *Anal Chem* **2003**, *75*, 4711-4717.

(129)   Simpson, P. C.; Roach, D.; Woolley, A. T.; Thorsen, T.; Johnston, R.; Sensabaugh, G. F.; Mathies, R. A. *Proc Natl Acad Sci* **1998**, *95*, 2256-2261.

(130)   Jacobson, S. C.; Hergenroder, R.; Moore, A. W., Jr.; Ramsey, J. M. *Anal Chem* **1994**, *66*, 4127-4132.

(131)   Jacobson, S. C.; Koutny, L. B.; Hergenroeder, R.; Moore, A. W.; Ramsey, J. M. *Anal Chem* **1994**, *66*, 3472-3476.

(132)   Shackman, J. G.; Watson, C. J.; Kennedy, R. T. *J Chromatogr A* **2004**, *1040*, 273-282.

(133)   Culbertson, C. T.; Jacobson, S. C.; Ramsey, J. M. *Anal Chem* **2000**, *72*, 5814-5819.

(134)   Davies, S. P.; Reddy, H.; Caivano, M.; Cohen, P. *Biochem J* **2000**, *351*, 95-105.

(135)   Cozza, G.; Bonvini, P.; Zorzi, E.; Poletto, G.; Pagano, M. A.; Sarno, S.; Donella-Deana, A.; Zagotto, G.; Rosolen, A.; Pinna, L. A.; Meggio, F.; Moro, S. *J Med Chem* **2006**, *49*, 2363-2366.

(136)   Sebastián, C.; Mostoslavsky, R. *Semin Cell Dev Biol* **2015**.

(137)   Ohla, S.; Beyreiss, R.; Scriba, G. K. E.; Fan, Y.; Belder, D. *Electrophoresis* **2010**, *31*, 3263-3267.

(138)   Abromeit, H.; Kannan, S.; Sippl, W.; Scriba, G. K. E. *Electrophoresis* **2012**, *33*, 1652-1659.

(139) Fan, Y.; Hense, M.; Ludewig, R.; Weisgerber, C.; Scriba, G. K. E. *J Pharm Biomed Anal* **2011**, *54*, 772-778.

(140) Perrin, D.; Frémaux, C.; Shutes, A. *Expert Opin Drug Dis* **2009**, *5*, 51-63.

(141) Shanmuganathan, M.; Britz-McKibbin, P. *Anal Chim Acta* **2013**, *773*, 24-36.

(142) Guetschow, E. D.; Steyer, D. J.; Kennedy, R. T. *Anal Chem* **2014**, *86*, 10373-10379.

(143) Cosgrove, M. S.; Bever, K.; Avalos, J. L.; Muhammad, S.; Zhang, X.; Wolberger, C. *Biochemistry* **2006**, *45*, 7511-7521.

(144) von Ahsen, O.; Bömer, U. *ChemBioChem* **2005**, *6*, 481-490.

(145) Maurer, B.; Rumpf, T.; Scharfe, M.; Stolfa, D. A.; Schmitt, M. L.; He, W.; Verdin, E.; Sippl, W.; Jung, M. *ACS Med Chem Lett* **2012**, *3*, 1050-1053.

(146) Sun, S.; Kennedy, R. T. *Anal Chem* **2014**, *86*, 9309-9314.

(147) Suenkel, B.; Fischer, F.; Steegborn, C. *Bioorg Med Chem Lett* **2013**, *23*, 143-146.

(148) Su, J.; Chang, C.; Xiang, Q.; Zhou, Z.-W.; Luo, R.; Yang, L.; He, Z.-X.; Yang, H.; Li, J.; Bei, Y.; Xu, J.; Zhang, M.; Zhang, Q.; Su, Z.; Huang, Y.; Pang, J.; Zhou, S.-F. *Drug Des Dev Ther* **2014**, *8*, 2555-2602.

(149) Kainkaryam, R. M.; Woolf, P. J. *Curr Open Drug Discov Devel* **2009**, *12*, 339-350.

(150) Hatakeyama, T.; Chen, D. L.; Ismagilov, R. F. *J Am Chem Soc* **2006**, *128*, 2518-2519.

(151) Oldenburg, K. R.; Zhang, J.-H.; Chen, T.; Maffia, A.; Blom, K. F.; Combs, A. P.; Chung, T. D. Y. *J Biomol Screen* **1998**, *3*, 55-62.

(152) Walling, L. A.; Peters, N. R.; Horn, E. J.; King, R. W. *J Cell Biochem* **2001**, *84*, 7-12.

(153) Du, W.-B.; Sun, M.; Gu, S.-Q.; Zhu, Y.; Fang, Q. *Anal Chem* **2010**, *82*, 9941-9947.

(154) Du, G.-S.; Pan, J.-Z.; Zhao, S.-P.; Zhu, Y.; den Toonder, J. M. J.; Fang, Q. *Anal Chem* **2013**, *85*, 6740-6747.

(155) Zhu, Y.; Zhang, Y.-X.; Cai, L.-F.; Fang, Q. *Anal Chem* **2013**, *85*, 6723-6731.

(156) Abate, A. R.; Hung, T.; Mary, P.; Agresti, J. J.; Weitz, D. A. *Proc Natl Acad Sci* **2010**, *107*, 19163-19166.

(157) Ahn, K.; Agresti, J.; Chong, H.; Marquez, M.; Weitz, D. A. *Appl Phys Lett* **2006**, *88*, 264105.

(158) Chabert, M.; Dorfman, K. D.; Viovy, J.-L. *Electrophoresis* **2005**, *26*, 3706-3715.

(159) Lee, H.; Xu, L.; Oh, K. W. *Biomicrofluidics* **2014**, *8*, 044113.

(160) Baroud, C. N.; Robert de Saint Vincent, M.; Delville, J.-P. *Lab Chip* **2007**, *7*, 1029-1033.

(161) McDonald, J. C.; Whitesides, G. M. *Acc Chem Res* **2002**, *35*, 491-499.

(162) Price, A. K.; Paegel, B. M. *Anal Chem* **2015**.

(163) Chen, Y.; Wijaya Gani, A.; Tang, S. K. Y. *Lab Chip* **2012**, *12*, 5093-5103.

(164) Courtois, F.; Olguin, L. F.; Whyte, G.; Theberge, A. B.; Huck, W. T. S.; Hollfelder, F.; Abell, C. *Anal Chem* **2009**, *81*, 3008-3016.

(165) Price, A. K.; MacConnell, A. B.; Paegel, B. M. *Anal Chem* **2014**, *86*, 5039-5044.

(166) Edwards, B. S.; Young, S. M.; Oprea, T. I.; Bologa, C. G.; Prossnitz, E. R.; Sklar, L. A. *Nat Protocols* **2006**, *1*, 59-66.

(167) Hayashi, S.; Hamaguchi, H.-o. *Chem Lett* **2004**, *33*, 1590-1591.

(168) Hayashi, S.; Saha, S.; Hamaguchi, H.-o. *IEEE Trans Magn* **2006**, *42*, 12-14.

(169) Nacham, O.; Clark, K. D.; Yu, H.; Anderson, J. L. *Chem Mater* **2015**, *27*, 923-931.

(170) Mao, L.; Elborai, S.; He, X.; Zahn, M.; Koser, H. *Physical Review B* **2011**, *84*, 104431.

(171) Wells, J. A.; McClendon, C. L. *Nature* **2007**, *450*, 1001-1009.

(172) Wilson, A. J. *Chem Soc Rev* **2009**, *38*, 3289-3300.

(173) Song, P.; Mabrouk, O. S.; Hershey, N. D.; Kennedy, R. T. *Anal Chem* **2012**, *84*, 412-419.

(174) Anderson, G. J.; M. Cipolla, C.; Kennedy, R. T. *Anal Chem* **2011**, *83*, 1350-1355.

(175)   Jin, S.; Anderson, G. J.; Kennedy, R. T. *Anal Chem* **2013**, *85*, 6073-6079.